

DAMAGE INDICES FOR REINFORCED CONCRETE FRAMES:
EVALUATION AND CORRELATION

by

ISABELLE VILLEMURE

B. Eng., École Polytechnique de Montréal, 1993

A THESIS SUBMITTED IN PARTIAL FULFILLMENT OF
THE REQUIREMENTS FOR THE DEGREE OF
MASTER OF APPLIED SCIENCE

in

THE FACULTY OF GRADUATE STUDIES

Department of Civil Engineering

We accept this thesis as conforming

to the required standard

THE UNIVERSITY OF BRITISH COLUMBIA

July 1995

© Isabelle Villemure, 1995

In presenting this thesis in partial fulfilment of the requirements for an advanced degree at the University of British Columbia, I agree that the Library shall make it freely available for reference and study. I further agree that permission for extensive copying of this thesis for scholarly purposes may be granted by the head of my department or by his or her representatives. It is understood that copying or publication of this thesis for financial gain shall not be allowed without my written permission.

Department of CIVIL ENGINEERING

The University of British Columbia
Vancouver, Canada

Date July 4th 1995

ABSTRACT

The purpose of this study was to assess the effectiveness of damage indicators for predicting damage in reinforced concrete structures. Two damage assessment approaches were investigated. One of these approaches leads to damage indices based on structural properties. The other approach leads to damage indices based on structural dynamic characteristics. Both approaches were used to characterize the damage of five 0.45 scale reinforced concrete bridge bents that were subjected to lateral slow cyclic loading at the Structures Laboratory of the University of British Columbia. These bents were tested as part of a seismic retrofit program undertaken by the Ministry of Transportation and Highways of British Columbia (MOTH), in collaboration with Klohn-Crippen Consultants and the University of British Columbia. The specimens underwent lateral slow cyclic loading which was monotonically increased until failure or very significant damage of the specimen occurred. During the loading process, load-deformation relationships were determined to assess structural properties of the specimens. Vibration measurement tests (ambient and impact testing) were performed at different stages of the loading cycles in order to identify the dynamic properties of the specimens.

Damage assessment based on structural properties, such as displacement, stiffness and energy absorption, consisted in the evaluation of three damage indices: displacement ductility, modified stiffness ratio and the modified Park and Ang index. For the five specimens tested in the laboratory, these three indices were evaluated at different stages of damage as the displacement level increased. Damage based on dynamic properties, such as natural frequencies and damping ratios, was assessed using three damage indices: ultimate stiffness degradation, maximum softening and normalized damping ratio.

For each damage index considered in this study, the specimens were ranked according to their performance and the results from these evaluations were compared with the physical damage observed at different stages of the load testing. The results of the study showed that the agreement between analytical predictions and experimental observations was, in general, satisfactory. This study also indicated that, while two of the structural damage indices could provide some indication on the failure mode, none of the modal damage indices could give specific information on the failure mode (shear/flexure). Finally, comparison of index values from the two approaches indicated that modal damage indices generally provide a better damage characterization than structural damage indices.

TABLE OF CONTENTS

	page
ABSTRACT	ii
TABLE OF CONTENTS	iv
LIST OF TABLES	viii
LIST OF FIGURES	ix
ACKNOWLEDGMENTS	xi
DEDICATION	xii
CHAPTER 1	
INTRODUCTION	1
1.1 PROBLEM OVERVIEW	1
1.2 OBJECTIVES AND OUTLINE OF STUDY	2
CHAPTER 2	
THEORETICAL BACKGROUND ON DAMAGE ASSESSMENT	4
2.1 DAMAGE ASSESSMENT BASED ON STRUCTURAL PROPERTIES	6
2.1.1 GLOBAL DAMAGE INDICES	6
2.1.2 LOCAL DAMAGE INDICES	7
2.1.2.1 NON-CUMULATIVE INDICES	8
2.1.2.2 CUMULATIVE INDICES	9
2.1.3 SUMMARY OF DAMAGE INDICES BASED ON STRUCTURAL PROPERTIES	13
2.2 DAMAGE ASSESSMENT BASED ON DYNAMIC PROPERTIES	14
2.2.1 GLOBAL INDICES	15
2.2.2 LOCAL INDICES	23
2.2.3 SUMMARY OF DAMAGE INDICES BASED ON DYNAMIC PROPERTIES	28
2.3 INTRODUCTION TO DAMAGE ASSESSMENT BASED ON NEURAL NETWORKS	30
2.3.1 TYPICAL INTERNAL STRUCTURE	31
2.3.2 TYPES OF NEURAL NETWORK	32
2.3.3 BACK-PROPAGATION NEURAL NETWORKS	32
2.3.3.1 DESCRIPTION OF THE NETWORK AND ITS OPERATION	32
2.3.3.2 NETWORK DEVELOPMENT	34
2.3.3.2.1 Input and Output Layers	35
2.3.3.2.2 Hidden Layers	35
2.3.3.2.3 Training Patterns	36
2.3.3.2.4 Training Process	37
2.3.3.2.5 Validation of Network	37
2.3.3.3 EXAMPLES OF APPLICATION TO DAMAGE ASSESSMENT	38
2.4 CONCLUDING REMARKS	39

CHAPTER 3

EXPERIMENTAL PROCEDURE	40
3.1 TEST OBJECTIVES	41
3.2 DESCRIPTION OF SPECIMENS	41
3.2.1 SPECIMEN OSB1	42
3.2.2 SPECIMEN OSB2	43
3.2.3 SPECIMEN OSB3	43
3.2.4 SPECIMEN OSB4	43
3.2.5 SPECIMEN OSB5	44
3.3 LOADING PROCEDURE	44
3.3.1 VERTICAL LOADING	45
3.3.2 LATERAL LOADING	45
3.3.3 STRUCTURE INSTRUMENTATION	46
3.4 DYNAMIC TESTING PROCEDURE	46
3.4.1 TYPE OF VIBRATIONS	47
3.4.1.1 AMBIENT VIBRATIONS	47
3.4.1.2 FORCED VIBRATIONS	47
3.4.2 STRUCTURE INSTRUMENTATION	47
3.4.2.1 ACCELEROMETERS	48
3.4.2.2 INSTRUMENTED HAMMER	51
3.4.3 DATA ACQUISITION SYSTEM	52
3.4.3.1 MEASUREMENT HARDWARE	53
3.4.3.2 MEASUREMENT SOFTWARE	53
3.4.3.2.1 Ambient Vibration Testing Parameters	54
3.4.3.2.2 Forced Vibration Testing Parameters	54
3.4.4 DYNAMIC TESTING SEQUENCES	56
3.4.4.1 PRELIMINARY AND FINAL SEQUENCES	56
3.4.4.2 INTERMEDIATE SEQUENCES	57
3.5 PRELIMINARY DESCRIPTION OF DAMAGE OBSERVED	58
3.6 CONCLUDING REMARKS	61

CHAPTER 4

DAMAGE ASSESSMENT BASED ON STRUCTURAL PROPERTIES	62
4.1 CHOICE OF DAMAGE INDICES	62
4.2 EVALUATION OF DAMAGE INDICES	63
4.2.1 DISPLACEMENT DUCTILITY	63
4.2.2 MODIFIED STIFFNESS RATIO	65
4.2.3 MODIFIED PARK AND ANG INDEX	66
4.3 RESULTS AND COMPARISONS OF INDICES	67
4.3.1 COMPARISON OF SPECIMEN BEHAVIORS	67
4.3.1.1 DUCTILITY DISPLACEMENT	67
4.3.1.2 MODIFIED STIFFNESS RATIO	69
4.3.1.3 MODIFIED PARK & ANG INDEX	71
4.3.1.4 SUMMARY OF SPECIMEN CLASSIFICATION	72
4.3.2 DAMAGE INDICES CORRELATION	73
4.3.3 COMPARISON OF NORMALIZED INDICES FOR EACH SPECIMEN	76
4.4 CONCLUDING REMARKS	78

CHAPTER 5

DAMAGE ASSESSMENT BASED ON MODAL PROPERTIES	80
5.1 CHOICE OF MODAL DAMAGE INDICES	80
5.2 EVALUATION OF NATURAL FREQUENCIES FROM EXPERIMENTAL DATA	81
5.2.1 THEORETICAL BACKGROUND	82
5.2.1.1 THE FOURIER TRANSFORM	82
5.2.1.2 INDICATORS OF NATURAL FREQUENCIES	83
5.2.1.3 NATURAL FREQUENCY RELATED TO DIFFERENT DIRECTIONS OF MOTION	86
5.2.2 EVALUATION OF NATURAL FREQUENCY	86
5.2.2.1 TYPICAL TIME SIGNALS	87
5.2.2.2 INITIAL STUDY OF NATURAL FREQUENCIES	89
5.2.2.3 FUNDAMENTAL LONGITUDINAL FREQUENCY STUDY	91
5.2.3 NATURAL LONGITUDINAL FREQUENCY HISTORY	94
5.3 EVALUATION OF DAMPING FROM EXPERIMENTAL DATA	98
5.3.1 THEORETICAL BACKGROUND	98
5.3.1.1 VISCOUS DAMPING	99
5.3.1.2 HYSTERETIC DAMPING	101
5.3.2 EVALUATION OF DAMPING	103
5.3.2.1 VISCOUS DAMPING	104
5.3.2.2 HYSTERETIC DAMPING	105
5.3.3 DAMPING HISTORY	105
5.4 EVALUATION OF DAMAGE INDICES	109
5.4.1 ULTIMATE STIFFNESS DEGRADATION	109
5.4.2 MAXIMUM SOFTENING	110
5.4.3 NORMALIZED DAMPING RATIO	110
5.5 RESULTS AND COMPARISON OF DAMAGE INDICES	111
5.5.1 COMPARISON OF SPECIMEN BEHAVIORS	111
5.5.1.1 ULTIMATE STIFFNESS DEGRADATION	112
5.5.1.2 MAXIMUM SOFTENING	114
5.5.1.3 NORMALIZED DAMPING RATIO	115
5.5.1.4 SUMMARY OF SPECIMEN CLASSIFICATION	117
5.5.2 DAMAGE INDICES CORRELATION	118
5.5.3 COMPARISON OF NORMALIZED INDICES FOR EACH SPECIMEN	121
5.6 CONCLUDING REMARKS	123

CHAPTER 6

COMPARATIVE ANALYSIS	125
6.1 DAMAGE INDICES CORRELATION	125
6.1.1 ULTIMATE STIFFNESS DEGRADATION	126
6.1.2 MAXIMUM SOFTENING	128
6.1.3 NORMALIZED DAMPING RATIO	131
6.1.4 SUMMARY OF INDICES CORRELATION	134
6.2 GENERAL COMPARISON OF DAMAGE ASSESSMENT APPROACHES	135
6.3 CONCLUDING REMARKS	137

CHAPTER 7

CONCLUSIONS AND FURTHER STUDIES	138
---------------------------------------	-----

REFERENCES	140
------------------	-----

APPENDIX A	146
APPENDIX B	162
B.1 TYPICAL TESTING PROCEDURE	163
B.2 DETAILED TESTING CHARACTERISTICS	164
B.2.1 SPECIMEN OSB1	164
B.2.2 SPECIMEN OSB2	166
B.2.3 SPECIMEN OSB3	167
B.2.4 SPECIMEN OSB4	169
B.2.5 SPECIMEN OSB5	171
B.3 DETAILED SENSOR LOCATION	173
B.4 HAMMER AND SENSOR SPECIFICATIONS	174
B.5 DETAILS ON PROCESSING OF LONGITUDINAL FREQUENCY	175
APPENDIX C	176
C.1 TYPICAL SPREADSHEET FOR DISPLACEMENT DUCTILITY- SPECIMEN OSB1	177
C.2 TYPICAL SPREADSHEET FOR MODIFIED STIFFNESS RATIO - SPECIMEN OSB1	178
C.3 TYPICAL SPREADSHEET FOR MODIFIED PARK AND ANG INDEX - SPECIMEN OSB1	179
APPENDIX D	181

LIST OF TABLES

CHAPTER 2	page
Table 2.1 Damage indices based on structural properties	14
Table 2.2 Global damage indices based on dynamic properties	29
Table 2.3 Local damage indices based on dynamic properties	30
CHAPTER 3	
Table 3.1 Ambient vibration testing characteristics	54
Table 3.2 Impact vibration testing characteristics	55
Table 3.3 Preliminary and final sequences	57
Table 3.4 Experimental lateral loading characteristics	58
CHAPTER 4	
Table 4.1 Ranking of specimen behaviors	72
CHAPTER 5	
Table 5.1 Natural frequencies of OSB1 extracted from impact vibrations	89
Table 5.2 Natural frequencies of OSB1 extracted from ambient vibrations	90
Table 5.3 Input/output combinations for longitudinal FRF calculations	94
Table 5.4 Fundamental natural longitudinal frequency history for each of the 5 specimens ...	94
Table 5.5 Viscous damping ratios	105
Table 5.6 Equivalent hysteretic damping ratios	107
Table 5.7 Ultimate stiffness degradation characteristics	113
Table 5.8 Maximum softening characteristics	115
Table 5.9 Normalized damping ratio characteristics	116
Table 5.10 Ranking of specimen behaviors	117
CHAPTER 6	
Table 6.1 Summary of index correlation	135

LIST OF FIGURES

CHAPTER 2	page
Figure 2.1 Fundamental period time history	17
Figure 2.2 Back-propagation neural network	32
CHAPTER 3	
Figure 3.1 Specimen OSB5 ready for testing	41
Figure 3.2 Experimental model of bent S28	42
Figure 3.3 Experimental setup	44
Figure 3.4 Load cycles in a single sequence	45
Figure 3.5 Typical tri-axial accelerometer setup	49
Figure 3.6 Installation device for accelerometers of OSB3 and OSB4	50
Figure 3.7 Setup for dynamic testing	51
Figure 3.8 Longitudinal impact applied with the instrumented hammer	52
Figure 3.9 Typical recording setup for vibration measurements	53
Figure 3.10 Low sampling rate [200 sps]	55
Figure 3.11 High sampling rate [1000 sps]	55
Figure 3.12 Hysteresis curves	60
CHAPTER 4	
Figure 4.1 Typical hysteresis loop and parameter definitions	64
Figure 4.2 Comparison of specimen behaviors: displacement ductility	68
Figure 4.3a Comparison of specimen behaviors: modified stiffness ratio	69
Figure 4.3b Comparison of specimen behaviors: modified Park and Ang index	71
Figure 4.4a Index correlation: modified stiffness ratio vs displacement ductility	74
Figure 4.4b Index correlation: modified Park and Ang index vs displacement ductility	75
Figure 4.4c Index correlation: modified Park and Ang index vs modified stiffness ratio	75
Figure 4.5 Comparison of normalized indices	78
CHAPTER 5	
Figure 5.1 Ambient vibration output signal	88
Figure 5.2 Impact vibration input and output signals	88
Figure 5.3 Fundamental natural mode shapes of OSB1	91
Figure 5.4 Comparison of FRF formulations	93
Figure 5.5 Sensitivity of natural longitudinal frequency to structural damage	96
Figure 5.6 Example of stiffness study for specimen OSB5	96
Figure 5.7 Viscously damped free-vibration response	100
Figure 5.8 Hysteretic damping from hysteresis loop	102

Figure 5.9 Sensitivity of viscous damping to structural damage	106
Figure 5.10 Sensitivity of hysteretic damping to structural damage	106
Figure 5.11 Modulation in the response time signals	108
Figure 5.12a Comparison of specimen behaviors: ultimate stiffness degradation	112
Figure 5.12b Comparison of specimen behaviors: maximum softening	114
Figure 5.12c Comparison of specimen behaviors: normalized damping ratio	116
Figure 5.13a Index correlation: ultimate stiffness degradation vs maximum softening.	119
Figure 5.13b Index correlation: ultimate stiffness degradation vs normalized damping ratio . .	120
Figure 5.13c Index correlation: normalized damping ratio vs maximum softening	121
Figure 5.14 Comparison of normalized damage indices	123

CHAPTER 6

Figure 6.1 Correlation between ultimate stiffness degradation and displacement ductility . . .	126
Figure 6.2 Correlation between ultimate stiffness degradation and modified stiffness ratio . .	127
Figure 6.3 Correlation between ultimate stiffness degradation and modified Park and Ang index	128
Figure 6.4 Correlation between maximum softening and displacement ductility	129
Figure 6.5 Correlation between maximum softening and modified stiffness ratio	130
Figure 6.6 Correlation between maximum softening and modified Park and Ang index	131
Figure 6.7 Correlation between normalized damping ratio and displacement ductility	132
Figure 6.8 Correlation between normalized damping ratio and modified stiffness ratio	133
Figure 6.9 Correlation between normalized damping ratio and modified Park and Ang index .	134

APPENDIX A

Figure Q-117-01 Pier S28	148
Figure Q-117-11 specimen OSB1	149
Figure Q-117-13 specimen OSB2	150
Figure Q-117-12 specimen OSB3	151
Figure Q-117-14 specimen OSB4	152
Figure Q-1 Elevation view of specimen OSB5.	153
Figure A.1 Typical accelerometer setup on a column	154
Figure A.2 Typical accelerometer setup on the cap beam	155
Figure A.3 Instrumented hammer	155
Figure A.4 Transverse impact applied with the instrumented hammer	156
Figure A.5 Vertical impact applied with the instrumented hammer.	157
Figure A.6 Data acquisition system	157
Figure A.7 Overall view of specimen OSB1 at failure.	158
Figure A.8 View of specimen OSB2 at failure (north column, east side)	158
Figure A.9 View of specimen OSB2 at failure (north column, west side).	159
Figure A.10 Overall view of specimen OSB3 at failure.	159
Figure A.11 Overall view of specimen OSB4 at failure.	160
Figure A.12 View of specimen OSB5 at failure (north half)	160
Figure A.13 View of specimen OSB5 at failure (south half)	161

ACKNOWLEDGMENTS

I would like to express my deepest gratitude to my thesis supervisor, Dr. Carlos E. Ventura, for his inestimable assistance and constant encouragement in the advancement and completion of this thesis. I would also like to gratefully acknowledge my thesis co-supervisor, Dr. Robert G. Sexsmith, for his excellent guidance throughout this research project.

I am indebted to my colleague Norman Schuster. During his graduate studies at the University of British Columbia, he upgraded the data acquisition software which was used in this study. Devoted and patient, he offered me helpful guidance and advice throughout the vibration testing program.

The financial support of the Natural Sciences and Engineering Research Council of Canada (N.S.E.R.C.) is gratefully acknowledged. This includes a Postgraduate Scholarship as well as Research Grants awarded to both Dr. C.E. Ventura and Dr. R.G. Sexsmith. The research was also made possible by financial support of the Ministry of Transportation and Highways of British Columbia.

Special thanks are expressed to Howard Nichol, earthquake laboratory technician, for his helpful assistance and constant technical support.

Furthermore, the helpful suggestions of colleagues Mahmoud Rezai and Vincent Latendresse are gratefully acknowledged as well as the contribution of Thomas Horyna in the development of two computer programs used in the analytical part of this study. I would also like to thank all of the other people who provided technical support in the testing of the specimens. These people include Paul Symons, Tony Cigic, Daryl English, Brad Kemp and Mike Baraka.

Finally, I would like to thank Dr. R. Foschi who, along with Dr. C. E. Ventura and Dr. R. G. Sexsmith, reviewed this thesis.

à Michelle et Pierre

CHAPTER 1

INTRODUCTION

1.1 PROBLEM OVERVIEW

During its lifetime, a structure is subjected to loads arising from different sources. Depending on the intended use and occupancy of the structure, serviceability loads produce stresses and deformations on the different structural components, in general, below critical levels. Although unusual, extreme loads, such as earthquakes and hurricanes, may generate stresses and deformations on the structural members that will be so high as to cause a certain level of damage or even failure of members, or the whole structure.

Over the last few decades, one of important areas of research for structural engineers has been the characterization and evaluation of structural damage. Considering the complexity involved in the structural degradation processes, quantifying damage often represents a difficult assignment. Different approaches have been developed to provide reliable predictions of the state of a damaged structure. Performed from analytical predictions or from experimental measurements, damage assessment investigates the potential or actual degradation state of a structure. Damage assessment techniques have been applied in different situations such as disaster planning, structural assessment, retrofit and repair operations, maintenance inspection and post-earthquake evaluation.

Among the different approaches to characterize damage, damage indices provide useful means to quantify damage of structures or rank their vulnerability relative to each other. Damage indices can be evaluated either based on the response of a structure to a particular loading pattern or based on the dynamic response of a structure. A different type of approach that has been recently developed considers the application of neural networks to the degradation process experienced by a structure.

Although damage assessment techniques are based on different concepts, they aim to quantify the same effect, structural degradation. However, investigating how different approaches characterize damage presents a topic of significant interest. Damage characterization is understood here to be how physical elements, such as displacement, crack propagation, yielding, stiffness degradation, etc., are taken into account in the rate of approach to failure of a damage index. Moreover, damage indicators of a same approach can quantify differently the structural degradation. Consequently, comparing damage indicators of a same approach is also of significant interest.

1.2 OBJECTIVES AND OUTLINE OF STUDY

In order to investigate different damage assessment approaches and different damage indicators of a same approach, a combined experimental and analytical program was developed and implemented during the course of this study. The objectives of this study were:

1. to measure structural and dynamic properties of the specimens tested;
2. to evaluate damage indices based on structural properties and damage indices based on modal properties;
3. to compare damage indices within a same approach;
4. to correlate damage indices obtained from the two different approaches.

A third approach, damage assessment based on neural networks, was also investigated. Since no conclusive developments were derived from this approach, results of this approach are not presented as part of this study.

This thesis describes how these objectives were implemented on an experimental program developed at the University of British Columbia. Chapter 2 presents a literature review of most commonly used damage indices, based on structural or modal properties, as well as an introduction to damage assessment based on neural networks. Chapter 3 describes the experimental procedure performed, including details on the

specimens tested and description of the loading and dynamic testing procedures. Chapter 4 investigates damage assessment based on structural properties and describes its application to the specimens tested in the laboratory. Damage assessment based on modal properties, also applied to the experimental specimens, is presented in Chapter 5. A comparative analysis of these two approaches is presented in Chapter 6. Finally, Chapter 7 summarizes results obtained from this study.

CHAPTER 2

THEORETICAL BACKGROUND ON DAMAGE ASSESSMENT

During its lifetime, the capacity of a structure may be reduced due to different types of structural faults, such as cracking, buckling, unbonding, corrosion losses, loosening of fastened parts and yielding of steel reinforcement. The complexity involved in these degradation processes sometimes limits their complete understanding. As a consequence, quantifying damage often represents a difficult assignment. Nevertheless, quantification of damage remains a useful assessment tool in several situations. Maintenance inspection and post-earthquake evaluation are examples of structure assessment requiring damage quantification. As a result, different approaches have been developed to provide reliable predictions of the state of a damaged structure. Three of these approaches are discussed below.

A first approach is based on the response of the structure to a particular loading pattern. Since seismic events present a significant damage threat, this approach usually considers structural degradation caused by earthquakes or cyclic loads. Response to these loadings is usually measured in terms of force applied and corresponding displacements experienced by the structure. Resulting load-deformation curves are commonly called hysteresis curves. These curves can either be predicted analytically with models of variable performance or determined experimentally. Since hysteresis curves obtained from experimental measurements imply partial or complete destruction of the structure under study, they contain information about degradation levels sustained by the structure. Maximum displacements experienced by the structure, stiffness degradation and levels of energy absorption can be determined from these hysteresis curves. Combination of these structural characteristics led to the development of a category of damage indices that provide quantification of damage levels sustained by the structure.

Modal analysis also provides information about structural damage. This approach is based on the concept that degradation of structural elements and/or joints alters the dynamic response of the structure. These changes in the vibration response are in turn reflected in the experimentally measured dynamic properties of the structure. The modal properties usually are the fundamental frequencies, damping ratios and mode shapes. They can be evaluated from processing of time histories obtained during vibration tests or recorded during an actual seismic event. They can also be predicted with analytical models of variable performance. Unlike structural damage indices, damage assessment based on experimental dynamic properties may involve either destructive or non-destructive measurement techniques. Combination of these dynamic properties or their relative changes has generated another category of damage indices.

The third approach, briefly discussed in this study, is damage assessment based on neural networks. Basically, application of neural networks attempts to overcome the complexity involved in damage assessment. By definition, neural networks are computing environments modelling a complex system behavior. In this case, the system behavior refers to the degradation process experienced by a structure. In order to model a system behavior, the network must initially be trained to a specific condition. For damage evaluation, the system is trained to assess a certain type of structural degradation. Thereafter, based on the training conducted, the network functions as an associative memory capable of diagnosing unknown degradation levels.

The following sections describe alternative ways of implementing these three approaches. Section 2.1 introduces damage indices based on structural properties. Damage indices based on dynamic properties are discussed in section 2.2. Finally, an introduction to damage assessment based on neural networks is presented in section 2.3.

2.1 DAMAGE ASSESSMENT BASED ON STRUCTURAL PROPERTIES

When subjected to an earthquake, a structure might suffer excessive deformations, causing structural damage in individual members or parts of the structure. Moreover, the repeated load reversals caused by the earthquake can generate low-cycle fatigue damage, leading to structural deficiencies in the system. The structure deterioration generally originates from a combination of these two effects. Consequently, damage indices based on structural properties usually include a large deformation term and/or a fatigue loading term. These damage indices can be evaluated locally on a particular member or globally on parts of the structure from measurements or predicted response to simple cyclic loadings. Several of the most commonly used global and local damage indices are presented in the following sections.

2.1.1 GLOBAL DAMAGE INDICES

Global indices, D_G , quantify damage for the complete structure, or for parts of the structure when several of its structural elements are considered. They provide an overall assessment of structure performance based on damage distribution and level of degradation sustained by its individual components. They are typically evaluated by weighting local damage indices of the different members composing the structure. Different types of weighting functions have been formulated to consider the state of heavily damaged individual elements.

The most common global index uses the amount of energy absorbed at different locations as a weighting function (Park, Ang and Wen, 1987, Chung et al, 1990, Kunnath et al, 1992). Evaluated for a complete structure of N elements or part of a structure composed of N members, the global damage index, D_G , is defined as:

$$D_G = \frac{\sum_{i=1}^N D_{L,i} E_i}{\sum_{i=1}^N E_i} \dots\dots\dots [2.1]$$

where $D_{L,i}$ is a local index evaluating damage at location i (see section 2.1.2) and E_i is the energy absorbed at that same location.

Severely damaged members of a structure can limit its overall stability. This is not reflected in the averaging effect of Equation 2.1. Hence, Bracci et al (1989) developed a global damage index that emphasizes the severity of damage in a structural member. It is expressed as:

$$D_G = \frac{\sum_{i=1}^N w_i D_{L,i}^{(b+1)}}{\sum_{i=1}^N w_i D_{L,i}^b} \dots\dots\dots [2.2]$$

High values of parameter b are used when more emphasis on the most severely damaged members is required. This formulation defines the weights w_i as the ratio of the gravity load supported by member i to the total gravity load on the structure. These weighting functions reflects the greater dependence of the overall structural stability to the damage occurring at the base of the structure. Tests performed on reinforced concrete frames (Bracci et al, 1989) verified the ability of the indicator to quantify damage. Corresponding index values showed good correlation with observed and measured damage.

2.1.2 LOCAL DAMAGE INDICES

Local indices, D_L , usually characterize damage of individual members or joints, and are typically based on ductility measurements, energy absorption or a combination of both. Some indices also model the accumulation of degradation induced by the cyclic part of the motion. Others are non-cumulative and

characterize a fixed damage state of the structure. Generally, local index values range between zero, for an undamaged structure, and one, for a collapsed structure. Commonly used local damage indices are described below.

2.1.2.1 NON-CUMULATIVE INDICES

The **displacement ductility**, μ_δ , represents the most elementary index to quantify structural damage (Newmark and Rosenblueth, 1974). It is defined as the ratio of the maximum displacement sustained by the structure to its yield displacement:

$$D_L = \mu_\delta = \frac{\delta_m}{\delta_y} = 1 + \frac{\delta_m - \delta_y}{\delta_y} \dots \dots \dots [2.3]$$

where δ_y is the yield displacement and δ_m represents the maximum displacement of each cycle. The displacement ductility index is based exclusively on peak displacement and it neglects the fatigue contribution of cyclic loading. Nevertheless, it is still used as damage indicator because of its simplicity in evaluation and practical interpretation (Sordo et al, 1989).

Banon et al (1981) developed a measure of the local stiffness degradation and called it the **flexural damage ratio (FDR)**. In terms of stiffnesses, it is expressed as:

$$D_L = FDR = \frac{k_0}{k_m} \dots \dots \dots [2.4]$$

where k_0 represents the initial tangent stiffness of the structural element considered while k_m refers to the maximum stiffness of this same member during a complete cycle. Considering a particular cycle, its maximum stiffness k_m is evaluated for both forward and reverse parts of the cycle and the minimum k_m value, yielding the maximum index value, is retained. Stiffnesses are, by definition, derived from the ratio of force over displacement. Therefore, they can be evaluated from hysteresis curves of the element studied. Based on experiments of reinforced concrete frames (Banon et al, 1981), FDR indicated

adequately damage originating from large deformations. The FDR is considered as a better damage indicator than displacement ductility since it takes into account stiffness and strength degradations in the deteriorated member.

Roufaiel and Meyer (1987a) used a modified version of this index, considering the increase in flexibility at maximum deformation and at failure state. Expressed in terms of stiffnesses, the **modified stiffness ratio**, *MSR*, is defined as:

$$D_L = MSR = \frac{k_f}{k_m} \cdot \frac{(k_m - k_0)}{(k_f - k_0)} \dots \dots \dots [2.5]$$

where k_f represents the stiffness of the structure at failure. The index retained is the maximum ratio considering both positive and negative cycles. Experimental data obtained from diverse laboratory specimens were used to verify the damage index. Corresponding index calculations indicated good correlation with residual strength and stiffness obtained from experimental specimens.

2.1.2.2 CUMULATIVE INDICES

The **cumulative ductility** (Banon et al, 1981) represents a measure of ductility and captures the effect of repeated loading on the structure. Considering M cycles of loading, it is expressed as:

$$D_L = \sum_{j=1}^M (\mu_{\delta,j} - 1) \dots \dots \dots [2.6]$$

where $\mu_{\delta,j}$ is the maximum displacement ductility at cycle j , defined by Equation 2.3. Tests of reinforced concrete frames, conducted by Banon et al (1981), showed that this index was closely associated with the hysteretic behavior of the structure. Note that while displacement ductility represents a measure of damage due to excessive deformations, cumulative ductility carry information on fatigue damage, inflicted by the cyclic part of motion.

The **Stephens & Yao index** (1987) was developed based on plastic displacement increments, $\Delta\delta_p$, for a complete cycle. Considering M cycles, it is expressed as:

$$D_L = \sum_{j=1}^M \left[\frac{\Delta\delta_p^+}{\Delta\delta_f} \right]^{1-br} \dots\dots\dots [2.7]$$

in which $\Delta\delta_p^+$ is defined as the value of the positive plastic decrement and $\Delta\delta_f$ is the positive plastic decrement in a single-cycle test to failure. Coefficient r represents the ratio of positive to negative plastic displacement increments, $\Delta\delta_p^+ / \Delta\delta_p^-$, for each cycle. Parameter b is a calibrated constant based on different type of structure and damage levels and it has a recommended value of 0.77. Based on Stephens and Yao experimental studies of two small structural systems, the index provided useful measures of damage sustained by these structures. However, calibration of parameter b represents a potential limitation of this method.

The **Wang & Shah index** (1987) was developed on the assumption that the rate of accumulation of damage is proportional to the damage already affecting the structure. They proposed the following exponential equation to characterize damage, based on M loading cycles:

$$D_L = \frac{\exp(s\alpha) - 1}{\exp(s) - 1} \dots\dots\dots [2.8]$$

in which,
$$\alpha = c \sum_{j=1}^M \frac{\delta_{m,j}}{\delta_f}$$

Parameters $\delta_{m,j}$ and δ_f are respectively the maximum displacement of cycle j , and the final displacement after the complete loading pattern of M cycles. Parameters c and s are constants with recommended values of 0.1 and 1.0 for well-reinforced concrete member. Small-scale reinforced concrete beam-column joint were used to verify the index ability to quantify structural degradation (Wang and Shah, 1987). Analytical models, based on damage index calculations, showed good correlations with experimental response of the

specimens subjected to different loading histories. However, parameter s , which appeared to be correlated to the member design properties, such as the amount of joint and beam reinforcement, limits the application of this method in general.

The **Jeong & Iwan index** (1988) quantifies damage under cyclic loading using an expression combining the effects of cycles at different amplitudes. It measures the influence of both duration and ductility of response. Considering P loading cycles of different amplitudes, it is defined as:

$$D_L = \sum_{k=1}^P \frac{n_k}{n_{f,k}} \dots \dots \dots [2.9]$$

where n_k is the number of cycles at amplitude k and $n_{f,k}$ is the number of cycles to failure at that same amplitude, evaluated as:

$$n_{f,k} \mu_{\delta,k}^s = c$$

Constants c and s have recommended values of 6.0 and 416 respectively for reinforced concrete structures. The index provided an adequate qualitative estimation of structural damage. However, calibration of parameters c and s , affected by the design details of the structure under study, is a limitation of the index.

The **Kratzig & al index** (1989) is based on the hysteretic energy absorbed by a member. Considering a positive loading cycle, the first load cycle at a given amplitude represents the *primary half cycle*. The subsequent cycle at the same or lower amplitude is denoted *follower cycle*. A similar definition is used for the negative part of a complete loading cycle. Positive and negative energy terms, denoted D^+ and D^- , are then evaluated as follows for each loading cycle j :

$$D_L^\pm = \frac{\sum_{i=1}^M E_{p,j}^\pm + \sum_{j=1}^M E_j^\pm}{E_f^\pm + \sum_{j=1}^M E_j^\pm} \dots \dots \dots [2.10]$$

where $E_{p,j}^\pm$ is the energy absorbed in a primary half cycle, E_j^\pm is the energy of the follower cycles and E_f^\pm is the energy absorbed in a monotonic test to failure. The overall damage index is finally expressed as:

$$D_L = D_L^+ + D_L^- + D_L^+ D_L^-$$

From various databases, obtained from laboratory experiments or on literature, Kratzig et al successfully verified the ability of the index to detect damage evolution in a structure. This index involves considerable calculation effort compared to other local indices including a fatigue damage term.

The **Park & Ang index** (1985) combined a deformation term and a hysteretic energy absorption term to take into account the peak deformation as well as the damage related to fatigue. The corresponding damage index is expressed as:

$$D = \frac{\delta_m}{\delta_f} + \beta \frac{\int_{E=E_1}^{E=E_M} dE}{F_y \delta_f} \dots \dots \dots [2.11]$$

The integral takes into account the accumulation of energy absorbed up to the cycle under study. Parameters δ_m and δ_f are respectively the maximum displacement of the cycle considered and the final displacement after the complete loading pattern of M cycles. F_y represents the yield strength of the structure. β is a strength degradation parameter and is assumed random with a mean of 0.27 and coefficient of variation of 0.6 (Ciampoli et al, 1989). For well-reinforced concrete, its value is 0.1. Limitations of the index could be associated to the calibration of β for the structure under study. This index has been calibrated and validated against a significant amount of observed seismic damage on different structures. It has been used in a number of seismic vulnerability studies and probabilistic studies (Ang,

1987, Barenberg and Foutch, 1988, Ciampoli et al, 1989, Seidel et al, 1989, Stone and Taylor, 1993).

The **modified Park & Ang index** (Kunnath et al, 1992) slightly transforms Equation 2.11 to consider only the permanent deformation in the first term. The index is expressed as:

$$D = \frac{\delta_m - \delta_y}{\delta_f - \delta_y} + \beta \frac{\int_{E=E_1}^{E=E_M} dE}{F_y \delta_f} \dots\dots\dots [2.12]$$

2.1.3 SUMMARY OF DAMAGE INDICES BASED ON STRUCTURAL PROPERTIES

Global and local damage indices are summarized in Table 2.1. Data required in calculation as well as calibrated parameters required in the formula are presented for each damage index. For more details on these structural damage indices as well as their background, one can consult the comparative study by Williams and Sexsmith (1994).

Index or Author(s)	Type	Equation Number	Experimental or Predicted Measurement(s) Required	Calibrated Parameter(s)
energy absorption	global	2.1	for each member i : <ul style="list-style-type: none"> • local index • hysteresis curve 	none
Bracci et al	global	2.2	for each member i : <ul style="list-style-type: none"> • local index • associated gravity load 	b
displacement ductility	local	2.3	displacement history	none
flexural damage ratio	local	2.4	hysteresis curves	none
modified stiffness ratio	local	2.5	hysteresis curves	none
cumulative ductility	local	2.6	displacement history	none
Stephens & Yao	local	2.7	hysteresis curves	b
Wang & Shah	local	2.8	displacement history	c, s
Jeong & Iwan	local	2.9	hysteresis curve fatigue failure data	c, s
Kratzig et al	local	2.10	hysteresis curves	none
Park & Ang	local	2.11	hysteresis curves	β
modified Park & Ang	local	2.12	hysteresis curves	β

Table 2.1 Damage indices based on structural properties

2.2 DAMAGE ASSESSMENT BASED ON DYNAMIC PROPERTIES

Modal testing can also be used to quantify damage. This approach often includes measurements of the structure vibrations due to a particular excitation. Time histories can also be directly recorded during a seismic event. Structural deterioration, affecting members and/or joints, cause changes in these measured dynamic responses of the structure. These changes in the vibration responses are, in turn, reflected in the

experimentally derived modal properties of the structure. Modal damage assessment is based on this concept of dynamic property changes. Natural frequencies, damping ratios and mode shapes represent the most common modal properties obtained from analytical processing of time histories. While these properties can be extracted from time histories of the structure, they can also be predicted analytically with finite element models.

Indices have been developed based on these modal properties or their relative changes due to degradation. Global or local modal damage indices can be used to assess damage of the structure. The damage can be severe and global in nature and significantly influence the overall response of the structure. In this case, global indices are used to give an estimation of existence of damage in the structure. However, more reliable local indices have been developed to diagnose localized or obscure damage, usually of very small extent and found at critical sections. Local indices provide information on both the extent of damage and its location.

2.2.1 GLOBAL INDICES

Global indices, D_G , assess the overall deteriorated state of the structure. Damage extent is evaluated on the basis of parameters reflecting global changes of modal characteristics of the structure. Global indices do not give adequate representation of the location of deterioration. Nevertheless, combined with other damage assessment means, such as experimental load-displacement curves, visual inspection of structure conditions or local damage indices, global indices may provide an efficient estimation of structure deterioration. Since the first fundamental mode is the easiest to capture experimentally, several indices described below are based exclusively on this first natural mode.

The first attempt to characterize global damage consisted of tracking the evolution of the fundamental period, T , or the **fundamental frequency**, f . Note that $T = 1/f$. This indicator was developed from laboratory experiments (Newmark and Rosenblueth, 1974) on reinforced concrete elements. As expected, this modal damage index requires identification of natural frequencies of the structure under study. Analytical processing of responses of the structure to external vibrations usually provide these natural frequencies. Evaluated for different damage states sustained by the structure, these natural frequencies are compared and their changes serve as damage indicator. Natural frequencies usually decrease with increasing structural degradation. In fact, Dowell (1979) reported that local stiffness degradation, characterizing structural damage, leads to a general shift of the natural frequencies towards lower values. The magnitude as well as the rate of frequency decrease can be used as damage indicator.

This index has been used and verified through different experimental damage assessments or structural comparisons. Haroun, Mourad and Flynn (1993) studied damage in reinforced concrete pier walls and observed a reduction in the natural frequencies, indicating stiffness degradation. Slastan and Pietrzko (1993) also related damage of concrete T-shaped beams with frequency shifts at every damage stage. Chen and Swamidass (1993) monitored frequency changes due to crack growth in a tripod tower platform made of acrylic plastic. Richardson and Mannan (1993) correlated frequency shifts with the presence of holes in a rectangular aluminium plate and in a steel plate structure.

The **ultimate stiffness degradation** (DiPasquale and Cakmak, 1987) uses the fundamental period of the undamaged structure as a reference indicator. Comparing subsequent fundamental periods to this reference period leads to the formulation of the damage index. Assuming that the fundamental period increases with damage, the index gives a positive value, increasing with the severity of damage. It is expressed as:

$$D_G = \frac{T_j - T_0}{T_0} \dots \dots \dots [2.13]$$

where T_0 is the fundamental period of the undamaged structure and T_j represents the fundamental period at cycle j . Tests performed on both full scale structure and experimental models indicated increase of the damage index with degradation of the structure. (Carydis and Mouzakis, 1986, Meyer and Roufaiel, 1984, Mihai et al, 1980, Ogawa et Abe, 1980).

Softening indices (DiPasquale and Cakmak, 1987, 1989, DiPasquale et al 1990) were developed from combinations of three characteristic fundamental periods (or frequencies) obtained at different states of the damage process. These periods can be evaluated on the basis of a single time response. From this time signal, analytical methods evaluate the fundamental period history by dividing the time history into a series of consecutive windows and matching an equivalent linear system to each window (DiPasquale and Cakmak, 1987, 1988). Figure 2.1 shows a period time history and three characteristic periods used in calculations of the softening index. Referring to this figure, T_0 , T_{max} and T_{dam} respectively correspond to the fundamental period of the undamaged structure, its maximum value during the response time history and the fundamental period of the damaged structure, respectively.

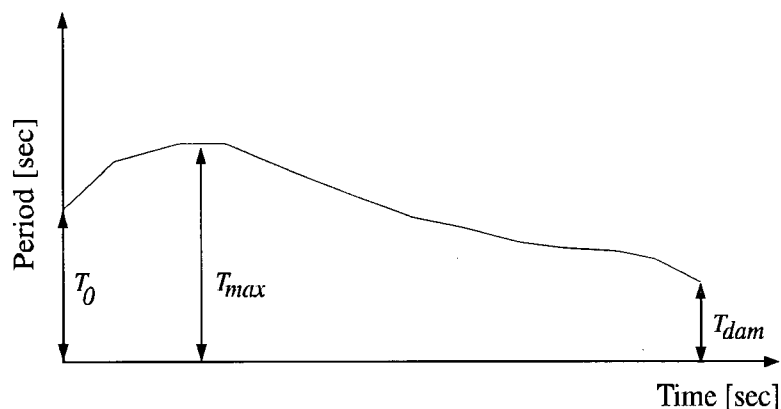


Figure 2.1 Fundamental period time history

DiPasquale and Cakmak (1989) developed the **final softening**, $D_{G,f}$, by comparing the fundamental period before and after damage has occurred. This index measures the average reduction in stiffness across the structure (DiPasquale et al, 1990). It is expressed as:

$$D_{G,f} = 1 - \frac{T_0^2}{T_{dam}^2} \dots\dots\dots [2.14]$$

Effects of nonlinearities, caused by plastic deformations and soil-structure interaction, led to the formulation of another index, the **plastic softening**, $D_{G,pl}$, (DiPasquale and Cakmak, 1989). This indicator isolates the nonlinear effects from the softening due to the stiffness degradation. (DiPasquale et al, 1990).

$$D_{G,pl} = 1 - \frac{T_{dam}^2}{T_{max}^2} \dots\dots\dots [2.15]$$

DiPasquale and Cakmak (1989) also developed an index that combines both stiffness degradation and plasticity effects. It is called the **maximum softening** and is denoted $D_{G,m}$:

$$D_{G,m} = 1 - \frac{T_0}{T_{ma}} \dots\dots\dots [2.16]$$

Of the softening indices, $D_{G,m}$ is considered the best damage indicator of the global damage state of the structure. This index provides a reliable estimate of presence of yielding within the structure. However, in order to determine the maximum period value, it requires knowledge of the structure time response. However, since only the final period value is required in Equation 2.14, $D_{G,f}$ evaluation can be performed on direct post-damage measurements.

Damage indices have also been developed to consider both deformation and fatigue damage contributing to the structure deterioration. A deformation term, δ_M , takes into account the peak displacement sustained by the structure while an energy-related term, δ_E , considers the deformation associated to the fatigue mechanism. The ultimate stiffness degradation (Equation 2.17) is used to consider the peak deformation. A cumulative softening takes into account the energy absorption (Equation 2.18). A linear combination of

these two contributions is defined as the **global softening index** (Equation 2.19) (DiPasquale & Cakmak, 1987). Considering M cycles:

$$\delta_{M,M} = \max_{j=1,M} \left[\frac{T_j - T_0}{T_0} \right] \dots \dots \dots [2.17]$$

$$\delta_{E,M} = \sum_{j=1}^M \left[\frac{T_j - T_0}{T_0} \right] \cdot \frac{s_j}{T_j} \dots \dots \dots [2.18]$$

$$D_{G,M} = \delta_{M,M} + \beta \delta_{E,M} \dots \dots \dots [2.19]$$

As previously, T_0 is the fundamental period of the undamaged structure and T_j represents the fundamental period at cycle j . Parameter s_j refers to the energy demand at cycle j while constant β is estimated from experimental measurements. Analysis of earthquake records of buildings provided verification of this method (DiPasquale & Cakmak, 1987). Evaluated separately, deformation and energy contributions (Equations 2.17 and 2.18) were consistently increasing with the level of damage. Hence, as expected, the global index, based on a the calibration parameter β , will definitely increase as well. Nevertheless, parameter β involves calibration for different structures.

Roufaiel and Meyer (1987b) also proposed a global index, combining deflections (at roof level) and the fundamental frequency of the structure before and after being damaged. Based on experimental data, relation between the maximum roof displacement and the frequency ratio was found as:

$$\delta_m = \delta_y + 14.2\delta_y (\sqrt{f_{und}/f_{dam}} - 1)$$

The global index, comparing permanent deformation at a particular cycle and at failure state, is then expressed as:

$$D_G = \frac{14.2\delta_y (\sqrt{f_{und}/f_{dam}} - 1)}{\delta_f - \delta_y} \dots \dots \dots [2.20]$$

The global damage index provided reasonably good indication of damage in low to medium rise structures. For tall buildings, the assessment method should include the effects of higher modes of vibration.

Samman and Biswas (1994b) experimented with different methods to investigate structure signatures. A signature generally consists in an average of frequency response functions (FRF) for a particular damage level. Signatures can be evaluated for different damage levels. Their methods is based on comparison of these signatures to assess structural degradation. They developed different recognition techniques to compare two signatures, a reference signature obtained from the undamaged structure and a second signature obtained from the same structure after an unknown level of degradation has occurred. Five of these methods are described in the following paragraphs.

The **waveform chain code (WCC)** compares two signature slopes and curvatures, previously evaluated from the digitized signals. A large differential value at a particular frequency is associated with a significant difference between the two signatures in the neighborhood of that frequency. This differential value is used as damage indicator. A mathematical procedure for calculation and comparison of slopes and curves can be found in Samman and Biswas (1994a). The WCC was applied on a scale bridge sustaining increasing crack lengths. Increase in slope and curvature differentials adequately captured increasing changes in the signatures due to damage (Samman and Biswas, 1994b).

The **adaptive template matching** performs point-by-point magnitude check in order to detect differences between two signatures. This method is called adaptive because of its magnitude dependence. A tolerance zone, in which an unknown signal is considered to be similar to a reference signal, is associated to a tolerance value β . As the difference between the signals increases, the minimum tolerance increases as well. Hence, the minimum tolerance to consider two signatures similar serves as damage indicator. Details on the theoretical procedure can be found in Samman and Biswas (1994a). From their

experimental studies on a scale bridge, the minimum average tolerance demonstrated monotonic increase with the increasing crack length (Samman and Biswas, 1994b).

Samman and Biswas also experimented with methods that compare explicitly FRF signatures, such as the **signature assurance criterion (SAC)** and the **cross signature assurance criterion (CSAC)**. The SAC value ranges between zero and one, with a unit value indicating two identical signals. For two signatures u and w , the SAC value is expressed as:

$$D_G = SAC(u, w) = \frac{(|u^T \cdot w|^2)}{(u^T \cdot u \cdot w^T \cdot w)} \dots \dots \dots [2.21]$$

Comparisons between an intact and a cracked scale bridge model showed diminution of the SAC index. However, those index changes were relatively small in amplitude (Samman and Biswas, 1994b).

The CSAC measures similarity of two sets of FRF signatures at a particular frequency. For two sets of signatures U and W , the k^{th} signature for the two sets, evaluated at frequency i , are u_{ki} and w_{ki} . Considering N^{sig} signatures in each set, the CSAC is then expressed as:

$$D_G = CSAC(i) = \frac{\sum_{k=1}^{N_{sig}} (|u_{ki} \cdot w_{ki}|)^2}{\sum_{k=1}^{N_{sig}} u_{ki}^2 \cdot \sum_{k=1}^{N_{sig}} w_{ki}^2} \dots \dots \dots [2.22]$$

The CSAC can range between zero and one, with a unit value for identical magnitudes at frequency i . Like the SAC, CSAC values should decrease with increasing damage. However, using signatures from bridge models, the CSAC was not successful in detecting simulated cracks (Samman and Biswas, 1994a).

The **Equivalent Level of Degradation System (ELOS)** represents a structural system, or transformer, which modifies an input signal to an output signal. The input corresponds to a response of an undamaged

structure while the output is associated to a response of the damaged structure. If there is no change between the input and the output, the transformer is considered passive since the level of degradation is zero. However, if the input and output are different, the transformer serves as damage indicator. The concept of transformer led to the development of two measures, the distortion identification function (DIF) and the normalized frequency ratio (NFR). These two real functions range between zero and one, where a unit value is associated with a zero level of degradation. The area under the these curves as well as their minimum and maximum values are used as features of recognition. Detailed mathematical procedure can be found in Samman and Biswas (1994a). Experimental studies showed that the area related to the DIF curve was the only feature of recognition showing a monotonic increase with crack length (Samman and Biswas, 1994b).

Damping dissipates vibrational energy, usually as friction heat (Richardson and Mannan, 1993). Structure deterioration creates an increase in damping, especially in nonlinear materials like concrete, where damping enhancement is related to cracking of the concrete and yielding of the steel reinforcement. **Normalized damping ratio changes** then serve as damage indicator, where increasing damage is associated to an increase in damping. Similarly to maximum stiffness degradation index, normalized damping changes can be evaluated as:

$$D_G = \frac{\xi_j - \xi_0}{\xi_0} \dots\dots\dots [2.23]$$

where ξ_0 is the initial damping ratio and ξ_j is the damping ratio at cycle j .

Some experimental studies confirmed the increasing trend of damping with structural deterioration. Haroun, Mourad and Flynn (1993) studied damage in reinforced concrete pier walls and observed damping enhancement with increasing deterioration. In their experiment of concrete T-shaped beams, Slastan and Pietrzko (1993) showed that damping increase indicated crack initiation. However, other experiments

concluded that the change of damping ratio with increasing damage was not very conclusive, showing large scatter (Chen and Swamidas, 1993, Cherng and Abdelhamid, 1994, Salawu and Williams, 1995). DiPasquale and Cakmak (1987) maintained that damping factors are entities of uncertain physical meaning and that their estimation, when the structure is in the non-linear phase, yields results of questionable reliability.

2.2.2 LOCAL INDICES

Local indices, D_L , usually assess both the extent of damage as well as its location. Consequently, their basic formulation is more complex than global indices, which essentially provide an estimation of the deterioration of the structure without locating the damage. For unevenly distributed degradation, where global assessment is inadequate, local indices become a valuable mean of damage evaluation.

As mode shapes represent amplitude or power of the motion, their changes reveal gain or loss of energy in each mode. Approaches using **direct mode shape assessment** as damage detection and location have been developed in the need of assessing localized or uneven damage distribution. Inspection and comparison of mode shapes before and after damage is used as damage indicator. Since localized or minor level damage usually affect higher modes, effective damage assessment should compare these higher modes. However, the process of exciting and identifying higher modes can be difficult (Raghavendrachar and Aktan, 1992). Salawu and Williams (1994) showed that the presence of damage at more than one location yielded to unreliable results when methods based on mode shapes were used.

Model Updating is a set of techniques using experimental data to adjust finite element models on the basis of the experimental dynamic behavior of the structure. Structural differences between the updated model and its undamaged version are attributed to damage. Typically, the largest reduction in structural parameters, estimated simultaneously at several potential damage sites, is associated with the most likely

damage location. Different updating algorithms have been developed on the basis of the experimentally obtained modal parameters. Some of them are presented below.

Raghavendrchar and Aktan (1992) used variations in the **flexibility matrix** as damage indicator. In contrast to inspection of individual mode shapes, the flexibility matrix sums the contributions of changes from several mode shapes. Hence, changes that are individually non significant add up, yielding to a more significant global contribution. Considering n identified mode shapes, the flexibility matrix can be expressed in terms of modal parameters as:

$$H = \Psi \begin{bmatrix} 1 \\ \vdots \\ 1/f^2 \end{bmatrix} \Psi^T \dots\dots\dots [2.24]$$

where ψ is a matrix of mass-normal mode shapes and $[1/f^2]$ is a diagonal matrix containing the reciprocals of the fundamental frequencies. A typical diagonal element of the flexibility matrix is given by:

$$H_{ii} = \sum_{j=1}^n \left[\frac{\Psi_{ij}}{f_j} \right]^2 \dots\dots\dots [2.25]$$

Experimental modal analyses were performed on a three-span bridge. Raghavendrchar and Aktan found that variations in the corresponding flexibility coefficients provided reliable damage indicators.

Lammens et al (1994) studied a **updating algorithm based on the frequency response function**. This method uses updating parameters, such as Young's modulus and Poisson's ratio, as damage indicators. These parameters are updated through a minimization procedure of dynamic residual forces. The minimization problem is solved with a least squares approach. They discussed the importance of the minimum number of updating frequencies and they also experimented different damping approaches. This updating procedure was applied on a polyvinyl chloride (PVC) plate to update given initial values of its Young's modulus and Poisson's ratio. Their study showed that updating frequencies away from the resonance peaks gave more stable updating parameters. Also, an undamped approach provided better

convergence of the updating parameters.

Hemez and Farhat (1992) developed an updating algorithm known as the **sensitivity based element by element (SB-EBE)** method. The algorithm is also based on a minimization of the modal dynamic residuals but the procedure also includes minimization of the static residuals. The minimization algorithm modifies physical parameters such as Young's modulus, density and thickness. Significant changes in these parameters serve as damage indicators. It was demonstrated that the algorithm worked very well for a cantilevered truss structure but had difficulty locating damage in a suspended truss, where higher modes had more effects (Doebling et al, 1992).

Kaouk and Zimmerman (1993) used a decoupled approach where the location and extent of damage are determined by two separate algorithms. First, the **modal force error criteria** (Ojalvo and Pilon, 1988) determined the location of damage. With the location determined, a minimum rank perturbation algorithm evaluates the extent of damage. This damage location/extent technique was applied to an experimental eight bay truss. The damage was clearly located in eleven out of fifteen damage cases and for all cases the extent algorithm performed well.

Casas and Aparicio (1994) experimented the minimization of a performance error, the **dynamic parameter identification**, by comparing experimental and finite element mode shapes and frequencies. The results of the algorithm provide equivalent moments of inertia for all elements of the finite element mesh. Variations in the moment of inertia, evaluated for all members, are used to assess the damage extent and location. Damage evaluated on experimental reinforced concrete beams was adequately located and quantified. However, success of the method depended on the number of frequencies used in the calculations. Their experimental studies indicated a minimum of two frequencies to adequately locate the cracked zone and obtain equivalent moments of inertia.

Cawley and Adams (1979) developed a minimization method, the **normalized percentage error (NPE)**, to identify the damage site and its mechanism. Computation of analytical fundamental frequency changes of several modes is performed for each possible damage mechanism and each location. Then, error between experimentally measured frequencies and theoretical frequency patterns are summed up to get the total error. The pattern giving the minimum total error is used as damage indicator on the extent and location. Penny et al (1993) combined the NPE with statistical methods in order to assess the quality of the predicted location of damage. Two coefficients, the **coefficient of determination (COD)** and the **normalized squared deviation (NSD)**, were used to verify the quality of the NPE values. Analyses of NPE together with its corresponding COD and NSD would provide higher confidence in the predicted damage location. Experimental studies performed on a steel frame showed that the combination of COD, NSD and NPE led to the correct location of damage site, even in the case where the NPE criterion had failed to identify the right damage location.

Hearn and Testa (1991) compared observed ratios of frequency changes and **characteristic ratios** to statistically locate damage. A characteristic ratio compares two natural frequencies and is expressed as:

$$CR = \frac{\Delta\omega_i^2}{\Delta\omega_j^2} \dots\dots\dots [2.26]$$

Observed ratios are directly computed from experimental frequencies. Characteristic ratios are evaluated analytically from potential patterns of damage. These ratios, evaluated for an individual member or for an ensemble of members, are computed entirely from initial quantities, such as initial member stiffness, initial mass and initial mode shapes. Damage location is determined by selecting the characteristic ratio pattern that most closely match the experimental ratios. Potential analytical characteristic ratio patterns must minimize a mean square deviation between the experimental and characteristic ratios. Laboratory experiments on a steel frame explored the effect of damage on this damage detection method. The use of observed frequency changes, in conjunction with characteristic ratio patterns, successfully identified two

types of damage sustained by the frame. However, for larger structures, it may be found that several characteristic ratio patterns all closely match a set of observed ratios, limiting the general applicability of the method.

Cherng and Abdelhamid (1994) have developed a **subspace correlation index (SSC)**. This method calculates a correlation matrix of two signal subspaces. Changes in mode shapes are related to values of the SSC matrix, serving as damage indicator. The algorithm associates the mode undergoing the largest change to the damage index. Numerical simulations performed on a three DOF system showed the ability of SSC index to identify the most changed mode.

For local damage assessment, assurance criterions were developed for comparison of mode shapes (Allemang and Brown, 1982, Wolff and Richardson, 1989). The **modal assurance criterion (MAC)** measures similarities between two sets of mode shapes, X and Y . For two corresponding k^{th} mode shapes x_k and y_k , extracted from sets X and Y , representing the same mode at different degradation states, the MAC value is expressed as:

$$D_L = MAC(x_k, y_k) = \frac{(|x_k^T \cdot y_k|^2)}{(x_k^T \cdot x_k \cdot y_k^T \cdot y_k)} \dots \dots \dots [2.27]$$

The **COMAC, coordinate modal assurance criterion** (Lieven & Ewins, 1988) evaluates the difference between two sets of mode shapes at a particular point on the structure. With x_{ki} and y_{ki} defining the values of two corresponding k^{th} mode shapes evaluated at location i , the COMAC value is expressed as:

$$D_L = COMAC(i) = \frac{\sum_{k=1}^{N_{modes}} (|x_{ki} \cdot y_{ki}|)^2}{\sum_{k=1}^{N_{modes}} x_{ki}^2 \sum_{k=1}^{N_{modes}} y_{ki}^2} \dots \dots \dots [2.28]$$

Some research has also been done on the use of strain gauges in modal testing (Bernasconi and Ewins 1989, Li et al. 1989, Tsang 1990). Strains and stresses are in fact the main parameters of interest in structural behavior. Experimental analysis was performed with the **strain frequency response function** (Chen & Swamidas, 1993), a transfer function between the output (strain level at the location under consideration) and the input (exciting forces). They found that the local strain changes are more sensitive to localized damage than global frequency or damping changes. However, this method assumes that potential critical sections are known before vibration testing is performed. Strain gauges were used in a modal test to detect a crack in a tripod tower platform model. Based on experimental results, strain FRF's showed very large changes with increasing crack size while acceleration FRF's indicated relatively small changes.

2.2.3 SUMMARY OF DAMAGE INDICES BASED ON DYNAMIC PROPERTIES

Following tables summarize damage indices based on analysis of modal properties. Table 2.2 presents global damage indices while Table 2.3 recall local damage indicators. Measurements required for evaluation of each index are also indicated.

Index or Author(s)	Equation Number	Measurements Required
frequency (or period) changes	n/a	frequency (or period) at the end of each cycle i
ultimate stiffness degradation	2.13	period history
final softening	2.14	period history
plastic softening	2.15	period history
maximum softening	2.16	period history
global softening index	2.19	period history energy demand for each cycle i
Roufaiel & Meyer	2.20	period history displacement history
WCC	see Samman and Biswas (1994a)	undamaged and damaged signatures
adaptive matching template	see Samman and Biswas (1994a)	undamaged and damaged signatures
SAC	2.21	undamaged and damaged signatures
CSAC	2.22	undamaged and damaged signatures
ELOS	see Samman and Biswas (1994a)	undamaged and damaged signatures
damping changes	2.23	damping at the end of each cycle i

Table 2.2 Global damage indices based on dynamic properties

Index or Author(s)	Formula	Measurements Required
mode shape assessment	n/a	mode shape history
flexibility matrix	2.24	frequency history mode shape history
FRF based algorithm	see Lammens et al (1994)	frequency history damping history FRF history
SB-EBE	see Doebling et al (1992)	frequency history dynamic mode shape history static mode shape history
Kaouk & Zimmerman	see Kaouk and Zimmerman (1993)	frequency history mode shape history
dynamic parameter identification	see Casas and Aparicio (1994)	frequency history mode shape history
NPE	see Penny et al (1993)	frequency history
characteristic ratios	2.26	frequency history
SSC	see Cherng and Abdelhamid (1994)	frequency history damping history
MAC	2.27	mode shape history
COMAC	2.28	mode shape history
strain FRF	see Chen and Swamidas (1992)	strain time signals

Table 2.3 Local damage indices based on dynamic properties

2.3 INTRODUCTION TO DAMAGE ASSESSMENT BASED ON NEURAL NETWORKS

Neural networks present a completely different approach for damage assessment to those discussed in the two previous sections. Neural networks are used to process information without a specific algorithm for different types of problems. That is, the same neural network can be used to solve different types of

problems. Unlike expert systems, neural networks do not require the knowledge of all the relationships between the components of the problem (Garrett, 1992). Hence, this concept is appealing to model systems where no currently acceptable theory exists for describing the components relationship or to assess complex phenomena or complex system behaviors, such as structural and material behaviors (Garrett, 1992). For example, the concept can be applied to simulate the altering process of an undamaged structure into its reciprocal, the damaged structure. More specifically, neural networks are used to capture mapping describing the relationships between two sets of data: a set of observable data (input layer) and a reciprocal set generated from a particular transformation of the original set (output layer). The neural network itself represents the altering process between the two sets. Neural networks are developed by *collecting* mapping examples relevant to the problem investigated, *designing* the neural network and finally *training* the network with the collected examples until the network behavior is validated. The neural network behavior is acceptable when the *expected* reciprocal set is generated from a given observable data set.

2.3.1 TYPICAL INTERNAL STRUCTURE

The internal arrangement of a neural network is modelled after the structure and operation of the brain. It consists of a highly interconnected network of numerous simple processing units, called neurodes. The neurodes are joined through many weighting connections. Each neurode typically receives many signals from neighbor neurodes or from external solicitations through its incoming connections. Although a neurode receives several incoming signals, it produces only one outgoing signal. Using the incoming signals, each unit is capable of simple computations to generate its outgoing signal. The outgoing signal depends on the number and amplitude of incoming neurodes as well as on the weights associated with each connection. By modifying the weighting connections, the neural network can learn a particular transformation pattern.

2.3.2 TYPES OF NEURAL NETWORK

Many types of neural networks have been developed by modifying the network topology, the neurode characteristics and the learning schemes. The network topology refers to the number of neurodes in the network as well as the weight pattern linking the neurodes between themselves. The mathematical relationship used to compute the neurode outcoming signal also lead to different types of neural network. Finally, different computational schemes have been elaborated to update the weighting connections in the training process. A few examples of neural networks are the Kohonen network, the back-propagation network, the counter-propagation network and the adaptive resonance network. An extensive summary of neural networks can be found in Caudill and Butler (1992). In civil engineering, **back-propagation neural networks** are commonly used by researchers to solve different types of problem (Elkordy et al, 1993). The following section details this type of neural network as well as the steps involved in its design. Application examples of the use of neural networks for damage assessment are also presented.

2.3.3 BACK-PROPAGATION NEURAL NETWORKS

2.3.3.1 DESCRIPTION OF THE NETWORK AND ITS OPERATION

A typical back-propagation network is shown in Figure 2.2. The neurodes are arranged in layers: an input layer, an output layer and a number of hidden layers. This type of network is fully interconnected, where each neurode in a lower level is connected to every neurode in the next higher level.

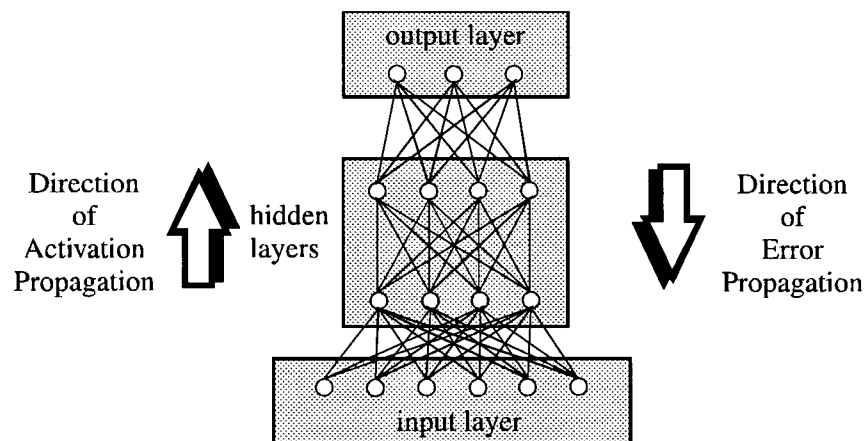


Figure 2.2 Back-propagation neural network

The function of the network is to compute a pattern of output from a pattern of input by propagating calculated outgoing signals through the weighting connections linking the neurodes. Activation of the network is initiated when the network is presented with a pattern of input, i.e. a set of observable data that reflects the excitation of the system by external sources. It is referred to as the *input layer* in Figure 2.2. The neurodes in the higher level receive this pattern of input and produce in return an outgoing signal which is transmitted to the next processing units. This outgoing signal is computed using the incoming signals and the weighting connections. First, the net input of neurode j , N_j , is calculated as:

$$N_j = \sum_{k=1}^M w_{jk} \cdot o_k \dots\dots\dots [2.29]$$

where M is the number of units incoming on neurode j and o_k refers to output signal travelling towards a particular neurode k . The weighting connection between neurodes j and k is symbolized by w_{jk} . Secondly, a level of activation, a_j , is evaluated for each neurode. It is usually evaluated with the sigmoid function:

$$a_j = f(N_j) = \frac{1}{1 + e^{-N_j}} \dots\dots\dots [2.30]$$

Finally, the outgoing signal of neurode j , o_j , is, in this type of network, the same as the activation value, where $o_j = a_j$.

This propagation process is repeated until the pattern of output, or the set of responses produced by the excited system, is obtained. In Figure 2.2, the *output layer* refers to this highest level of neurodes. The neurodes composing the *hidden layers* carry, in their weight connections, additional information to simulate the mapping between the input and output layers. They allow the network to generate its own rich and complex model of the system.

A correct behavior of the network is obtained when the expected output is actually produced at the output layer of the network initially presented with the given input at the input layer. As mentioned previously, a

neural network is not based on theoretical relationships existing between neurodes. Instead, it is trained to perform this correct computation. The training takes place in an iterative fashion. For each output, it first involves computing an output error, E , by comparing the calculated output to the expected output. This error usually refers to a degree of dissimilarity between the output computed through the neural network and the expected output. The training procedure then back-propagates this output error in lower layers by modifying the weighting connections linking the processing units. In the process of back-propagating the output errors, these errors E 's must also be evaluated for the hidden layers, where a more complex procedure is followed. The modification of the strengths of the connections is based on the generalized delta rule, which defines the change in a given weighting connection as:

$$\Delta w_{jk} = \beta E f(N_j) \dots \dots \dots [2.31]$$

where β is a learning constant, or a measure of the rate at which the learning process should take place. This parameter ranges between zero and one.

Once the updated weights are computed, the output layer can be re-evaluated and compared to the expected output. If the output error is still above a certain threshold value, then the error is back-propagated again, and so forward until the network behavior is validated. The nature and the extent of the training sample, composed of pairs of input and output layers, will significantly influence the efficiency of the training process. More details on the mathematical background used in the back-propagation network can be found in Caudill and Butler (1992).

2.3.3.2 NETWORK DEVELOPMENT

The development of a typical back-propagation neural network involves five principal steps. They can be summarized as follows:

1. selection of neural representation for input and output layers;
2. selection of network internal structure, i.e. characteristics of hidden layers;
3. selection of training pattern characteristics;

4. actual training of the neural network;
5. validation of the designed neural network.

These steps are described in the following sections, including some indications for the particular case of damage assessment.

2.3.3.2.1 Input and Output Layers

The selection of the network input and output representation is dependent on the type of problem to be solved. The input set refers to observable data, or parameters that can be rather directly estimated. On the other hand, the output set represents data usually difficult to evaluate directly from information already available. The main function of a neural network is actually to provide useful means to derive these output data sets. In the case of damage assessment, presence or absence of damage in a specific location, vibration responses and dynamic properties are examples of parameters that can be observed or measured directly on the structure under study while the output layer usually refers to parameters closely associated to stiffness reduction, providing relevant information on the structural degradation of a system.

2.3.3.2.2 Hidden Layers

The number of hidden layers as well as the number of processing units in each hidden layer can vary from one network to another. Hidden layers of a same network can contain a different number of neurodes. Despite restrictions imposed by the software used, there is usually no limit in the number of hidden layers that can be used.

While the input and output layers are very much dependent of the type of problem to be solved, the choice of hidden layers is not as straightforward. There are no specific rules in the design of hidden layers. It is rather an iterative process, that experience with neural network development can partly overcome. However, some basic rules can facilitate this task. For example, Caudill and Butler (1992) suggest that, for a fastest training, a reasonable range for the number of neurodes in the hidden layers is 50% to 150% of the

number of training patterns to learn. However, fastest training is not always the best training in terms of the network's capability to recognize unknown patterns. The number of hidden-layer neurodes should preferably be less than the number of learning patterns. This consideration will avoid the network to memorize the training patterns by allowing each neurode to exactly recognize one input pattern instead of generating its internal network. Observing these basic rules, it should also be noted that a complex problem will be easily solved with an extensive hidden layer network. This will allow the network to develop a richer and more complex internal network and, consequently, will provide a better mapping of the real problem.

2.3.3.2.3 Training Patterns

Training patterns are in the form of couples of input/output sets. Presented to the network, these training patterns enable the network to create its own complex internal connections based on the update of the weighting links. Since the network only learns from the data sets to which it is exposed, the patterns used in the training process are determinant in the way the network will react to unknown input patterns. The patterns can vary in number as well in the nature of cases considered. The more complex the problem to solve, the more patterns will be necessary to obtain a correct behavior of the neural network. Similarly, the more different cases covered by the training process, the better behavior the network will give to unknown patterns.

In the case of damage assessment, two category of patterns can be used to perform the training process. First, they can be accumulated over time from measurements referring to the actual damage states as sustained by the structure. Considering that the number of patterns needed to complete an efficient training process is often significant, this first approach is often difficult to implement. Using analytically generated states of damage then represents an attractive option. This approach refers to the use of Finite Element Models to create training samples of the specimen under study.

2.3.3.2.4 Training Process

Once the network architecture and the training cases have been selected, the actual training of the network through a learning algorithm represents the next step of the network development. When a new network is to be trained, the following steps, for a single cycle, are implemented as follows, for each training pattern:

1. a training couple of input/output is presented to the network;
2. the output pattern produced by the network is compared to the expected output, producing an error;
3. the error is back-propagated to the hidden layers;
4. the weighting connections are modified according to the error back-propagation rule implemented in the network.

This process is repeated several times for the complete set of training patterns until a specified error tolerance is obtained. The success and efficiency of the training process depends on the network characteristics, i.e. on the input, output and hidden layers representation. Unfortunately, as mentioned previously, the state of technology is not well enough defined to provide specific rules to implement an efficient learning procedure, regarding the network internal structure (Caudill and Butler, 1992). The learning process also depends on the learning constant β . No theoretical rule guides the choice of β value. However, for a more difficult the problem, a slower learning must take place. This means that the learning constant should be small. For example, on extremely complex problems, it is suggested that β values should range between 0.05 and 0.005 (Caudill and Butler, 1992).

2.3.3.2.5 Validation of Network

The last step in the development of a neural network is to verify how well the network behaves when presented with patterns for which it was not trained. In other words, the ability of the network to generalize for unknown cases is verified by assessing how well the network recognize all the features and sub-features implied in the training patterns (Garrett, 1992). As for the training patterns, unknown patterns can be obtained either from experimental measurements or from analytical data sets.

2.3.3.3 EXAMPLES OF APPLICATION TO DAMAGE ASSESSMENT

Neural networks are currently used by structural engineers and researchers to assess structural damage. This section presents some examples of back-propagation networks used in the detection of structural degradation.

Wu et al (1992) used neural network to recognize individual member damage from the measured response of structures. They applied their method to a three-story frame, instrumented with accelerometers. Structural degradation was simulated by stiffness reduction. The input layer to the neural network was taken as the Fourier spectra of the relative accelerations recorded at a particular floor. It was represented by numerous neurodes, each of them representing a portion of the frequency spectrum. The output layer consisted of neurodes representing the damage condition (presence or absence of damage) for different members of the structure. After training, the network was presented with unknown states of damage. The original network did not show very good results. It was then modified by adding an extra hidden layer and providing two sets of Fourier spectra instead of one in the input layer. After training, the resulting network was capable of correctly identifying most types of damage but was unable to diagnose adequately all of them.

Elkordy et al (1993) used neural networks to identify changes in the vibrational signatures of an experimental five-story steel frame. To overcome the difficulty of developing over time an extensive training sample set, they investigated the use of analytically generated training samples to train neural networks. The training samples were obtained from finite element models of the five-story steel frame. Damage states of the structure were simulated by gradual reduction of bracing areas in the finite element model. The input layers were the percent change in mode shapes, normalized with respect to the top of the structure. The output layers were related to the presence of damage at particular location (where 1=damage exists and 0=no damage) and the corresponding extent of degradation. The networks were verified with an experimental steel frame. Mode shapes were measured by analyzing signals recorded by

accelerometers mounted on the specimen. The neural networks trained with analytical data provided very good results when presented to these experimental input data. Hence, the neural networks were able to diagnose the damage sustained by the structure.

Other applications of neural network for damage assessment can be found in Elkordy et al (1992), Szewczyk and Hajela, (1994) and Chen and Shah (1992).

2.4 CONCLUDING REMARKS

This chapter discussed damage assessment based on structural properties and damage assessment based on modal properties. Basic concepts of damage assessment based on neural networks were also introduced. Except for damage assessment based on neural networks, these approaches will be applied to specimens tested in the wake of this study. Exploratory work on the neural network approach was also considered in this study. Since no extensive study of this method was investigated, no results of this approach are presented in this thesis.

The following chapter describes the experimental procedure performed, including details on the specimens tested as well as description of the loading and dynamic testing procedures. A preliminary description of damage observed on the specimens is also presented.

CHAPTER 3

EXPERIMENTAL PROCEDURE

The Ministry of Transportation and Highways of British Columbia (MOTH) sponsored an extensive seismic testing program on large scale models of the piers of Vancouver's Oak Street Bridge. This was done in conjunction with the seismic retrofit of the bridge. The major part of the MOTH sponsored work consisted of slow cyclic testing of the models under lateral load. These test were performed in the Structures Laboratory of the University of British Columbia (U.B.C.) from September 1993 to September 1994. The MOTH test program (Anderson et al, 1995) provided a unique opportunity to investigate damage assessment techniques in conjunction with the slow cyclic lateral load tests.

Figure Q117-01 (drawing from Klohn-Crippen Consultants) of Appendix A shows bent S28, considered representative of many similar bents in other bridges that may require retrofit. Five reinforced concrete frames, the original design of S28, and four retrofitted versions of that same bent, were tested in the laboratory. One of the retrofitted versions of the bent is shown in Figure 3.1. Specimens underwent lateral slow cyclic loading monotonically increasing up to failure or very high damage state. Vibration tests were performed between degradation cycles to assess modal properties of the specimens.

This chapter includes details on the testing procedures performed on the five specimens. Test objectives are presented in the first section. Section 3.2 describes the experimental specimens. Lateral and vertical loading procedures as well as details on the vibration testing procedure can be found in Sections 3.3 and 3.4 respectively. Finally, Section 3.5 gives a preliminary description of damage observed on the five specimens.

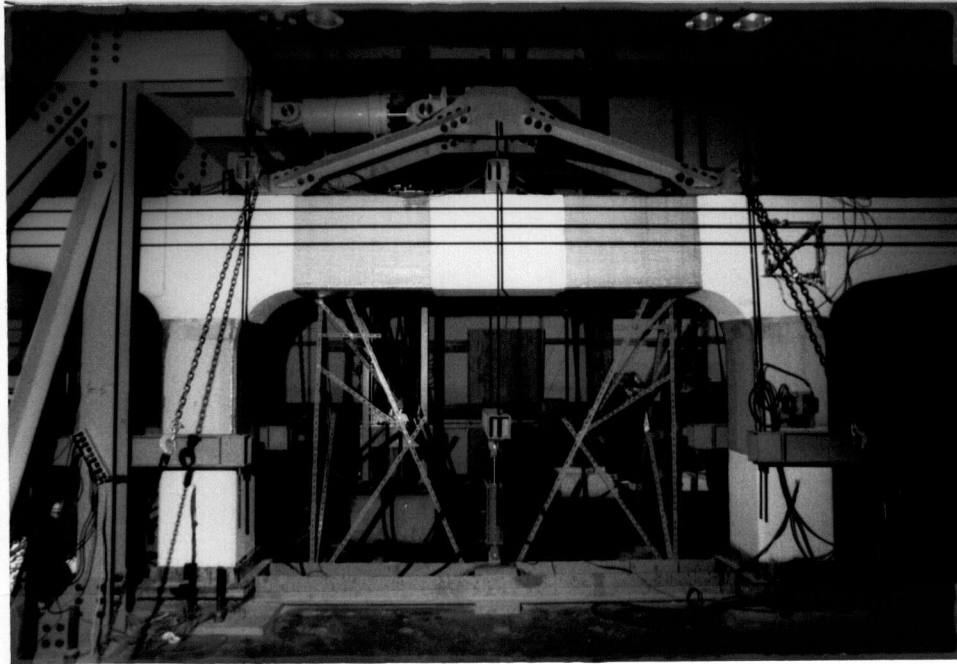


Figure 3.1 Specimen OSB5 ready for testing

3.1 TEST OBJECTIVES

Three principal objectives guided this experimental program. They are defined below:

1. To measure, in terms of loads and displacements, structural responses of the specimens subjected to slow lateral cyclic loading.
2. To develop a hammer test procedure for forced vibration testing of small size civil engineering structures;
3. To measure vibrations of both input and output signals at each displacement level, using both ambient and impact vibration testing.

3.2 DESCRIPTION OF SPECIMENS

Dimensions of the U.B.C. Structures Laboratory and required loading levels both limited the overall size of the specimens. These restrictions, as well as convenience in scaling bar sizes, led to a 0.45 linear scale specimen representing one of the bents of the Oak Street Bridge in Vancouver. Five specimens were tested

as part of this experimental program. The first specimen was modelled to match the original design of the Oak Street Bridge bent S28. The other four specimens modelled retrofitted versions of that same bent. The overall dimensions of the five bents were 7.06 m in width by 2.75 m in height. The as-built model was denoted OSB1 while the other four were labeled OSB2 through OSB5 with numbering referring to the order of testing. Figure 3.2 shows the scale model of bent S28. Construction of all five specimens was done by a precast concrete manufacturer in the Vancouver area, APS located in Langley.

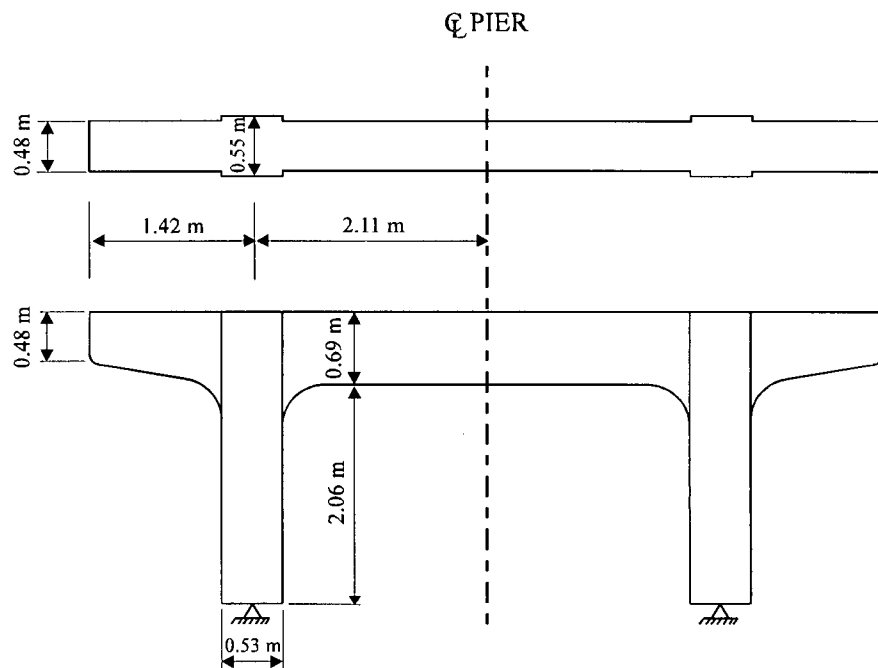


Figure 3.2 Experimental model of bent S28

3.2.1 SPECIMEN OSB1

The first specimen tested represented the as-built design of the actual Oak Street Bridge bent. The frame was made of reinforced concrete. Material strengths were adequately reproduced to match those of the original bent. Sizes of longitudinal reinforcement, stirrups and ties were scaled down to 0.45. More details concerning these material properties can be found in Anderson et al (1995). As shown in Figure 3.1, only the top half of the columns were modelled, from the column inflection point to the top of the bent. The

bending moment being zero at the inflection point, it was structurally convenient to design a hinge bearing support at the bottom end of the specimen columns. Modelling half of the columns also reduced considerably the overall height of the specimen. Drawing of specimen OSB1 can be found in Figure Q117-11 of Appendix A. These structural characteristics are also applicable to specimens OSB2, OSB3, OSB4 and OSB5.

3.2.2 SPECIMEN OSB2

The retrofit of OSB2 modified the cap beam but the columns remained as in the original bent. The retrofit consisted of coring the cap beam along its longitudinal axis and grouting two post-tensioned tendons in the cap beam. Details on the retrofit of specimen OSB2 can be found in Figure Q117-13 of Appendix A.

3.2.3 SPECIMEN OSB3

Both the cap beam and the columns were retrofitted on specimen OSB3. A reinforced concrete beam was fixed under the existing middle part of the cap beam. Rods were cored through the existing cap beam and prestressed vertically to anchor that underbeam to the existing cap beam. The columns were retrofitted with 6.35 mm (1/4") steel jackets. For more details on OSB3 retrofit, see Figure Q117-12 of Appendix A.

3.2.4 SPECIMEN OSB4

Retrofit scheme of specimen OSB4 also included retrofit of both the cap beam and the columns. A prestressing tendon was grouted in the cap beam along its longitudinal axis. Vertical post-tensioned tendons were also cored in the middle part of the cap beam. 6.35 mm (1/4") steel jackets were used to retrofit the columns. Details on the retrofit of OSB4 are available in Figure Q117-14 of Appendix A.

3.2.5 SPECIMEN OSB5

A fiberglass retrofit technique was used on specimen OSB5. Fiberglass membranes were epoxy-glued on concrete regions to be retrofitted. Membranes were fixed on both the columns and the middle part of the cap beam. The retrofit also included external ungrouted prestressing along the longitudinal axis of the cap beam. Three tendons were post-tensioned on each side of the cap beam. More details on the OSB5 retrofit can be found in Figure Q-1 of Appendix A.

3.3 LOADING PROCEDURE

Two types of loading were simulated during the testing. Vertical loads simulated the superstructure dead load transferred on the bents and the appropriate selfweight of the bents. Lateral loads consisted of slow cyclic loading with displacement amplitudes increased at each new damage level. The experimental setup is shown in Figure 3.3.

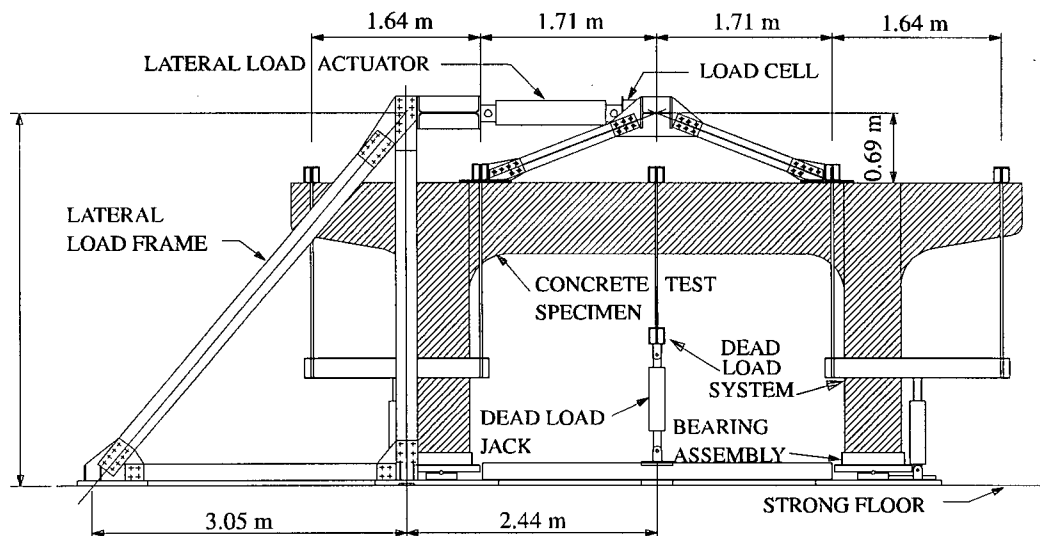


Figure 3.3 Experimental setup

3.3.1 VERTICAL LOADING

The original bridge superstructure framed into the bridge bent at five bearing points (see Figure Q117-01 of Appendix A). Corresponding scale dead loads were evaluated at 169 kN per bearing support (see Anderson et al (1995) for calculations). Specimen vertical loading was consequently applied at the five respective locations on the specimen. Simulated dead loads remained constant throughout the testing procedure. They were transferred by vertical Dywidag bars pulling down on the bent. These bars were connected to a system of five hydraulic jacks anchored to the strong floor of the laboratory.

3.3.2 LATERAL LOADING

The lateral loads were cycled and increased in amplitude until failure or very high damage of the bent occurred. The quasi-static cyclic pattern simulated more severe load-displacement history than that imposed by most earthquakes. Each sequence, producing to increasing levels of damage, consisted of three complete cycles, forward and reverse, at the same displacement level. Figure 3.4 shows a typical loading sequence.

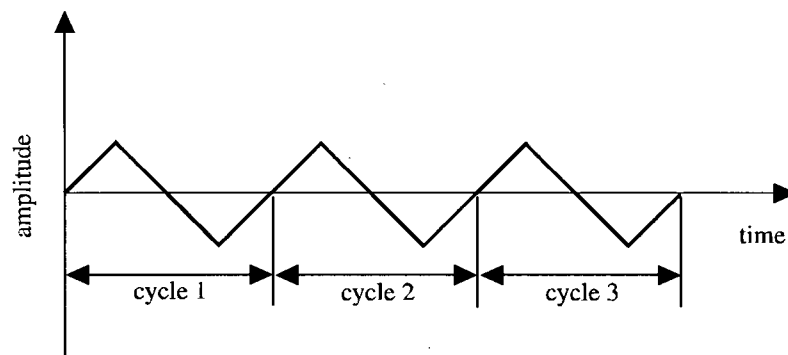


Figure 3.4 Load cycles in a single sequence

The testing procedure was under load control up to the yield load (see Anderson et al (1995) for details on the yield strength estimation). Cycles subsequent to yielding condition were under displacement control until failure of the bent occurred. The displacement ductility index, based on the yield displacement, was used to determine the following lateral loading sequences. Typical ductility values were 0.75, 1.0, 1.5, 2.0,

3.0, 4.0, 6.0, 9.0 and 12.0. Ductility level $\mu = 12.0$ represented an upper displacement ductility limit imposed by the experimental apparatus.

Lateral loading was applied through a horizontal jack along an axis parallel to the cap beam of the bent. This actuator had a maximum loading capacity of 1000 kN. A reaction frame was designed to withstand the full capacity of the horizontal actuator. The lateral load was applied at a level that would simulate the deck inertial loads. From the original design, the lateral loads were expected to be transferred through the two interior bearings closest to the columns. Consequently, a triangular truss connected to those two bearings was designed to carry the loads from the actuator to the structure.

3.3.3 STRUCTURE INSTRUMENTATION

Each specimen was instrumented with LVDT's and strain gauges fixed at several locations of the bent. Test data was collected by a computerized data acquisition system which recorded changes in displacements and strains as the damage increased. Lateral loads were controlled and recorded through a load cell fixed on the lateral loading setup. More details on the recording procedure are available in Anderson et al (1995).

3.4 DYNAMIC TESTING PROCEDURE

Dynamic testing and measurement were the main interests of the study presented here. Two types of vibration tests were performed on the bents: ambient vibration testing and impact testing. The ambient vibration technique, which was already a validated technique at U.B.C., was used for result validation purposes. Forced vibration testing represented the main vibration technique investigated in this study. In order to relate increasing damage and dynamic property changes, measurements were required at different stages during the testing sequences. Hence, vibration tests were performed before the specimen had

suffered any damage and after each sequence or ductility level sustained.

3.4.1 TYPE OF VIBRATIONS

Ambient and impact vibrations were used to excite the specimens. General characteristics of each type of vibration are presented below.

3.4.1.1 AMBIENT VIBRATIONS

Ambient vibrations arise from air flow, technical apparatus, machinery and common activity vibrations. In that case, the force applied to the structure cannot be controlled. It is assumed to have white noise characteristics, i.e. uniform frequency content. From the theory based on ambient vibrations, frequencies and mode shapes can be evaluated by simultaneously measuring vibrations at several locations on the structure. One can refer to Felber (1993) for theoretical background of ambient vibration data analysis.

3.4.1.2 FORCED VIBRATIONS

Forced vibrations involved exciting the structure with a known external excitation. In this study, impact loads were imposed on the structure by striking the structure with an instrumented hammer. Unlike the ambient test, the force induced on the structure is known and can be measured. The force level applied by the hammer was recorded by the data acquisition system.

3.4.2 STRUCTURE INSTRUMENTATION

Response of a specimen, generated by either ambient and forced vibrations, was measured by accelerometers. In the impact vibration testing, the level of excitation of the structure was measured through the instrumented hammer.

3.4.2.1 ACCELEROMETERS

Accelerometers converted the structure's vibrations into electronic signals. Force balanced accelerometers (FBA's 11) were used during this testing program. Acceleration up to $\pm 0.5g$ can be measured by these sensors. More details on the accelerometer specifications can be found in Appendix B. These accelerometers transmitted their signals to the acquisition system through shielded cables. Eight sensors were available in the testing system.

Accelerometers were mounted on steel plates which were bolted on the concrete structure. Figure 3.5 shows three accelerometers placed orthogonally on the column of specimen OSB1. Accelerations were measured in the three principal orthogonal directions: the longitudinal direction, in the plane of the bent and parallel to the cap beam, the transverse direction, perpendicular to the plane of the bent, and the vertical direction, in the plane of the bent and parallel to the columns.

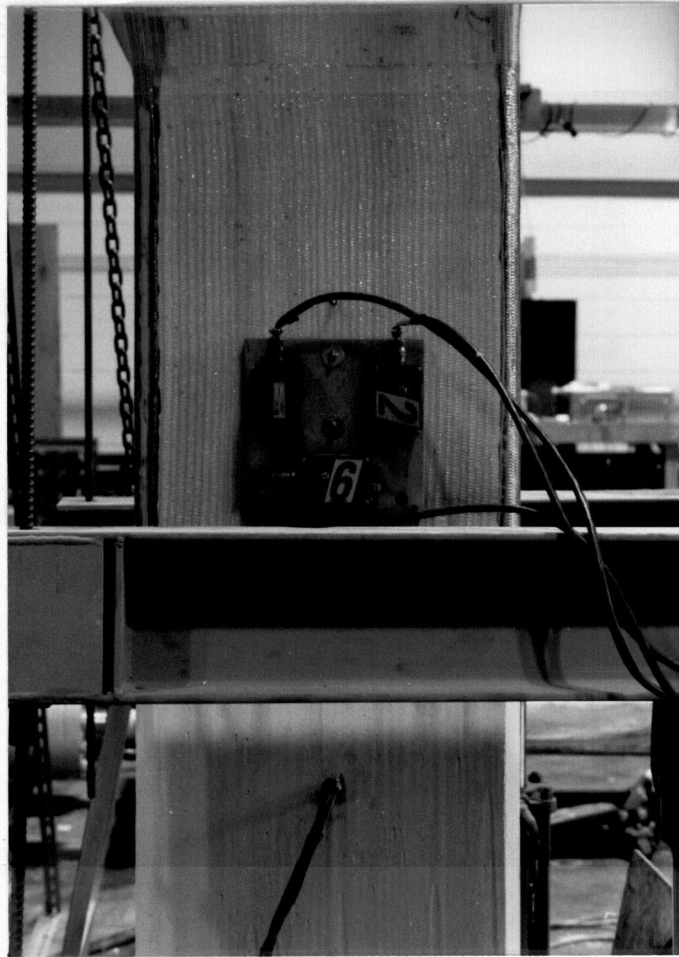


Figure 3.5 Typical tri-axial accelerometer setup

For specimens OSB3 and OSB4, the steel plates could not be directly installed on the circular steel jackets retrofitting the columns. For those two specimens, the column plates were mounted on a transfer device which was fixed to the steel jackets. This installation device is shown in Figure 3.6. For specimen OSB5, steel plates supporting the accelerometers were anchored directly through the fiberglass membranes retrofitting the bent.



Figure 3.6 Installation device for accelerometers of OSB3 and OSB4

Since only eight sensors were available, two setups of the accelerometers were used to measure the induced vibrations on the bents. Figure 3.7 shows the sensor locations. Together, these two setups totalized 16 measurements. They recorded vibrations at six locations of the bent: four on the cap beam and two on the sides of the columns. The longitudinal sensor of node 5, duplicated in setup no.2, served as the reference sensor for ambient vibration analysis. For specimen OSB1, only eight recording channels were available in the acquisition system. Since the hammer required one channel, measurements from vertical sensors of node 1 and node 6 were not recorded during impact testing of specimen OSB1. For the other four specimens, the acquisition system was upgraded to 16 channels and the hammer channel was not interfering with sensors of node 1 and node 6, which then recorded response time histories of the specimen.

Figures A.1 and A.2 of Appendix A show typical accelerometer setup on the column and cap beam respectively.

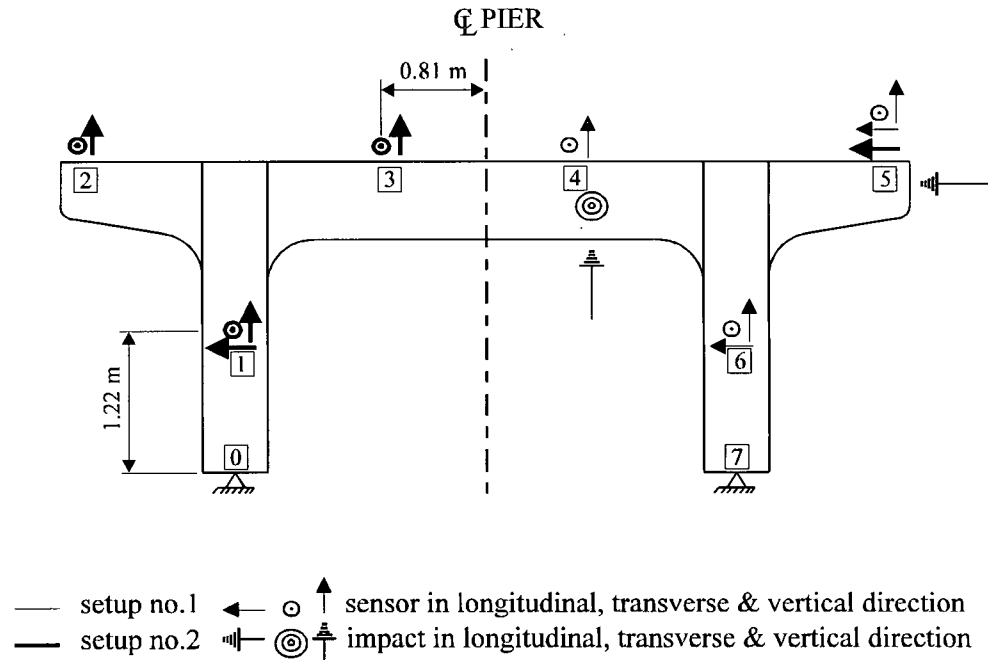


Figure 3.7 Setup for dynamic testing

3.4.2.2 INSTRUMENTED HAMMER

In the impact testing procedure, an impulse hammer was used to excite the structure. This hammer consists of an integral piezoelectric force sensor. This sensor utilizes self-generating quartz crystals to generate an output signal which is exactly analogous to the impact force of the hammer. Figure A.3 of Appendix A shows the instrumented hammer used in the impact testing. Details on the hammer specifications can be found in Appendix B.

Hammer impacts were input on the structure at three different locations and in three different directions as shown in Figure 3.7. The directions of impact corresponded to the three principal orthogonal directions. The longitudinal impacts were applied at the end of the cap beam. The transverse and vertical impacts were input in the middle part of the cap beam. Figure 3.8 shows how hammer impacts were input

longitudinally at the end of the cap beam. Examples of typical transverse and vertical impacts are shown in Figures A.4 and A.5 of Appendix A.



Figure 3.8 Longitudinal impact applied with the instrumented hammer

3.4.3 DATA ACQUISITION SYSTEM

The data acquisition system includes measurement hardware and software. Measurement hardware comprises physical instrumentation and apparatus used to record vibrations while measurement software refers to computer programs performing acquisition of the discretized signals.

3.4.3.1 MEASUREMENT HARDWARE

The same acquisition hardware was used for both ambient and impact testing procedure. The computerized acquisition data system comprised a conditioner, an analog/digital converter and a 486 PC computer. The conditioner filtered and amplified the signals. The A/D converter then transformed the continuous signal in a series of discretized data. Finally, the computer recorded and saved the vibrations measured on the bent. Figure 3.9 shows a schematic view of the acquisition system. Figure A.6 of Appendix A shows the actual acquisition system used during vibration testing of the specimens. More details on the acquisition hardware can be found in Schuster (1994).

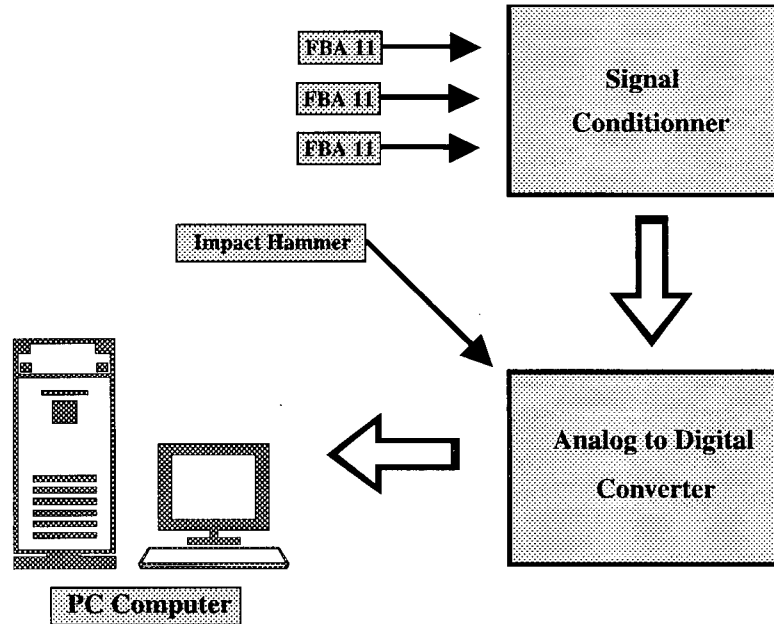


Figure 3.9 Typical recording setup for vibration measurements

3.4.3.2 MEASUREMENT SOFTWARE

Measurement software differed slightly for ambient and impact testing. This section provides details on recording parameters used in each testing procedure. For both ambient and impact testing, a 50 Hz low-pass filter was used to condition the signals before recording was processed.

3.4.3.2.1 Ambient Vibration Testing Parameters

The computer program used to record the ambient vibrations was developed at U.B.C. by Yee and Felber (1993). Modifications and improvements of the original version were done by Schuster (1994). Ambient vibration tests were performed at a sampling rate of 200 samples per second (sps), corresponding to a Nyquist frequency of 100 Hz. For specimen OSB1, a total of 32768 data points were recorded for each channel. For specimens OSB2 to OSB5, a total of 16384 data points per channel were recorded. The frequency resolution was fixed by the ambient vibration analysis program. Based on a segment length of analysis of 4096 points, the frequency resolution was of 0.049 Hz. Table 3.1 summarizes the experimental characteristics for each specimen. Description of the ambient vibration testing procedure can be found in Felber (1993) and Schuster (1994).

Specimen	Sampling Rate [sps]	Time Resolution [sec]	Recording Segment Length [points]	Total Recorded Samples [points]	Frequency Resolution [Hz]
OSB1	200	0.005	4096	32768	0.049
OSB2	200	0.005	4096	16384	0.049
OSB3	200	0.005	4096	16384	0.049
OSB4	200	0.005	8192	16384	0.049
OSB5	200	0.005	8192	16384	0.049

Table 3.1 Ambient vibration testing characteristics

3.4.3.2.2 Forced Vibration Testing Parameters

The computer program used to record the ambient vibrations is also a modified version the original software developed at U.B.C. by Felber (1993). The ambient vibration acquisition program was adapted to impact testing by Schuster (1994). Four sets of impact were induced per ductility level. Each set of impacts consisted of four consecutive hammer blows. Two sets of hammer impact were induced along the longitudinal axis of the cap beam, the direction of the lateral loading cycles. The two other sets were in the

transverse and vertical directions. Table 3.2 summarizes the experimental measurement characteristics for each specimen. Detailed description of impact vibration procedure can be in Appendix B.

Specimen	Sampling Rate [sps]	Time Resolution [sec]	Recording Segment Length [points]	Frequency Resolution [Hz]	Averaged Impact Peak Force [kN]
OSB1	200	0.005	4096	0.049	6.58
OSB2	200	0.005	4096	0.049	6.58
OSB3	1000	0.001	16384	0.061	17.12
OSB4	1000	0.001	16384	0.061	10.45
OSB5	1000	0.001	16384	0.061	11.61

Table 3.2 Impact vibration testing characteristics

For specimens OSB1 and OSB2, the time resolution was 0.005 sec. It was reduced to 0.001 sec for specimens OSB3, OSB4 and OSB5. The frequency resolution was about the same for all five specimens. The time resolution was improved by increasing the sampling rate. However, augmenting the sampling rate too much would have impaired the frequency resolution. The duration of sampling was then increased to preserve a similar frequency resolution. Anomalies observed in the time signals of the hammer impact justified these recording changes. Figures 3.10 and 3.11 show typical time histories of the hammer for low and high sampling rates.

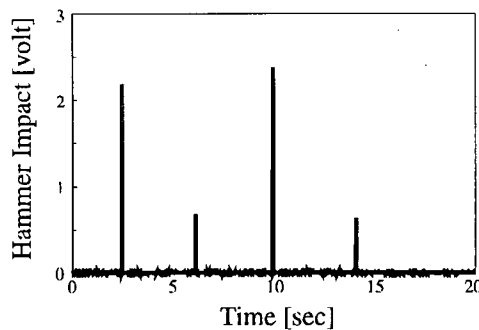


Figure 3.10 Low sampling rate [200 sps]

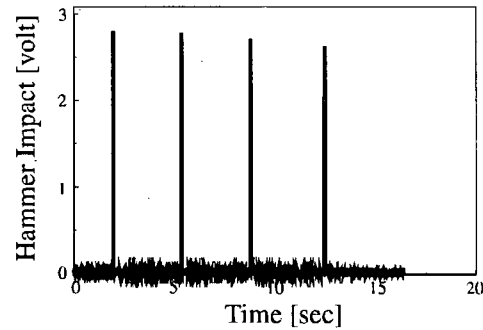


Figure 3.11 High sampling rate [1000 sps]

The time signal recorded at low sampling rate shows considerable variation of the peak values of the hammer blows. On the other hand, the high sampling rate indicates relatively constant peak value. The lower sampling rate sometimes missed the peak value of the hammer, recording different peak amplitudes from one impact to the other. The high sampling rate correctly captured the peak value. Table 3.2 shows that the averaged impact peaks for OSB1 and OSB2 are lower than those for OSB3, OSB4 and OSB5. Different tests performed on the hammer showed that a minimum sampling rate of 900 sps was required to capture the hammer peak. Frequency domain analyses (see Chapter 5), which used ratios of output to input signals, were also affected by this recording problem.

3.4.4 DYNAMIC TESTING SEQUENCES

A typical dynamic test included two types of testing sequences, with specific objectives for each sequence type. Description of these sequences are presented below.

3.4.4.1 PRELIMINARY AND FINAL SEQUENCES

Preliminary sequences were recorded before the specimen had suffered any structural damage. Vibrations from setups no.1 and no.2 were measured in these sequences. Measurements from the complete structure permitted to relate the natural frequencies to their corresponding mode shapes.

In these sequences, measurements were recorded for different combinations of dead load and lateral actuator conditions. They represented useful tools for future analytical modelling of the bents. Table 3.3 summarizes the preliminary sequences recorded for each specimen. A total of 8 consecutive sequences were measured. The sequence order was planned to minimize the number of sensor relocations for different setups and considered the fact that the actuator installation was not a simple operation compared to the activation of the dead load.

Sequence No.	Actuator Condition	Dead Load Condition	Setup No.
1	out	off	1
2	out	off	2
3	out	on	2
4	out	on	1
5	in	on	1
6	in	on	2
7	in	off	2
8	in	off	1

Table 3.3 Preliminary and final sequences

Final sequences were performed after failure or very high damage of the bent had occurred. The sequences described for preliminary testing were repeated, in reverse order, in the final sequences.

3.4.4.2 INTERMEDIATE SEQUENCES

During lateral loading cycles, corresponding to increasing damage of the bent, frequency changes comprised the main interest of the dynamic testing. Consequently, only accelerometers from setup no.1 recorded signals to accelerate the testing procedure. Measurements from setup no.2, which discretized the complete structure together with setup no.1, were not needed for further data processing.

Detailed experimental dynamic testing parameters are summarized in forms of tables used during the actual testing. For each specimen, these experimental datasheets include details on ductility levels tested, sequences, filenames, global gains, filters, etc. They can be found in Appendix B.

3.5 PRELIMINARY DESCRIPTION OF DAMAGE OBSERVED

A qualitative assessment of the test results can be done by examining hysteresis loops and types of damage observed in each specimen. Hysteresis curves are shown in Figure 3.12. In these figures, the joint displacement, is the average horizontal displacement measured at the two joints and the base shear represents the total base shear or the applied lateral load. Table 3.4 summarizes some experimental characteristics obtained from the lateral loading procedure, including the yielding displacement, Δ_y , the maximum ductility level sustained, μ_{\max} , and the corresponding maximum load.

Specimen	Δ_y [mm]	μ_{\max} Sustained	Maximum Load [kN]
OSB1	6.35	4	267
OSB2	11.43	6	467
OSB3	11.43	12	489
OSB4	10.92	12	489
OSB5	11.43	12	480

Table 3.4 Experimental lateral loading characteristics

The original design, specimen OSB1, showed a very poor and brittle behavior. During testing, diagonal shear cracks, associated with negative moment, developed in the middle part of the cap beam. These cracks substantially increased in width with increasing damage level. Low concrete compressive strength in the cracked zones led the structure to failure at a ductility level of 4. Hysteresis loops of specimen OSB1 (Figure 3.12a) clearly indicate the poor seismic behavior. Figure A.7 of Appendix A shows specimen OSB1 at failure state.

Specimen OSB2, retrofitted with longitudinal prestressing in the cap beam, showed improvements of both strength and ductility levels, as shown in the hysteresis loops of specimen OSB2 (Figure 3.12b). As for specimen OSB1, diagonal shear cracks developed in the middle part of the cap beam but their width was

limited to a relatively low level. However, the columns showed progressive flexural cracking with increasing damage level. This structural degradation led the specimen to a sudden column shear failure at a ductility level of 6. Figures A.8 and A.9 of Appendix A show details of the columns damage.

The underbeam retrofit in specimen OSB3 limited the shear cracking developed in the cap beam. Significant cracking progressed in the joint regions, causing spalling of the concrete cover and buckling of bars at high ductility levels. The specimen ultimately failed in flexure above the steel jackets retrofitting the columns at a ductility level of 12. Overall, hysteresis loops of specimen OSB3 (Figure 3.12c) indicate a good performance compared to the original design. Damaged specimen OSB3 is shown in Figure A.10 of Appendix A.

Hysteresis curves of specimen OSB4, with vertically and horizontally prestressed cap beam as well as steel jackets, are shown in Figure 3.12d. Behavior similar to OSB3 caused a flexure failure in the column above the steel jackets. Specimen OSB4 also sustained a ductility level of 12. Figure A.11 of Appendix A shows specimen OSB4 at failure state.

The fiberglass and external prestressed retrofit, specimen OSB5, showed less cracking than the other specimens. However, flexure cracking was progressing in the columns. Due to limitation of the experimental setup, complete failure of the specimen was not achieved and the specimen reached ductility 12 with no extensive damage. Hysteresis loops are presented in Figure 3.12e. Details of the damaged columns can be viewed in Figures A.12 and A.13 of Appendix A.

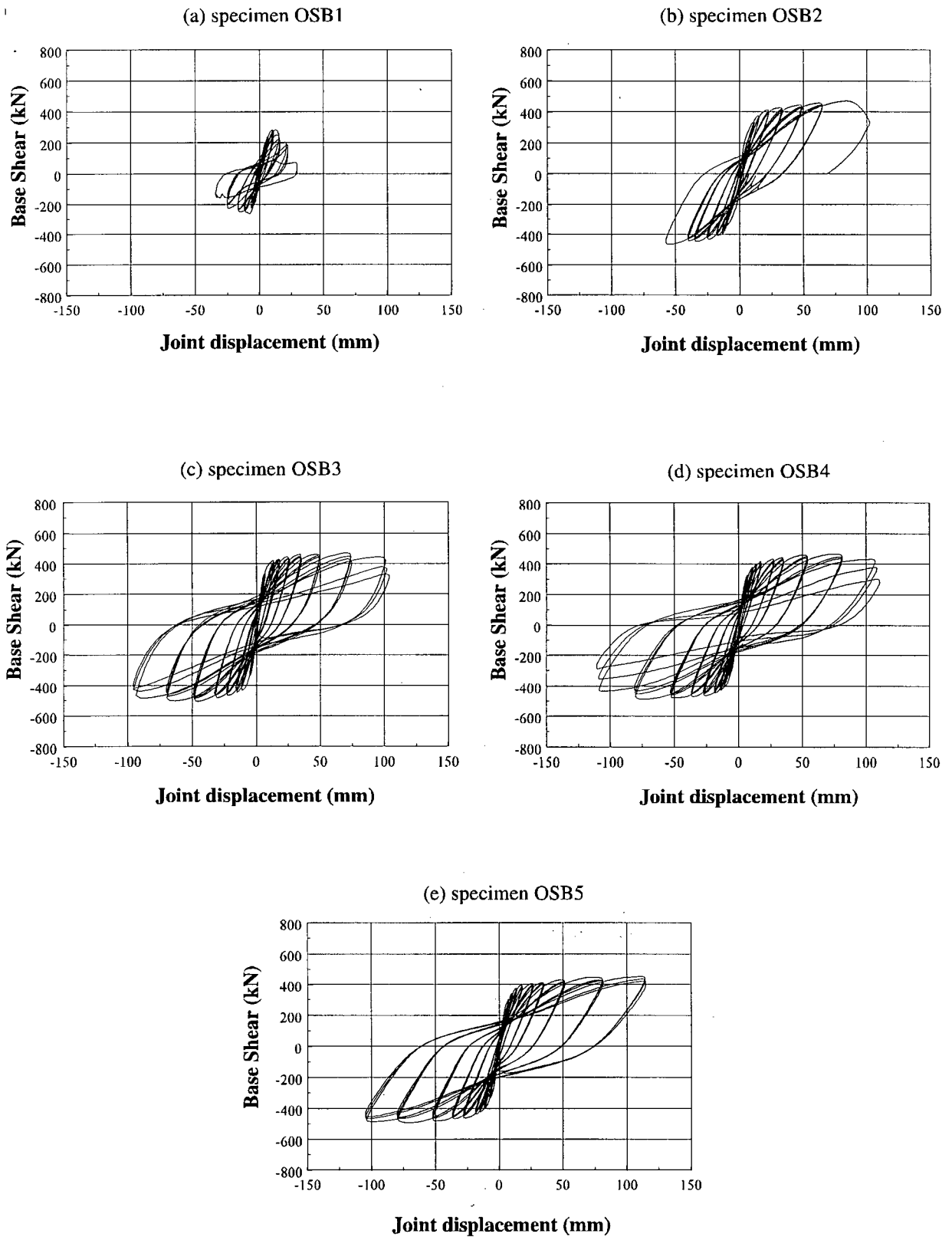


Figure 3.12 Hysteresis curves

3.6 CONCLUDING REMARKS

This chapter described the experimental procedure performed on the five specimens. The lateral and vertical loading procedures as well as the vibration testing were detailed. Observations of the damage sustained by the specimens were also described based on the hysteresis curves obtained experimentally. The following chapter investigates damage assessment based on structural properties, such as displacement, stiffness and energy absorption.

CHAPTER 4

DAMAGE ASSESSMENT BASED ON STRUCTURAL PROPERTIES

Damage indices show promise of providing a useful means to quantify damage sustained by a structure which was subjected to severe loading, such as a seismic event. Damage indices based on structural properties are evaluated here using information from the structural response of the specimens studied.

Based on the failure modes observed for the five specimens, three of the structural damage indices presented in Chapter 2 were chosen to quantify degradation levels of the specimens tested. In Section 4.2, calculation procedures of the damage indices are described and applied to the five bridge bents tested in the laboratory. Finally, index values obtained are compared and used to evaluate the specimen performance.

4.1 CHOICE OF DAMAGE INDICES

From test results of the bridge bents, two specimens failed in shear (OSB1, OSB2) while the remaining three (OSB3, OSB4, OSB5) failed or suffered very high damage in flexure. In order to compare adequately the specimen behaviors, the damage indices used had to provide acceptable damage assessment for both flexural and shear modes of failure. For practical reasons, it was convenient to consider each bent as an individual member so that a single local index would suffice to assess damage. Thus, the local index would also serve as a global index of a single-element structure.

Most of local structural indices presented in Chapter 2 were initially developed and validated for flexural modes of failure. Williams et al (1995) investigated methods to quantify shear-dominated damage with some of these flexural-based indices. In that study, different local indices were applied as per their original definition. Others were modified for a more appropriate formulation to evaluate shear-dominated

response, i.e. in terms of force-displacement instead of moment-curvature relationships. The local damage indices described in Chapter 2 refer to these modified version of the indices. Using a series of combined shear and flexural cyclic tests, eight local damage indices were evaluated and their ability to quantify shear-dominated damage was examined. A comparative analysis between these indices was also performed.

The Williams study found no particular correlation associating damage indices and shear modes of failure. Damage index values were basically deformation dependent, with the energy dissipation term having only a negligible effect. Basic indices, typically defined as a single term based on large deformation, provided more realistic evaluation of damage than complex indices, involving both a large deformation term and a cyclic loading term. Although damage indices were not very good at assessing shear damage, the three following local indices were considered adequate for evaluation of shear damage response: **displacement ductility**, **modified stiffness ratio** and **modified Park and Ang index**. These three local indices, adequate for both flexural and shear failure, were chosen to assess structural damage in the five specimens tested.

4.2 EVALUATION OF DAMAGE INDICES

This section describes the steps involved in the evaluation of displacement ductility, modified stiffness ratio and modified Park and Ang index.

4.2.1 DISPLACEMENT DUCTILITY

As mentioned in section 2.1.2.1, displacement ductility, μ_δ , is expressed as:

$$\mu_\delta = \frac{\delta_m}{\delta_y} = 1 + \frac{\delta_m - \delta_y}{\delta_y} \dots\dots\dots [4.1]$$

In this study, the displacement δ , referring to both δ_y and δ_m , was defined as the lateral average joint displacement. Two LVDT's, installed on each of the two beam/column joints, measured the lateral joint displacements throughout the loading procedure. Readings obtained from these two LVDT's were calibrated and averaged. The yield displacement δ_y was taken as 4/3 of the displacement measured at 75% of the yield strength. Yield strength was estimated analytically prior to testing. For each cycle, a positive and a negative maximum displacement (δ_i^+ and δ_i^-) were obtained from the recorded data. Figure 4.1 shows schematic definition of these symbols. The maximum absolute value of δ_i^+ and δ_i^- was retained for index calculation.

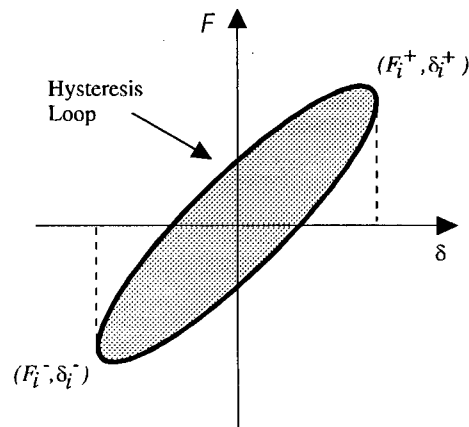


Figure 4.1 Typical hysteresis loop and parameter definitions

Displacement ductility at each load cycle can be calculated as follows:

- **step 1:** find δ_y from 4/3 of the displacement measured at 75% of the yield strength;
- **step 2:** for each cycle i , do:
 1. find δ_i^+ ;
 2. find δ_i^- ;
 3. find $\delta_{i,m} = \max(\delta_i^+, \text{abs}(\delta_i^-))$;
 4. evaluate Equation 4.1

A typical displacement ductility spreadsheets is presented in Appendix C.

4.2.2 MODIFIED STIFFNESS RATIO

In Section 2.1.2.1, the modified stiffness ratio, D , was defined as:

$$D = \frac{k_f}{k_m} \cdot \frac{(k_m - k_0)}{(k_f - k_0)} \dots\dots\dots [4.2]$$

Stiffnesses are expressed in this case as ratios of force over displacement, $k = F / \delta$. As for the ductility index, the displacement δ was taken as the lateral average joint displacement. The force was defined as the total base shear induced on the bents, equivalent to the total lateral load induced by the actuator. This force was measured by a load cell installed on the lateral loading setup. The lateral loads were recorded and used, together with the displacements, to generate hysteresis curves of the specimens. These hysteresis loops were used to compute the index.

In Equation 4.2, the initial tangent stiffness k_0 refers to the yielding condition and can be expressed as $k_0 = F_y / \delta_y$. The secant stiffness at failure k_f refers to the final condition and can be defined as $k_f = F_f / \delta_f$. Finally, $k_{m,i}$ refers to the maximum stiffness at each half cycle, forward and reverse, and is expressed as $k_{i,m} = F_i / \delta_i$. The stiffness index is evaluated for positive and negative half cycles and the maximum value is retained.

Calculation steps of modified stiffness ratio for each load cycle are summarized below:

- **step 1:** find δ_y and F_y from 4/3 of the displacement and load measured at 75% of the yield strength;
- **step 2:** calculate k_0 ;
- **step 3:** find δ_f and F_f from displacement and load at cycle of final sequence;
- **step 4:** calculate k_f ;
- **step 5:** for each cycle i , do:
 -
 - 1. find δ_i^+ and corresponding value for F_i^+ ;
 - 2. calculate $k_{i,m}^+$;
 - 3. calculate D_i^+ using Equation 4.2;
 - 4. find δ_i^- and corresponding value for F_i^- ;
 - 5. calculate $k_{i,m}^-$;

6. calculate D_i^- using Equation 4.2;
7. $D_i = \max(D_i^+, D_i^-)$.

A typical spreadsheet of modified stiffness ratio calculations can be found in Appendix C.

4.2.3 MODIFIED PARK AND ANG INDEX

Modified Park and Ang index comprises a deformation term and a cumulative energy term. From Section 2.1.2.2, this is expressed as:

$$D = \frac{\delta_m - \delta_y}{\delta_f - \delta_y} + \beta \frac{\int dE}{F_y \delta_f} \dots \dots \dots [4.3]$$

As before, displacement terms are associated to the lateral average joint displacements. The displacement $\delta_{i,m}$ represents the maximum value between δ_i^+ and δ_i^- . In the energy part of the equation, the integral evaluates the energy dissipated by the specimen. The energy that an elasto-plastic system dissipates in a cycle of deformation is proportional to the amplitude of the cycle. Hence, the shaded area in Figure 4.1 corresponds to the energy for one cycle. Total energy dissipated was obtained by adding individual cycle energy. The trapezoidal rule was used to evaluate energy dissipation from the hysteresis curves. The recommended value for β was 0.1. Calculation steps of modified stiffness ratio for each load cycle are summarized below:

- **step 1:** find δ_y and F_y from 4/3 of the displacement and load measured at 75% of the yield strength;
- **step 2:** find δ_f from displacement at cycle of final sequence;
- **step 3:** for each cycle i , do:
 1. find δ_i^+ ;
 2. find δ_i^- ;
 3. find $\delta_{i,m} = \max(\delta_i^+, \text{abs}(\delta_i^-))$;
 4. evaluate $D_{i,def}$ the deformation term of Equation 4.3;
 5. evaluate $D_{i,energy}$ the energy term of Equation 4.3;
 6. evaluate $D_i = D_{i,def} + D_{i,energy}$.

A typical spreadsheet for this index is presented in Appendix C.

4.3 RESULTS AND COMPARISONS OF INDICES

4.3.1 COMPARISON OF SPECIMEN BEHAVIORS

Three damage indices were evaluated on specimens OSB1 to OSB5. They represent a useful mean to compare specimen responses to the loading procedure. Specimen performances were compared by examining individually each of the indices evaluated on the five specimens tested. Figures 4.2, 4.3a and 4.3b show comparisons of displacement ductility with respect to nominal ductility as well as modified stiffness ratio and modified Park and Ang index with respect to displacement ductility. Nominal ductility is defined here as the reference ductility levels used during the experimental procedure.

4.3.1.1 DISPLACEMENT DUCTILITY

Figure 4.2 shows the variations of displacement ductility indices with increasing deterioration of each specimen expressed in terms of nominal ductility. It can be seen in Figure 4.2 that index values range from 0 to 12. Damage indices reached 5.41 (OSB1), 6.86 (OSB2), 12.01 (OSB3), 11.42 (OSB4) and 11.33 (OSB5). These values were obtained at failure of the specimen except for OSB5, for which complete failure was not achieved because of experimental setup limitations.

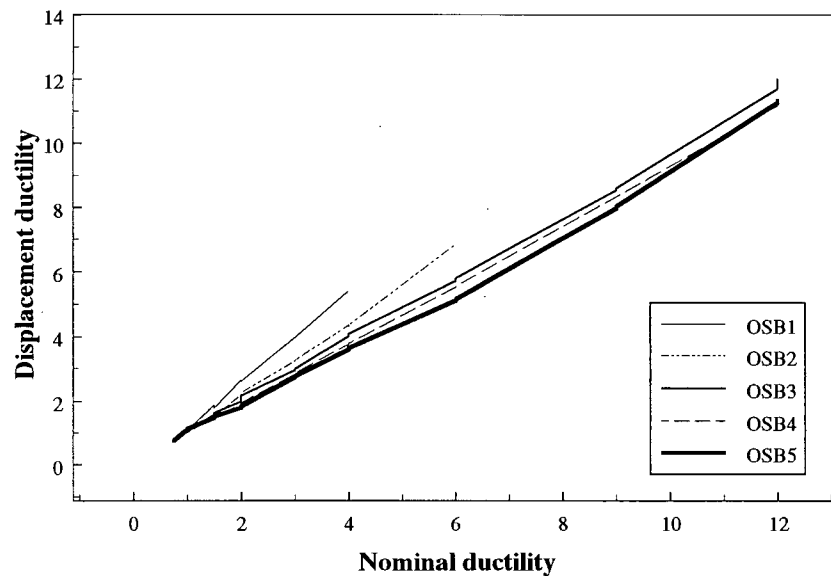


Figure 4.2 Comparison of specimen behaviors: displacement ductility

Figure 4.2 also shows the correlation between the nominal ductility and the calculated ductility indices. As these two parameters quantify the same effect, a close correlation is expected. While a good correlation is found for specimens OSB3, OSB4 and OSB5, the nominal ductilities for specimens OSB1 and OSB2 tend to underestimate the displacement ductility indices calculated from experimental data. The actual damage levels sustained are then undervalued for these two specimens. In fact, the curve slopes are greater than unity for specimens OSB1 and OSB2. The computed slope of the fitted line, obtained from a linear regression analysis for each of the specimens, was 1.44 for OSB1, 1.14 for OSB2, 0.95 for OSB3, 0.93 for OSB4 and 0.91 for OSB5. These observations suggest that calculated ductilities should be used as damage level indicators instead of nominal ductilities in future index comparisons.

Since ductility represents a key property of a structure subjected to seismic loading, good performance of a specimen is associated with a high index value. Based on this concept, OSB1 (5.41) gave the poorest performance, followed by OSB2 (6.86), OSB4 (11.42), OSB3 (12.01) and finally OSB5 (11.33).

Specimen OSB5 could have sustained higher ductility levels with enhanced capabilities of the experimental setup.

4.3.1.2 MODIFIED STIFFNESS RATIO

Figure 4.3a shows the relationship between the modified stiffness ratio index and the calculated ductility (Equation 4.1). As indicated in the previous section, damage levels were associated to the real ductility levels sustained by the specimens. Index values range from 0 to about 3. Maximum indices obtained at failure or very high damage were 1.0 (OSB1), 2.82 (OSB2), 1.68 (OSB3), 1.61 (OSB4) and 1.36 (OSB5).

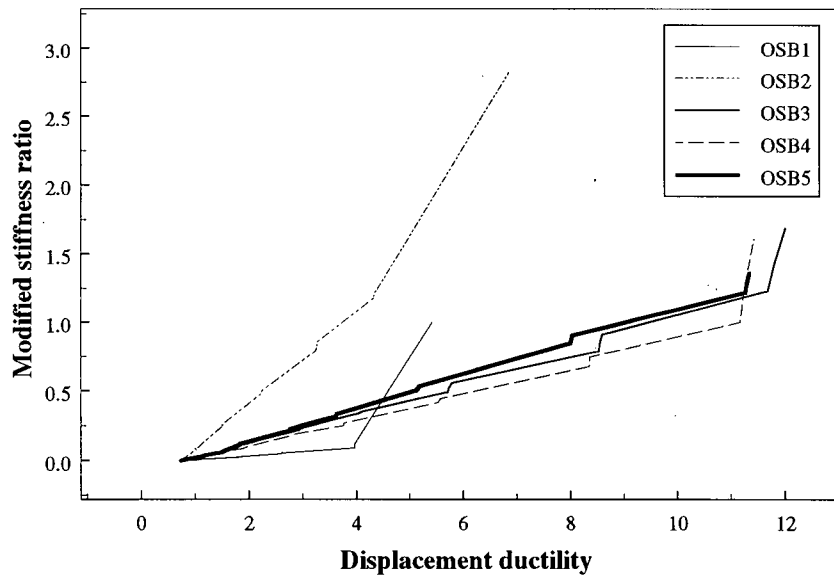


Figure 4.3a Comparison of specimen behaviors: modified stiffness ratio

Figure 4.3a shows dissimilar graph trends. For specimens OSB3 to OSB5, damage rates are relatively similar in magnitude. Index values are gradually increasing through the different damage states. On the other hand, specimens OSB1 and OSB2 display discontinuities in their degradation process. The discontinuities divide the response in two degradation rates: an initial low damage rate and a subsequent higher damage rate. For specimen OSB1, the slope increased about 20 times (from 0.03 to 0.61) at ductility 4, giving a slope change of 0.58. Specimen OSB2, with an initial slope of 0.12, suddenly shifted

to 0.64 at ductility 4.5, showing an increase of about 5 times its initial damage rate. The corresponding slope change is 0.52. Averaged slopes were estimated by linear regressions performed on the index data.

Recalling the failure modes for each specimen, the shear failures can be associated to trends presenting sharp discontinuities and flexural failure modes to gradual increasing trends. Hence, the index differentiated brittle from ductile behavior, with the presence or absence of sharp slope changes in the index trend. The index definition, based on stiffness indicators, can explain these observations, where a significant reduction in stiffness is usually associated with a sudden brittle damage. Consequently, if failure is obtained, the modified stiffness ratio can provide information on the failure mode of the specimen studied.

Two classification approaches can be used to assess performance of specimens. The index value corresponding to a fixed ductility level provides a first comparison tool. A high index value is associated with a significant stiffness degradation. This classification would rank the specimens like OSB2, OSB1, OSB5, OSB3 and OSB4 as poorest to best performance, with very similar performances for specimens OSB3 to OSB5. However, hysteresis curves clearly indicated that OSB2 showed improved behavior compared to OSB1, which would question the validity of this classification approach. Variation of degradation rates represent another mean for comparing specimen performances. For the three flexural failures, referring to specimens OSB3 to OSB5, the slope change is more or less zero. Their slope values are also very similar: 0.13 (OSB3), 0.11 (OSB4) and 0.12 (OSB5). For specimens OSB1 and OSB2, which suffered from shear failure respectively in the cap beam and the columns, the damage rate increases (0.58 for OSB1 and 0.52 for OSB2). According to this classification, the ranking would be, starting with the poorest performance, OSB1, OSB2, and specimens OSB3 to OSB5 with similar behavior. This classification method, associated with the failure mode, gave a ranking consistent with experimental observations and hysteresis curves.

4.3.1.3 MODIFIED PARK & ANG INDEX

Figure 4.3b shows variations of the modified Park & Ang index with calculated ductility levels sustained by the specimens. Index values range from 0 to about 3. The maximum index values obtained at failure reached 1.87 (OSB1), 2.92 (OSB2), 2.35 (OSB3), 2.12 (OSB4) and 2.39 (OSB5).

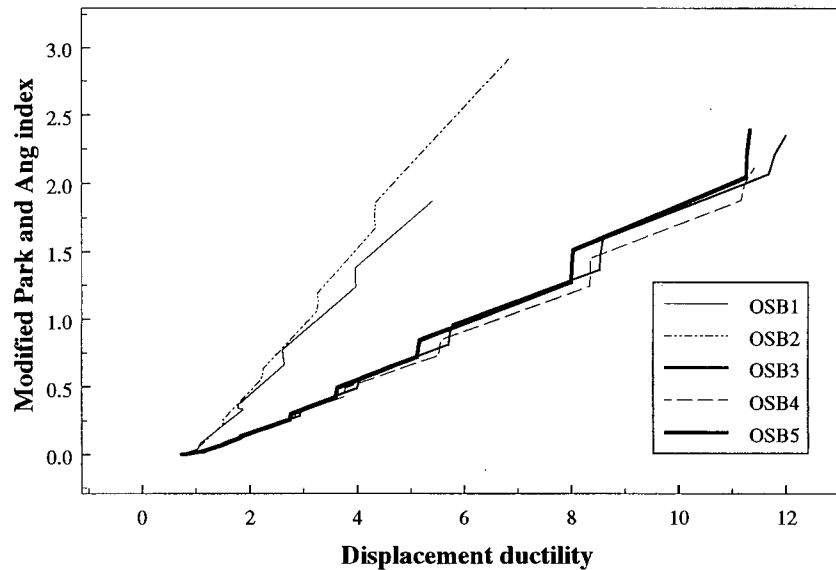


Figure 4.3b Comparison of specimen behaviors: modified Park and Ang index

As for the two previous indices, specimens OSB3 to OSB5 indicate similar damage rate and index magnitudes. Trends of specimens OSB1 and OSB2 are also comparable. However, their degradation increases at a higher rate than the three other specimens. Slope values obtained from linear regression are respectively 0.41, 0.50, 0.20, 0.19 and 0.21 for the five specimens tested.

Unlike the modified stiffness ratio, this index presents no significant variation in the degradation rate, previously related to the type of failure. Different slope values suggest a separation of the specimens in two categories like OSB1/OSB2 and OSB3/OSB4/OSB5. Recalling that OSB1 and OSB2 failed in shear and that OSB3, OSB4 and OSB5 failed in flexure, the failure mode could be associated to the slope magnitude. A high slope would in this case indicate a brittle mode of failure while a low damage rate

would represent a ductile failure mode. However, general application of this classification approach would require more case studies. If the ranking method is validated, a threshold value could eventually be defined to differentiate the two failure modes.

The specimen performance can be based on the index value for a fixed damage level. In that case, the specimens would be ranked like OSB2, OSB1, and OSB3 to OSB5 with similar behavior. If the slope is assumed an adequate performance indicator, the specimens would be ranked OSB2, OSB1, and OSB3 to OSB5 with similar behavior. These two comparison approaches are not consistent with previous conclusions from hysteresis curves, where OSB2 indicated improvement in its seismic response compared to OSB1.

4.3.1.4 SUMMARY OF SPECIMEN CLASSIFICATION

For each damage index evaluated, Table 4.1 provides a summary of specimen ranking, starting with the poorest specimen behavior. Three classification approaches were used to assess performance of the specimens: the maximum index value, the degradation rate, referring to the curve slope, and, finally, the variation of this damage rate. Note that observations of damage and hysteresis loops suggested a ranking like OSB1, OSB2, OSB3, OSB4 and OSB5.

Damage Index	by Peak Value	by Damage Rate	by Damage Rate Gradient
displacement ductility	OSB1, OSB2, OSB4, OSB3, OSB5	n/a	n/a
modified stiffness ratio	OSB2, OSB1, OSB5, OSB3, OSB4	n/a	OSB1, OSB2, OSB3, OSB4, OSB5
modified Park & Ang index	OSB2, OSB1, OSB3, OSB4, OSB5	OSB2, OSB1, OSB3, OSB4, OSB5	n/a

Table 4.1 Ranking of specimen behaviors

4.3.2 DAMAGE INDICES CORRELATION

Correlation studies evaluated the similarity between damage characterization provided, at different states of damage, by each index. Damage characterization is understood here to be how physical elements, such as displacement, crack propagation, yielding, stiffness degradation, etc., are taken into account in the failure process defined in a particular damage index. Damage indices were normalized, with respect to their peak value, to facilitate the comparison of their relative ability to assess damage. That is, a failure state refers to a *unit* value for all indices considered. Figures 4.4a to 4.4c show relationships obtained comparing modified stiffness ratio and modified Park and Ang index with displacement ductility as well as modified Park and Ang with modified stiffness ratio.

Similar damage characterization of two normalized indices would be indicated by a unit slope. That is, for a particular damage state, the two indices would attribute a similar degree of structural damage, or, in other words, they would converge to failure at a similar rate. On the other hand, curves above this unit line would suggest that the ordinate index converges more rapidly to failure than the abscissa index. Curves below the unit reference line would indicate that the abscissa index converges faster to failure than the ordinate index.

From Figures 4.4a, 4.4b and 4.4c, comparable rate of approach to failure was obtained from a comparison of the modified Park and Ang index and the displacement ductility, where all five specimens showed the similar graph trends. Also, looking at the three comparisons, this damage characterization similarity is improved for specimens with flexural failure mode.

Figure 4.4a compares normalized modified stiffness ratio and normalized displacement ductility. The comparison shows diverse trend types. Stiffness ratio seems to converge less rapidly to failure than displacement ductility. This is verified for all five specimens. However, the comparison curves seem

closer to a unit slope when the failure mode is ductile, as for specimens OSB3, OSB4 and OSB5. This observation suggests that ductility and stiffness ratio converge to failure at comparable rates when the failure mode is flexural.

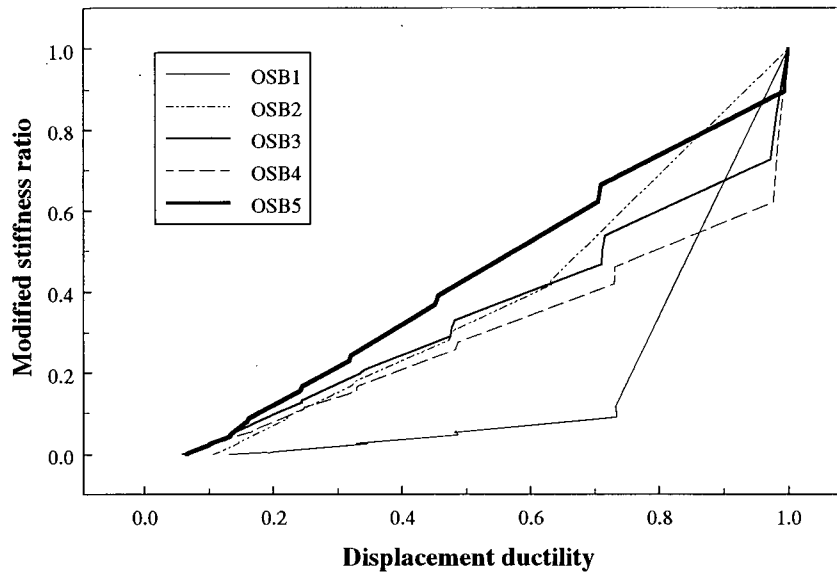


Figure 4.4a Index correlation: modified stiffness ratio vs displacement ductility

Figure 4.4b compares modified Park and Ang index to displacement ductility. This graph shows the least scattered data among the three index comparisons studied. The comparison of normalized indices produces a correlation almost perfect for all five specimens. These two indices were then assumed to converge to failure at similar rate for either failure modes.

Figure 4.4c compares the modified Park and Ang index to the modified stiffness ratio. The comparison gives diverse graph trends. As in the comparison with displacement ductility, modified stiffness ratio seems to converge to failure more slowly than the Park and Ang index.

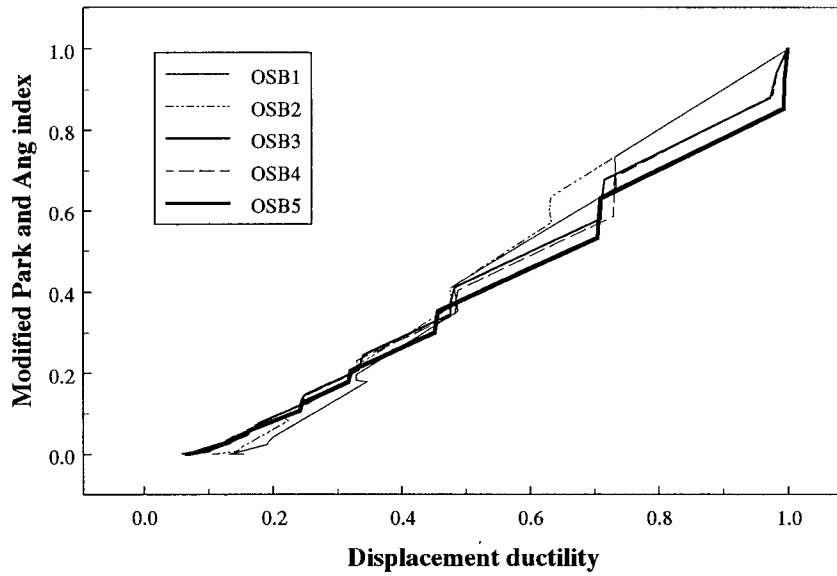


Figure 4.4b Index correlation: modified Park and Ang index vs displacement ductility

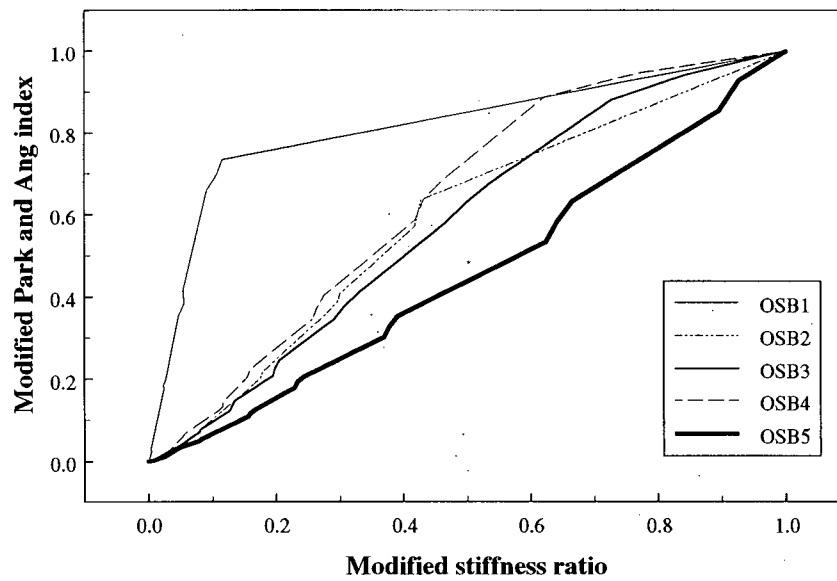
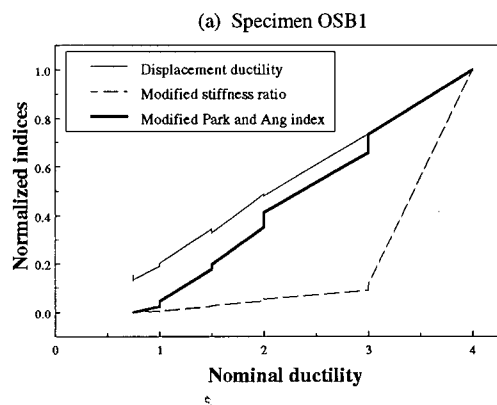


Figure 4.4c Index correlation: modified Park and Ang index vs modified stiffness ratio

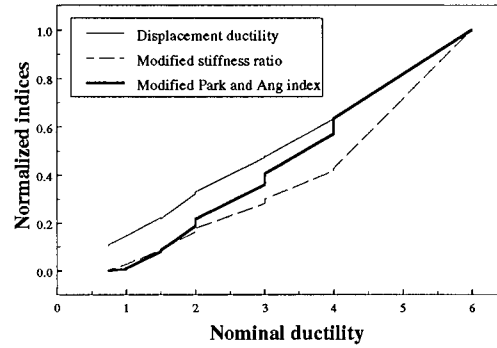
4.3.3 COMPARISON OF NORMALIZED INDICES FOR EACH SPECIMEN

For each specimen, the three indices calculated were normalized with respect to their peak value and plotted on a graph. Figures 4.5a to 4.5e show the resulting plots. For all five specimens, displacement ductility corresponds to the highest damage index values. The second largest index is the modified Park and Ang index followed by the modified stiffness ratio, except for specimen OSB5.

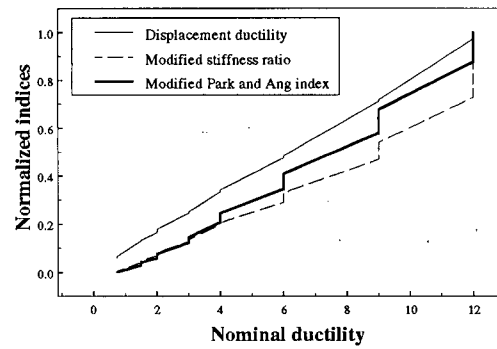
Two classification parameters are used to examine these figures. Considering an individual specimen, the relative slope of each normalized index represents one of these indicators. Figure 4.5 indicates that significant similarity between relative slope magnitudes refer to specimens with ductile failure mode. For example, specimen OSB1 show more variation in its normalized slopes than specimen OSB5. Secondly, the proximity of the curves represents another informative parameter. Graphs related to specimens with brittle failure modes show more distant curves than the ones associated to ductile failure modes. These two classification parameters suggest a performance ranking of OSB1, OSB2, OSB4, OSB3 and OSB5, consistent with experimental observations.



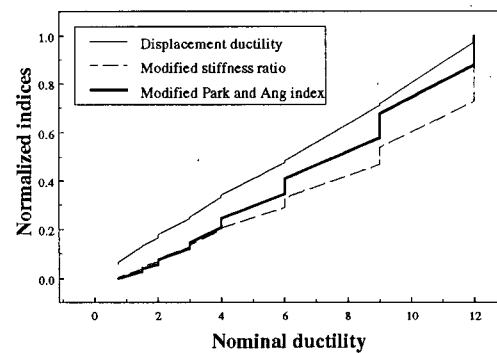
(b) Specimen OSB2



(c) Specimen OSB3



(d) Specimen OSB4



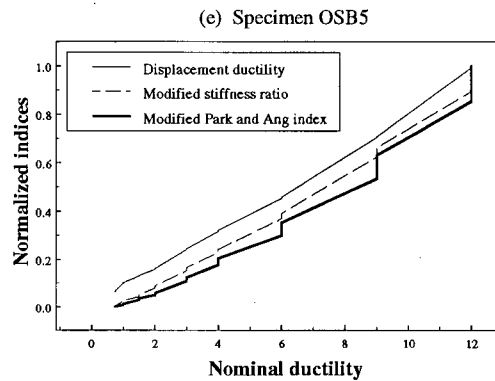


Figure 4.5 Comparison of normalized indices

4.4 CONCLUDING REMARKS

This chapter investigated damage assessment based on structural properties, such as displacement, stiffness and energy absorption. For the five specimens tested in the laboratory, three indices were evaluated at each of their nominal ductilities.

Based on these index values, specimen performance was compared and ranked according to different classification approaches. Two of the structural indices investigated, the **modified stiffness ratio** and **modified Park and Ang index**, could provide indication on the failure mode. For the specimen behavior comparison, two approaches gave a ranking similar to the one suggested by the observations of damage and the hysteresis loops: the **highest value of displacement ductility** and the **damage rate gradient of the modified stiffness ratio**.

A correlative analysis of the indices was performed in order to determine the similarity between damage characterization provided by each index. When normalized indices were compared, similar rates of approach to failure were obtained from a comparison between the **modified Park and Ang index** and the **displacement ductility**, while modified stiffness ratio seemed to converge less rapidly to failure than

displacement and modified Park and Ang index.

The following chapter explores damage assessment based on modal properties. As for structural damage indices, modal damage indices are evaluated for every nominal ductility sustained by each of the five bent specimens.

CHAPTER 5

DAMAGE ASSESSMENT BASED ON MODAL PROPERTIES

The dynamic response of a structure can be significantly affected by degradation of its structural elements and/or joints. Changes in the structure can be detected by the experimentally measured dynamic properties of the structure. As discussed in Chapter 2, modal damage indices are calculated from equations combining selected dynamic properties or their relative changes. Modal properties used to evaluate indices are usually the fundamental frequencies (or periods), damping ratios and mode shapes.

This chapter discusses the application of modal damage assessment techniques on the five specimens tested in the laboratory. The natural frequencies and damping ratios of each specimen were obtained from the dynamic tests. Three damage indices, derived from these two modal properties, were chosen to quantify damage levels of each specimen and are discussed in Section 5.1. Sections 5.2 and 5.3 describe the extraction of natural frequencies and damping ratios from vibration data obtained experimentally. These experimental dynamic properties are used to compute modal damage indices (Section 5.4). Based on the index values, Section 5.5 discusses the relative performance of the five specimens studied. Correlation between these three damage indices is also presented in this section.

5.1 CHOICE OF MODAL DAMAGE INDICES

The modal properties extracted from the experimental dynamic measurements limited the choice of modal damage indices. For each damage level, measurements obtained from the vibration tests provided two modal properties: natural frequencies and damping ratios. As indicated in the experimental testing procedure, vibrations from setups no.1 and no.2 were recorded before and after the loading sequences, while only setup no.1 was measured during the actual loading sequences. Since natural frequencies and

damping ratios can be obtained from only a few measurements, it was convenient to obtain these for each loading level. Identification of mode shapes requires a detailed discretization of the structure (setups no.1 and no.2) and thereafter longer testing durations. Because of time constraints, this was not performed for all damage levels, but only for the undamaged structure and for the structure at failure state. Considering that damage assessment had to be performed for each damage level, the choice of modal damage indices was limited to indicators derived from natural frequencies and/or damping ratios.

The type of specimen tested, a cap beam supported on two columns, also guided the choice of modal damage indices. Considering its relative structural simplicity, each specimen was treated as a single structural member. For a single element structure, local damage indices can be used as well as global indices. Local indices evaluate damage of individual element, while global indices can be applied to a structure composed of one member only. Consequently, the use of a global damage index was considered to quantify structural degradation of the bents.

Three modal damage indices, global in their definition and derived from natural frequencies or damping ratios, were chosen to assess degradation of the specimens. **Ultimate stiffness degradation** and **maximum softening** were evaluated on the basis of changes in natural frequencies (or periods) with damage level, termed here as the *frequency (or period) history*. The variation of damping through the loading procedure, referred to as the *damping history*, was used to evaluate a third global damage index, the **normalized damping ratios**.

5.2 EVALUATION OF NATURAL FREQUENCIES FROM EXPERIMENTAL DATA

Ultimate stiffness degradation (Equation 2.13) and maximum softening (Equation 2.16) can be derived from period (or frequency) history. For each specimen, a frequency history was assembled from vibration

data measured at each ductility level sustained. Ultimate stiffness degradation and maximum softening indices were then evaluated for each damage level.

This section discusses the theoretical background on identification of natural frequencies from experimental dynamic measurements. These analytical procedures are then applied to data obtained from the dynamic tests performed on the five specimens. A frequency history for each of the five specimens is presented and discussed for each damage level sustained.

5.2.1 THEORETICAL BACKGROUND

Measurements obtained from experimental modal testing are usually in the form of discretized time signals. Modal properties can be derived from direct time-domain analysis of these measurements. However, applying a particular transform algorithm on these time signals can lead to a more efficient procedure for determining modal properties. The Fourier Transform converts time-domain signals to their reciprocals in another domain, the frequency domain. Several relationships, derived in the frequency domain, provide useful information to identify natural frequencies. The background of the frequency-domain relationships used in this study is presented in the following sections.

5.2.1.1 THE FOURIER TRANSFORM

As stated earlier, vibration signals are measured in terms of an amplitude-versus-time function, referred to as a time history record. The Fourier Transform converts signals from the time domain, t , to the frequency domain, f . If $X(f)$ refers to the Fourier Transform of a time signal $x(t)$, their relationship can be expressed as:

$$X(f) = \int_{-\infty}^{+\infty} x(t) e^{-i2\pi ft} dt \dots\dots\dots [5.1]$$

Conversely, if $X(f)$ is known, then the inverse Fourier Transform will give $x(t)$:

$$x(t) = \int_{-\infty}^{+\infty} X(f) e^{i2\pi ft} df \dots\dots\dots [5.2]$$

The reciprocal functions $x(t)$ and $X(f)$ are said to be Fourier Transform pairs. The Fourier Transform is generally evaluated in a discrete form. The Fast Fourier Transform (FFT) algorithm, introduced first by Cooley and Tukey (1965), allows very efficient and accurate evaluations of the discrete Fourier Transform and its inverse.

The evaluation of a convolution integral (in the time domain) for dynamic analysis can be efficiently performed in the frequency-domain using the FFT. In this case, it is only required to obtain the FFT of the two functions involved in the convolution, computing their product and converting the result back in the time-domain by means of the inverse FFT. Although the process seems to require several steps, it is more computationally efficient than the direct computation of the convolution integral.

Analysis in the frequency domain also provides a clear representation of the frequency content of a particular signal. Different relationships, derived from the Fourier Transform of time signals, use this particularity to help determine the natural frequencies of a structural system.

5.2.1.2 INDICATORS OF NATURAL FREQUENCIES

Different frequency domain relationships can be used to identify fundamental frequencies. Some require input and output measurements while others only need output signals. This is important since some dynamic testing procedures measure both input and output signals while others only measure output signals. For example, a hammer test procedure usually measures input and output signals while ambient vibration testing only records output signals. Hence, the choice of natural frequency indicators depends on the type of dynamic testing performed.

For cases where **only output signals are measured**, the auto- or power spectral density (PSD) usually serves as natural frequency indicator. The PSD of a time-domain signal, $x(t)$, can be expressed as:

$$S_{xx}(f) = X^*(f) \cdot X(f) \dots\dots\dots [5.3]$$

in which $S_{xx}(f)$ is the PSD value at frequency f . $X(f)$ is the Fourier Transform of $x(t)$ (refer to Equation 5.1) and $X^*(f)$ is the complex conjugate of $X(f)$.

The auto-spectral density $S_{xx}(f)$ provides description of the frequency content of the original function $x(t)$. Peak values of the PSD indicate which are the dominant frequencies in the signal, some of which may be natural frequencies of the measured system. PSD's of several time signals can also be averaged to provide an accurate estimation of natural frequencies.

When **input and output signals are recorded**, the frequency response function (FRF) can also serve as fundamental frequency indicator. The frequency response function has several formulations, all derived from frequency domain relationships involving Fourier Transform of input and output signals. FRF reveals a frequency content associated to the structure studied, its peak values indicating potential natural frequencies.

A first formulation of FRF requires the Fourier Transforms of both input and output signals. Let $X(f)$ and $Y(f)$ be the Fourier Transform of the input and output signals, respectively. Then, the ratio of these two functions $H(f)$ defines the FRF as:

$$H(f) = \frac{Y(f)}{X(f)} \dots\dots\dots [5.4]$$

In this case, the FRF formulation contains noise in both the input and the output time signals. Natural frequencies can also be identified from two other FRF formulations, $H_1(f)$ and $H_2(f)$. The $H_1(f)$ estimator accounts for output measurement noise only while $H_2(f)$ only considers input measurement noise. They

result from combining auto- and cross-spectral densities. $H_1(f)$ is expressed as:

$$H_1(f) = \frac{X^*(f)}{X^*(f)} \cdot \frac{Y(f)}{X(f)} = \frac{S_{xy}(f)}{S_{xx}(f)} \dots \dots \dots [5.5]$$

The auto-spectral density of the input, $S_{xx}(f)$, was previously defined in Equation 5.3. The cross-spectral density, $S_{xy}(f)$, involves both the input and output signals and can be written as:

$$S_{xy}(f) = X^*(f) \cdot Y(f) \dots \dots \dots [5.6]$$

The other FRF estimator, $H_2(f)$, is determined as:

$$H_2(f) = \frac{Y^*(f)}{Y^*(f)} \cdot \frac{Y(f)}{X(f)} = \frac{S_{yy}(f)}{S_{yx}(f)} \dots \dots \dots [5.7]$$

where $S_{yy}(f)$ represents the power-spectral density of the output and $S_{yx}(f)$ is the cross-spectral density between output and input time signals $y(t)$ and $x(t)$. The latter is expressed as:

$$S_{yx}(f) = Y^*(f) \cdot X(f) = S_{xy}^*(f) \dots \dots \dots [5.8]$$

$H_1(f)$ and $H_2(f)$ are the two most common methods used to evaluate FRF since they provide an improved control on the noise contamination of the time signals compared to $H(f)$. However, $H_1(f)$ and $H_2(f)$ respectively under- and over-estimates the true FRF values. $H_1(f)$ is more accurate at antiresonance frequencies while $H_2(f)$ gives better estimates at resonance frequencies. These characteristics of $H_1(f)$ and $H_2(f)$ can be used together to obtain accurate estimates of FRF values, taking into account noise contamination in both the input and the output time signals. In order to reduce the biased error in all the frequency range, Park (1993) developed an improved FRF estimator, H_s , converging to $H_1(f)$ at antiresonance frequencies and $H_2(f)$ at resonance frequencies. Evaluation of H_s is primarily based on a scale factor δ , usually defined as a ratio between PSD's of input and output measurement noise. He suggested two methods to optimize this parameter. One algorithm is based on the estimation error of FRF's and requires a recursive process. The other method involves the coherence function and uses a

nonrecursive process. Once δ is known, H_s magnitude can be evaluated as:

$$|H_s| = \frac{1}{2} \left[|H_2| - \frac{\delta}{|H_1|} + \sqrt{\left(|H_2| - \frac{\delta}{|H_1|} \right)^2 + 4\delta} \right] \dots\dots\dots [5.9]$$

In the above equation, H_1 , H_2 and H_s respectively refer to $H_1(f)$, $H_2(f)$ and $H_s(f)$. The derivations of equation 5.9 as well as details of the recursive and non-recursive methods can be found in Park (1993).

The nonrecursive algorithm used is presented in more detail in Appendix D.

5.2.1.3 NATURAL FREQUENCY RELATED TO DIFFERENT DIRECTIONS OF MOTION

Natural frequencies of interest are generally associated with a specific direction of motion, either translations or rotations. In the case where only output signals are used in calculations, PSD's can be computed for individual signals as well as from their linear combinations. For two signals measuring vibrations in the same direction, PSD of their addition will enhance the contribution of frequencies associated with translation only since the torsional components are removed. On the other hand, PSD of their subtraction will enhance the contribution of natural frequencies associated with the torsional component of motion. When response and excitation signals are recorded, FRF's of input and output in the same direction can directly determine natural frequencies in that direction. For example, an impact in the vertical direction and a response signal in the same direction will provide indicators of vertical natural frequencies.

5.2.2 EVALUATION OF NATURAL FREQUENCY

As mentioned in the previous section, time histories of output signals, and input signals when recorded, can be combined in different frequency domain relationships to identify natural frequencies. In the dynamic testing performed on the bent specimens, time histories were recorded with two types of vibration tests, hammer test and ambient vibration test. This section presents typical time signals obtained from these two dynamic tests and describes the extraction procedure of natural frequencies based on

experimental measurements obtained. Initial analyses were performed on Specimen OSB1, mainly to investigate the extraction procedure based on hammer test measurements. Subsequently, a more detailed dynamic analysis was performed to extract fundamental frequency histories for the longitudinal direction. This direction was considered the most relevant direction of motion as it was in the direction of the applied lateral loading.

5.2.2.1 TYPICAL TIME SIGNALS

For both impact and ambient vibration testing, responses of the specimens were measured in the three principal orthogonal directions: longitudinal, transverse and vertical. No input signals were measured in the ambient vibration test, for which, by definition, the force applied to the structure cannot be controlled but is assumed to have significant amount of energy within the frequency range of interest. In the hammer test, excitation time histories were measured by the instrumented hammer. Figure 5.1 presents a typical output signal recorded during ambient vibration test. A typical hammer excitation signal is shown in Figure 5.2a and corresponding response signal, measured on the specimen, is plotted in Figure 5.2b. Acceleration amplitude of these time signals are recorded in volts, which can be converted in percentage of g 's (gravitational acceleration).

The random nature of ambient vibrations is well reflected in Figure 5.1. As mentioned in the experimental procedure, ambient vibrations are induced by external unspecified sources. On the other hand, input and output signals originating from the hammer test show particular trends (Figure 5.2). The input signal is a high-amplitude short-duration signal, typical for an impulse excitation. The response signal indicates a typical free-vibration motion, exponentially decreasing with time due to damping forces. These typical trends were also observed in the transverse and vertical directions of motion.

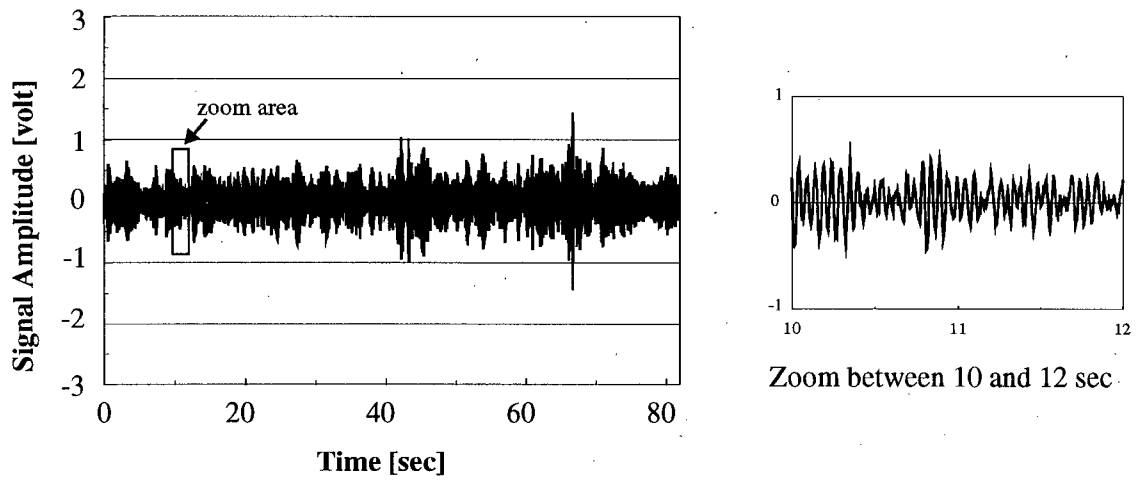


Figure 5.1 Ambient vibration output signal

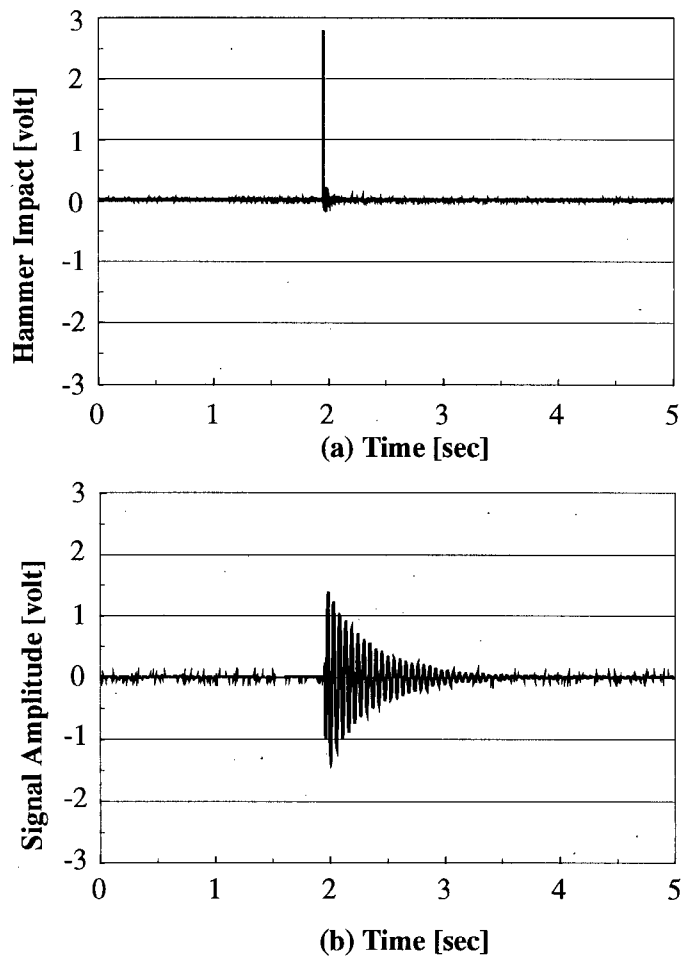


Figure 5.2 Impact vibration input (a) and output (b) signals

5.2.2.2 INITIAL STUDY OF NATURAL FREQUENCIES

This study included estimation of natural frequencies in longitudinal, transverse and vertical directions. Natural frequencies were first evaluated using input and output time signals measured in the hammer test. They were also evaluated from ambient vibration measurements and, subsequently, compared to the ones calculated from hammer test. These initial analyses were performed on the undamaged Specimen OSB1 with the vertical loading simulators activated and the lateral actuator installed.

Analysis of impact test measurements was based on evaluation of FRF's. In order to identify frequencies in the three directions studied, FRF's were evaluated using combinations of input and associated output signals recorded in the same direction. Calculations were performed using a computer program, FRF (Horyna, 1995), based on the evaluation of $H_I(f)$. For each combination, peak values of the FRF's, indicators of potential natural frequencies, were investigated and associated to corresponding natural modes. Considering a particular direction of motion, natural frequencies, obtained from signal combinations in that direction, were averaged to provide a reliable estimation. Table 5.1 summarizes signal combinations used for each direction of motion analyzed. Resulting values of natural frequencies, obtained from these calculations, are also presented. For the response signals (e.g. 5L), the first digit (5) refers to the node number where the sensor was located (refer to Figure 3.7). The second character (L) corresponds to the direction of measurement (L=longitudinal; T=transverse; V=vertical).

Direction of Motion	Excitation Signal	Response Signals Averaged	Natural Frequency [Hz]
longitudinal	longitudinal impact (setup no.1 or no.2)	1L, 2L, 5L, 6L	20.3
transverse	transverse impact (setup no.1 or no.2)	1T, 2T, 3T, 4T, 5T, 6T	5.9
vertical	vertical impact (setup no.1 or no.2)	2V, 3V, 4V, 5V	62.4

Note: Test conditions were: undamaged specimen, vertical load on and actuator connected.

Table 5.1 Natural frequencies of OSB1 extracted from impact vibrations

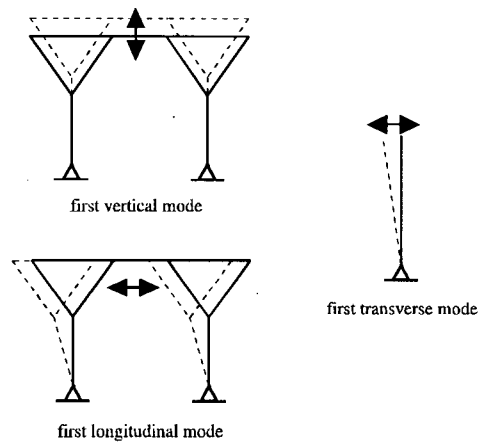
The ambient vibration data analysis performed used PSD's (Equation 5.3) and visualization of mode shapes to identify natural frequencies in the three principal directions. PSD's of output signals were investigated for each direction of motion studied. For each direction, a computer program, P2 (EDI, 1994), was used to evaluate PSD's associated to time signals in each direction. The program computed the average of normalized PSD's in order to obtain a representative estimation of natural frequencies in that direction. Resulting peak values of the averaged normalized PSD's served as potential natural frequency indicators. Validation of peak values as natural frequencies was completed by visual investigation of mode shapes. Mode shapes, corresponding to these peak values, were visualized using computer program VISUAL (Felber, 1993). Based on calculations with ambient vibration measurements, this program animates the structure motion at different frequencies and helps in the identification of mode shapes and natural frequencies. Table 5.2 gives details on output signals included in the analysis and indicates the natural frequencies in each direction.

Direction of Motion	Signals Averaged	Natural Frequency [Hz]
longitudinal (setup no.1 or no.2)	1L, 2L, 5L, 6L	19.6
transverse (setup no.1 or no.2)	1T, 2T, 3T, 4T, 5T, 6T	6.1
vertical (setup no.1 or no.2)	2V, 3V, 4V, 5V	59.2

Note: Test conditions were: undamaged specimen, vertical load on and actuator connected.

Table 5.2 Natural frequencies of OSB1 extracted from ambient vibrations

Fundamental longitudinal, transverse and vertical mode shapes; corresponding to the natural frequencies evaluated, are presented in Figure 5.3.



Figures 5.3 . Fundamental natural mode shapes of OSB1

For each direction, fundamental frequencies evaluated from the hammer test and the ambient test provided comparable values (see Tables 5.1 and 5.2). Hence, the extraction procedure, based on impact vibration measurements obtained experimentally, was considered adequate for identification of natural frequencies.

5.2.2.3 FUNDAMENTAL LONGITUDINAL FREQUENCY STUDY

Natural frequencies in the longitudinal direction were of interest in this study since substantial structural damage was expected from the loading in that direction. Fundamental longitudinal frequencies were evaluated for each specimen at each ductility level reached. Since dynamic testing was performed between sequences of actual loading of the specimens, vibration measurements were performed with vertical constant loading applied to the specimen and the lateral actuator system attached to the structure. Consequently, as in the preliminary study, longitudinal frequencies referred to the specimens under their experimentally setup conditions and not as free standing structures.

Prior to computation of frequency histories for each specimen, three FRF's formulations, presented previously, were compared in order to verify the adequacy of the FRF program used in the preliminary analysis. For comparison purposes, $H_1(f)$, $H_2(f)$ and $H_3(f)$ (Equations 5.5, 5.7, 5.9) were computed for

several combinations of longitudinal input and output. Figure 5.4 shows a typical comparison of these three FRF formulations.

At the low frequency range, the three FRF formulations show a rather low correlation between them. However, at the frequency range of interest, located in the neighborhood of the peak value, there is good agreement between the three FRF formulations. A close look in this peak region indicates slight differences in the plotted curves. In fact, assuming that $H_s(f)$ provides the exact frequency response function, $H_1(f)$ and $H_2(f)$ respectively under- and over-estimates the true FRF value. However, the natural longitudinal frequency, indicated by the *location* of the peak value, presents no significant variation. Consequently, the FRF computer program based on $H_1(f)$ was considered adequate to assess natural longitudinal frequency changes.

Each frequency evaluated was based on different sets of FRF calculations. Each set included impacts in the longitudinal direction and corresponding responses. As mentioned in the experimental procedure, two series of impacts were performed in the longitudinal direction for each ductility sequence (see Section 3.4.3.2.2). Since only setup no.1 was measured during the actual loading procedure, each series of impacts had only two accelerometers recording longitudinal vibrations (refer to Figure 3.7). Hence, a total of four FRF combinations (2 impact series x 2 sensors) were evaluated for each damage level. Natural longitudinal frequencies were subsequently averaged over the four combinations investigated.

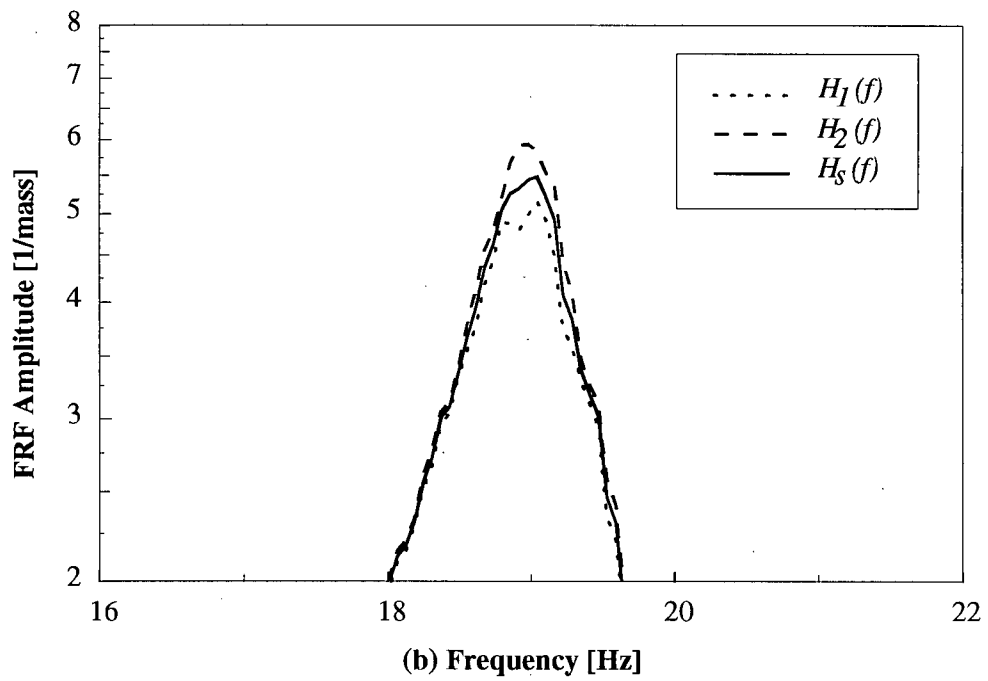
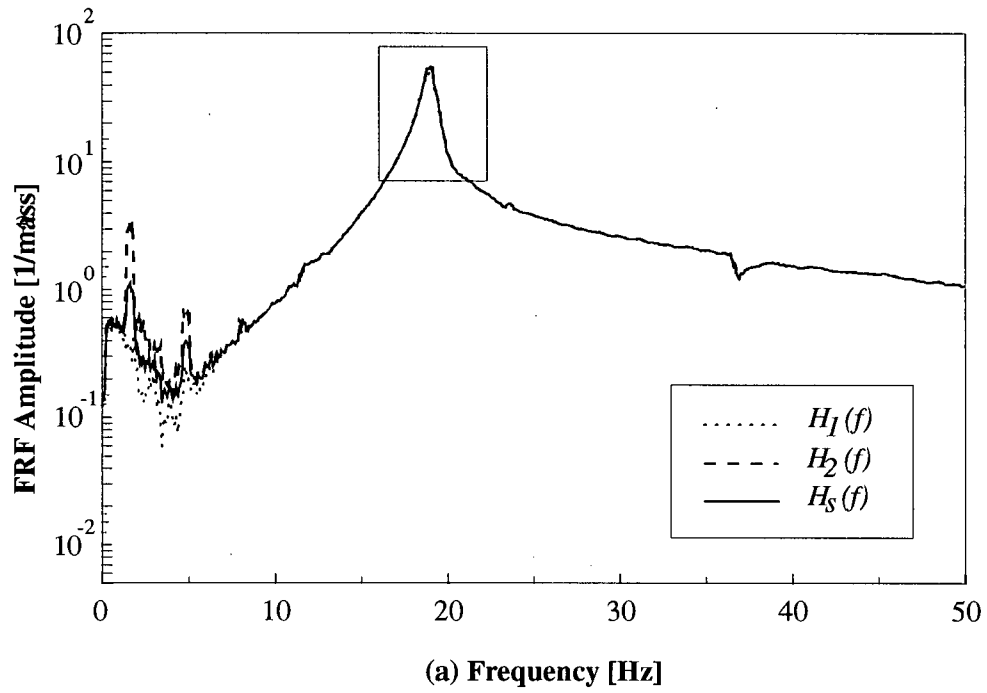


Figure 5.4 Comparison of FRF formulations: global (a) and zoom area (b)

Table 5.3 summarizes these four combinations. The results are presented and discussed in the following section.

Longitudinal Impact Set No.	Input Signal	Output Signal
1	longitudinal impact	5L
1	longitudinal impact	6L
2	longitudinal impact	5L
2	longitudinal impact	6L

Table 5.3 Input/output combinations for longitudinal FRF calculations

5.2.3 NATURAL LONGITUDINAL FREQUENCY HISTORY

Based on the extraction procedure presented above, natural longitudinal frequency history was evaluated for each specimen tested. Details of frequency processing is presented in Appendix B. Table 5.4 summarizes frequency history obtained for each specimen.

Ductility Level	f_L [Hz] Specimen OSB1	f_L [Hz] Specimen OSB2	f_L [Hz] Specimen OSB3	f_L [Hz] Specimen OSB4	f_L [Hz] Specimen OSB5
$\mu = 0$	20.3	20.1	22.3	21.0	18.9
$\mu = 0.75$	18.8	18.2	19.9	20.6	16.3
$\mu = 1$	17.5	17.1	*	20.4	20.8
$\mu = 1.5$	16.1	15.9	19.4	20.0	20.4
$\mu = 2$	15.1	18.0	18.2	19.2	19.1
$\mu = 3$	13.2	17.2	17.4	18.3	17.7
$\mu = 4$	13.0	11.5	17.0	18.0	18.1
$\mu = 6$	n/a	13.3	16.6	17.7	17.7
$\mu = 9$	n/a	n/a	16.1	17.2	17.0
$\mu = 12$	n/a	n/a	14.6	14.6	17.2

* no vibration measurements recorded

Table 5.4 Fundamental natural longitudinal frequency history for each of the 5 specimens

As indicated in Table 5.4, natural longitudinal frequencies range between 18.9 and 22.3 for the undamaged specimens and between 13.0 and 17.2 for specimens at failure state. Structural degradation is usually associated with an overall stiffness diminution. Since natural frequency is proportional to the square root of stiffness, an increase in structural damage (lowering of the stiffness) should correlate with a global decrease in natural frequency (see Chapter 2). This is clearly demonstrated by the overall frequency trends.

Figure 5.5 shows a graphical representation of the frequency histories. Looking at this figure, it can be seen that the rate of frequency decay differs from one specimen to another. For example, specimen OSB1 suggests a fast decreasing rate while specimen OSB5 indicates slow rate of frequency decay. Specimens OSB1, OSB3 and OSB4 indicate constant decreasing trend with increasing damage. However, detailed observations of Figure 5.5 indicate that for specimens OSB2 and OSB5 the fundamental longitudinal frequencies appear to increase for certain damage levels.

To verify these increases in frequency for specimens OSB2 and OSB5, impact time histories, associated to these frequency irregularities, were investigated in more detail. In order to obtain a better frequency resolution in the FRF curves, these original time signals were padded with zeros and re-evaluated. The resulting fundamental longitudinal frequencies showed no variation when compared with the initial frequency estimations. It was concluded that the calculation procedure was accurate and that the irregularities might be related to the time signal recorded. The ambient vibration measurements were then analyzed. For the ductility levels indicating anomalies, natural frequencies, evaluated using longitudinal PSD's, were compared with those obtained from hammer test measurements. The results correlated very well. It was then concluded that these frequencies were somewhat reflecting structural conditions of the structure considered.

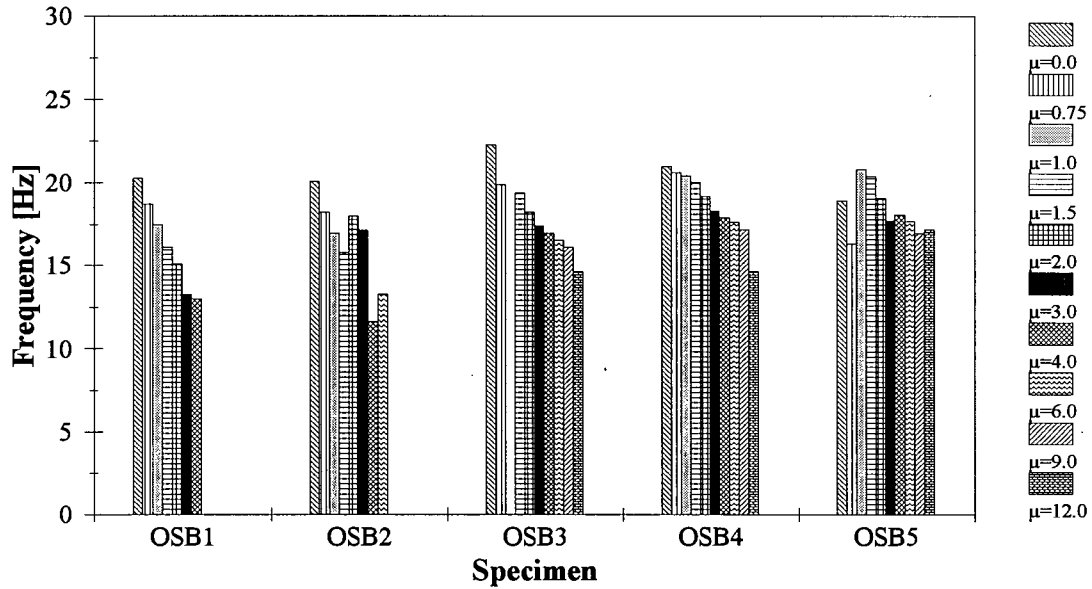


Figure 5.5 Sensitivity of the natural longitudinal frequency to structural damage

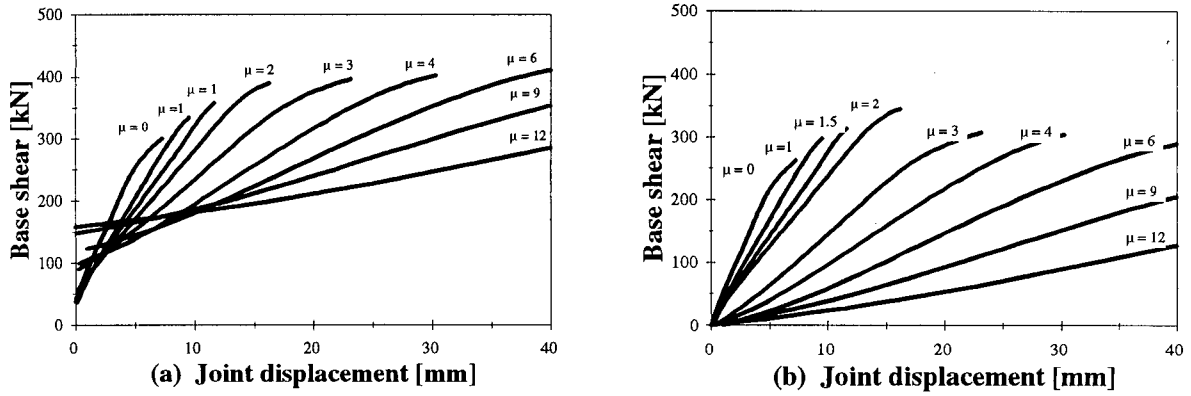


Figure 5.6 Example of stiffness study for specimen OSB5: global (a) and zero slope (b)

As no inconsistencies could be related to the time signals, the frequency anomalies of OSB2 and OSB5 had to be explained by means other than signal analysis. An approach based on the structural response of the specimens was then investigated. Assuming that these frequencies were accurate, this approach suggested a partial recovery in the structure stiffness. To explore this stiffness recovery assumption, experimental stiffnesses were estimated using hysteresis loops recorded during lateral loading. These stiffnesses corresponded to the initial slopes in the hysteresis curves. For a particular ductility level, the corresponding stiffness referred to the *initial tangent stiffness* of the *first cycle for the subsequent ductility level*. If the recovery assumption holds, these relative stiffnesses would show the same variation trend than the corresponding frequency history. Comparison of the initial slopes did not provide conclusive results. No recovery in the stiffness was noticed but a constant decrease of slopes with increasing damage levels was observed. An example of the initial tangent stiffness for specimen OSB5 at each ductility level is shown in Figure 5.6. Comparison of slope values clearly demonstrated no recovery in stiffness.

The type of retrofit was also investigated as a possible explanation of the anomalies in the frequency histories. As described in Chapter 3, specimen OSB2 was retrofitted with its cap beam prestressed longitudinally while external prestressing and fiberglass were used to retrofit specimen OSB5. The retrofit scheme of specimen OSB4 also included prestressing of the cap beam and its corresponding frequency trend did not indicate any anomalies. It was concluded that anomalies of the frequency history for specimen OSB2 were not related to its retrofit scheme. For specimen OSB5, the technical literature did not suggest particular behavior of fiberglass with increasing cracking of the corresponding retrofitted members. It was then concluded that anomalies of specimen OSB5 were not associated with its retrofit scheme.

As no other explanations could be provided, frequency anomalies were associated to uncontrolled experimental factors. Structural effects associated to the truss frame, the jack pressure residual and the pin

support represent factors that could have modified the real structure response. Frequencies corresponding to the irregular ductility levels were used without any modifications in further studies.

5.3 EVALUATION OF DAMPING FROM EXPERIMENTAL DATA

Evaluation of normalized damping ratios (Equation 2.23) is derived from damping history. Two types of damping were evaluated, viscous damping and hysteretic damping. At each loading level sustained by the specimen, these damping ratios were extracted respectively from vibration measurements or recorded hysteresis loops. Modal damage assessment, based on normalized damping ratios, was then completed for each specimen.

This section presents the theoretical background for evaluation of viscous and hysteretic damping from test data. These extraction procedures are then applied on data obtained from experimental tests performed on the five specimens. Damping histories are finally presented for each specimen.

5.3.1 THEORETICAL BACKGROUND

The motion of a structure is resisted by several kinds of damping forces, originating from air resistance and/or internal or external frictions. These forces are opposed to the direction of motion of the structure. Viscous damping, Coulomb friction and hysteretic (or structural) damping represent different types of damping forces restraining the movement of a system. From a practical point of view, damping forces are considered complex in nature and difficult to quantify. However, several damping extraction procedures have been derived to quantify damping forces. The following sections discuss two of them: viscous and hysteretic damping forces.

5.3.1.1 VISCOUS DAMPING

The equation of motion governing the free-vibration of a viscously damped single-degree-of-freedom system (SDOF) is:

$$mu'' + cu' + ku = 0 \dots\dots\dots [5.10]$$

where m , c and k are the mass, viscous damping and stiffness constants, respectively. Symbols u , u' and u'' refer to displacement, velocity and acceleration time histories, respectively. The free-vibration response of this system is:

$$u(t) = \rho e^{-\omega \xi t} \cdot \sin(\omega_d t + \phi) \dots\dots\dots [5.11]$$

Parameters ρ and ϕ respectively represent the amplitude and phase angle of the response. They are evaluated from initial conditions of displacement and velocity. The system natural angular frequency, ω , is evaluated from the structure stiffness and mass constants,

$$\omega = \sqrt{\frac{k}{m}} \dots\dots\dots [5.12]$$

and the damped natural frequency, ω_d , is defined as:

$$\omega_d = \omega \sqrt{1 - \xi^2} \dots\dots\dots [5.13]$$

The parameter ξ represents the damping ratio, defined as a fraction of the critical damping. It is related to the damping constant with $\xi = c/2\omega m$.

For structural systems and most of mechanical systems, the damping is in general less than critical. An underdamped free-vibration response of a SDOF system is shown in Figure 5.7.

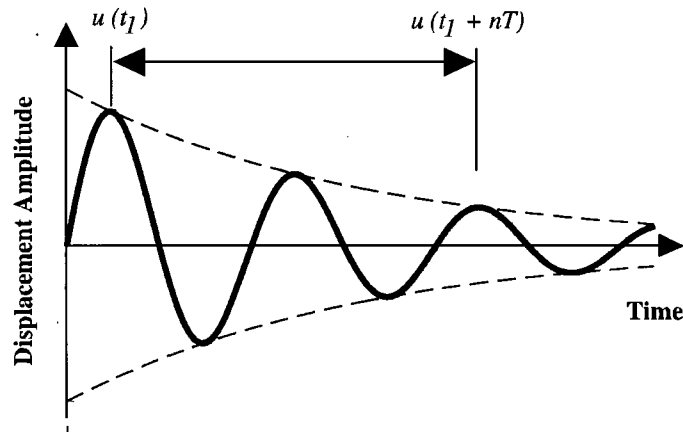


Figure 5.7 Viscously damped free-vibration response

The underdamped free-vibration response decreases in amplitude with each new cycle of motion. Equation 5.11 indicates that the displacement amplitude actually decays exponentially with time. The rate of decrease depends on the damping ratio ξ . In order to evaluate ξ value, let's consider the decrease in displacement after one cycle. Denoting the displacement at time t_1 by $u(t_1)$, then

$$u(t_1) = \rho e^{-\omega \xi t_1} \cdot \sin(\omega_d t_1 + \phi) \dots\dots\dots [5.14]$$

After a complete cycle of period $T=2\pi/\omega_d$, the displacement is

$$u(t_1 + 2\pi/\omega_d) = \rho e^{-\omega \xi (t_1 + 2\pi/\omega_d)} \cdot \sin(\omega_d t_1 + \phi) \dots\dots\dots [5.15]$$

The ratio of $u(t_1)$ and $u(t_1 + 2\pi/\omega_d)$ provides a measure of the reduction in displacement. The natural log of this ratio, called the logarithmic decrement, δ , is constant and is given as:

$$\delta = \ln \left\{ \frac{u(t_1)}{u(t_1 + 2\pi/\omega_d)} \right\} \dots\dots\dots [5.16]$$

Using Equations 5.14 and 5.15, equation 5.16 can be reduced to

$$\delta = 2\pi \xi \frac{\omega}{\omega_d} = 2\pi \frac{\xi}{\sqrt{1-\xi^2}} \dots\dots\dots [5.17]$$

from which ξ can be found to be

$$\xi = \frac{\delta}{\sqrt{4\pi^2 + \delta^2}} \dots \dots \dots [5.18]$$

Considering n cycles of motion, the displacement will decrease from $u(t_1)$ to $u(t_1 + nT)$, giving a ratio of

$$\frac{u(t_1)}{u(t_1 + nT)} = e^{2\pi\xi n\omega/\omega_d} \dots \dots \dots [5.19]$$

The natural log of this ratio gives

$$\ln \left\{ \frac{u(t_1)}{u(t_1 + nT)} \right\} = 2\pi\xi n \frac{\omega}{\omega_d} = n\delta \dots \dots \dots [5.20]$$

The viscous damping ratio, ξ , is then a function of δ , which in turn can be evaluated from amplitudes derived from underdamped free-vibration displacement signals.

5.3.1.2 HYSTERETIC DAMPING

As mentioned previously, hysteretic or structural damping refers to internal friction arising within the structure. Internal friction generates heat due to the relative motion of material particles. This heat, or loss of energy, is associated to degradation of the structure. It can be measured by the load-deformation curve, commonly called hysteresis loop. The area enclosed by a complete loop of this curve represents the loss of energy per cycle. Figure 5.8 shows a typical hysteresis loop. The shaded area is related to the loss of energy for a particular cycle.

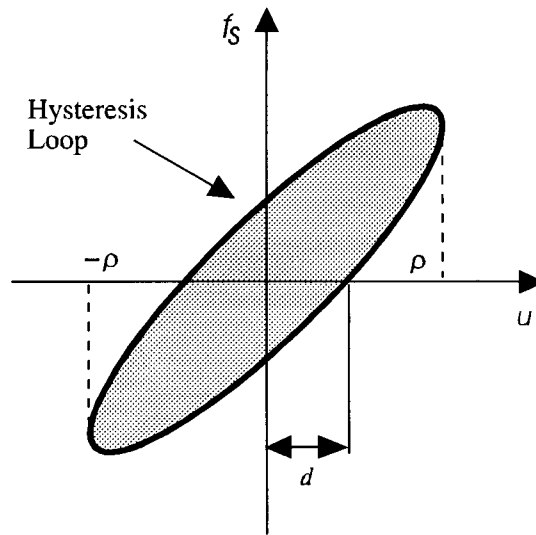


Figure 5.8 Hysteretic damping from hysteresis loop

In the case of hysteretic damping, the equation of motion is expressed as:

$$mu'' + F_s(u) = 0 \dots\dots\dots[5.21]$$

where $F_s(u)$ is a non-linear function of displacement representing the restoring capacity of the system.

This force can be expressed in terms of the displacement and velocity of the system as:

$$F_s(u) = ku + \frac{\eta k}{\omega} u' \dots\dots\dots[5.22]$$

Constant η is the hysteresis damping fraction and ω is the undamped angular natural frequency in the free-vibration case. Correlating this equation with the viscous damping equation of motion (Equation 5.10), an equivalent viscous damping, c_h , can be determined as:

$$c_h = \frac{\eta k}{\omega} \dots\dots\dots[5.23]$$

Knowing that $c=2\xi\omega m$, this equation becomes, after some algebraical manipulations,

$$\xi_h = \frac{\eta}{2} \dots\dots\dots[5.24]$$

Constant η can be obtained by substituting the free-vibration response (Equation 5.11) and its first

derivative in the $F_s(u)-u$ relationship. The corresponding function refers to a load-displacement curve or hysteresis loop. Consequently, its enclosed area corresponds to the loss of energy for one cycle. It can be shown that, for free-vibration response (Equation 5.11), the $F_s(u)-u$ curve represents an ellipse, such as the one shown in Figure 5.8. The parameters d and ρ in the figure are respectively defined as permanent displacement and maximum displacement sustained during the cycle. Based on the ellipse equation, d and

$$\rho \text{ must satisfy: } d = \rho \frac{\eta}{\sqrt{1 + \eta^2}} \dots\dots\dots [5.25]$$

$$\text{or, inversely, } \eta = \frac{d}{\sqrt{\rho^2 - d^2}} \dots\dots\dots [5.26]$$

Equation 5.24 indicates that the equivalent damping ratio, ξ_h , can be evaluated from constant η , which, in turn, is computed on the basis of two hysteretic parameters, d and ρ . Hence, if the hysteresis curves are obtained experimentally, measures of d and ρ will provide the hysteresis damping fraction, half of which gives the equivalent viscous damping ratio.

5.3.2 EVALUATION OF DAMPING

The two damping approaches described above, viscous and hysteretic, were applied to the five specimens tested in the laboratory. Viscous damping was calculated from vibration measurements while hysteretic damping was estimated from hysteresis loops measured during the loading procedure.

Damping ratios, both viscous and hysteretic, were evaluated for all specimens and each ductility level. Since dynamic testing was performed between sequences of actual loading of the specimens, vibration responses were measured with vertical loading applied and actuator system positioned. Consequently, as in the frequency study, damping ratios referred to the specimens under their experimentally setup conditions.

5.3.2.1 VISCOUS DAMPING

As shown in the damping theoretical background, evaluation of viscous damping using the logarithmic decrement is based on free-vibration displacement time signals. The random nature of ambient vibrations do not satisfy the free-vibration assumption. Moreover, other methods of damping evaluation from ambient vibrations do not generally provide reliable damping estimations (refer to Schuster, 1994). Consequently, estimation of viscous damping do not use these measurements. However, the impact responses satisfy this free-vibration pattern. In fact, the hammer impulse, related to an impulse-momentum relationship, can be translated in an initial velocity condition. By definition, an initial velocity generates a free-vibration displacement response. In this study, response time signals refer to acceleration time histories and it would appear that the method described above is not directly applicable. However, the viscous damping concept can be easily expanded to acceleration time signals. It can be shown that the damping approach is still valid with acceleration time signals, and therefore the measurements recorded during the hammer test were used in equation 5.20 without the need to convert them into displacement time histories.

For each ductility level, two damping estimations were performed, each of which was based on an individual response signals. As described in the experimental procedure, each set of impacts contained responses to four hammer blows. The longitudinal sets were used for damping evaluation. These time signals were conditioned with low-pass filters prior to damping computations. In order to obtain a more reliable estimation, parameter δ (Equations 5.20) was evaluated using several cycles. Once δ was evaluated, the damping ratio was obtained using Equation 5.18. Average of the two damping estimations was retained as damping ratio for the corresponding damage level. Conditioning process as well as investigation of time signal amplitudes were performed using computer program Ultra (Felber, 1993).

5.3.2.2 HYSTERETIC DAMPING

Hysteretic damping is based on the structure load-displacement curves. Hysteresis loops obtained for each specimen were presented in Chapter 3. As mentioned in the experimental procedure, each load sequence consisted of three complete load cycles, forward and reverse, each reaching the same displacement level. The last cycle, corresponding to the most damaged state, was used for damping estimation. For this cycle, parameters d and ρ had to be determined for each ductility level. With d and ρ , the hysteresis damping fraction η could be evaluated using Equation 5.26. Finally, the equivalent viscous damping ratio was computed using Equation 5.24.

5.3.3 DAMPING HISTORY

Based on the extraction procedures presented above, viscous and hysteretic damping histories were evaluated for each specimen tested. Tables 5.5 and 5.6 summarize these damping values while Figures 5.9 and 5.10 present the results in graphical form.

Ductility Level	ξ_v [%] Specimen OSB1	ξ_v [%] Specimen OSB2	ξ_v [%] Specimen OSB3	ξ_v [%] Specimen OSB4	ξ_v [%] Specimen OSB5
$\mu = 0$	3.25	3.61	3.04	3.02	3.49
$\mu = 0.75$	3.27	3.54	3.36	2.63	4.04
$\mu = 1$	3.74	3.32	*	2.07	2.05
$\mu = 1.5$	4.17	3.08	2.07	2.09	2.31
$\mu = 2$	4.60	2.83	1.81	1.98	2.19
$\mu = 3$	**	1.35	1.67	1.66	1.59
$\mu = 4$	**	5.74	1.56	1.50	1.52
$\mu = 6$	n/a	6.55	1.63	1.33	1.43
$\mu = 9$	n/a	n/a	1.56	1.50	1.18
$\mu = 12$	n/a	n/a	2.30	2.07	1.27

* no vibration measurements recorded / ** assumption of viscous damping not applicable

Table 5.5 Viscous damping ratios

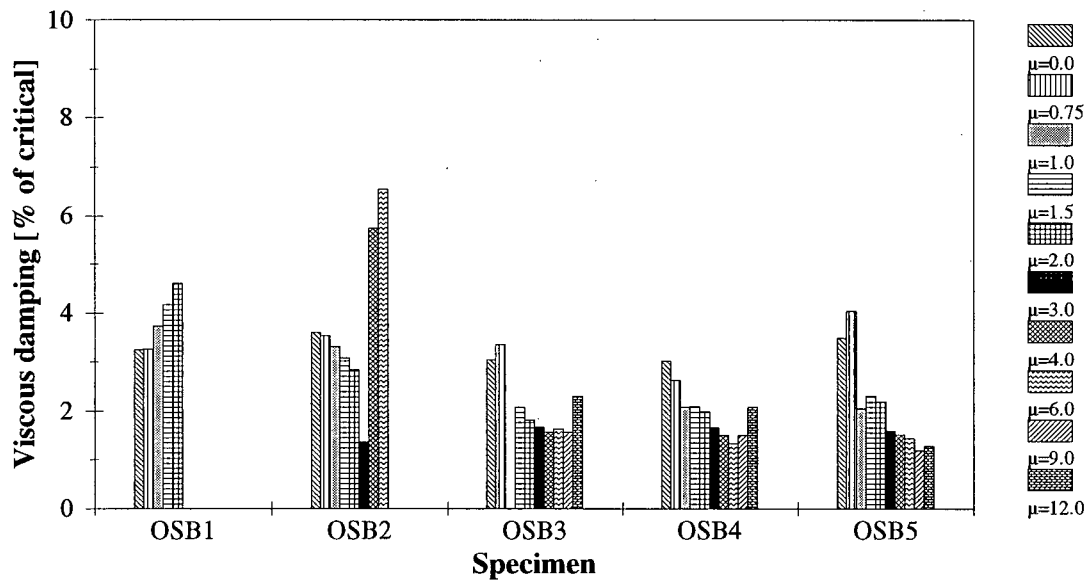


Figure 5.9 Sensitivity of viscous damping to structural damage

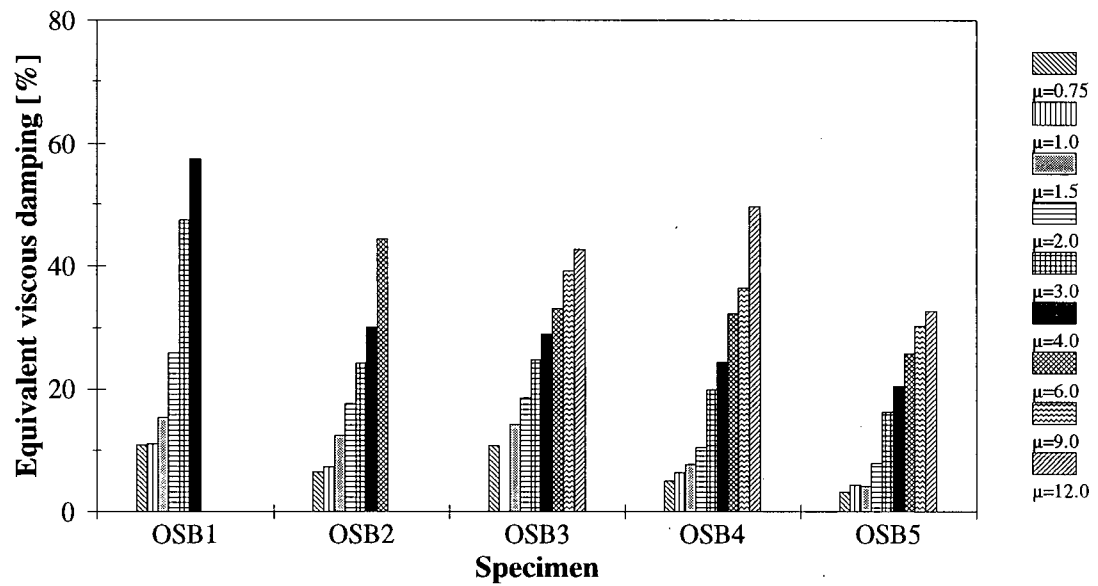


Figure 5.10 Sensitivity of hysteretic damping to structural damage

Ductility Level	ξ_h [%] Specimen OSB1	ξ_h [%] Specimen OSB2	ξ_h [%] Specimen OSB3	ξ_h [%] Specimen OSB4	ξ_h [%] Specimen OSB5
$\mu = 0.75$	10.86	6.48	10.78	4.91	3.20
$\mu = 1$	11.05	7.31	*	6.36	4.37
$\mu = 1.5$	15.40	12.38	14.19	7.71	4.14
$\mu = 2$	25.84	17.55	18.46	10.37	7.93
$\mu = 3$	47.30	24.12	24.67	19.80	16.13
$\mu = 4$	57.39	29.89	28.86	24.21	20.43
$\mu = 6$	n/a	44.32	33.01	32.18	25.79
$\mu = 9$	n/a	n/a	39.15	36.30	30.12
$\mu = 12$	n/a	n/a	42.63	49.61	32.55

* no vibration measurements recorded

Table 5.6 Equivalent hysteretic damping ratios

From Tables 5.5 and 5.6, it can be seen that the two types of damping do not provide comparable values. For viscous damping, values range between 1% and 7%. Equivalent hysteretic damping estimates, ranging between 3% and 58%, are much higher values than those for viscous damping.

It is interesting to note that viscous damping was affected by modulation appearing in the time signals of the damaged structures. This phenomenon is shown in Figure 5.11 where a comparison of response signals for two different damage level is presented. It can be seen that modulation is present in the degraded structure and consequently alters the exponential decay. For specimen OSB1, a viscous damping mechanism could not be assumed for some high ductility levels where presence of modulation in the time signals was significantly altering the exponential decay.

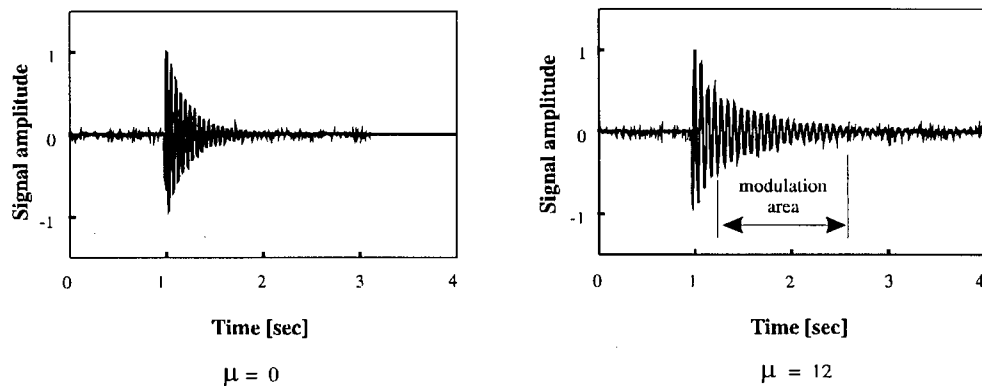


Figure 5.11 Modulation in the response time signals

As indicated in Figures 5.9 and 5.10, the two types of damping investigated show quite different trends. For viscous damping, histories indicate no clear trend with increasing damage. Except for specimen OSB1, which shows increasing damping, the ratios suggest an overall decrease with ductility levels. However, detailed observations of the trends indicate quite scattered values. At high damage levels, the significant presence of modulation in time signals affected the exponential decay, typically associated with the free-vibration response of an underdamped system. Hence, viscous ratio was not considered a reliable damping mechanism to characterize the behavior of these structures.

Unlike viscous damping, hysteretic damping indicates definite trends with ductility levels. In fact, all five specimens show increasing hysteretic damping values with increasing degradation. It was previously shown that hysteretic damping forces are related to internal friction restraining the structure behavior. As more internal friction occurs with degradation of the system, hysteretic damping forces should theoretically increase with damage. Figure 5.10 confirmed this observation. Hysteretic damping was then considered a reliable indicator of damping experienced by the specimens. However, the rate of increase slightly varies from one specimen to another. For example, specimen OSB1 indicates very higher

increasing rate when compared to the four other specimens tested.

In summary, a viscous mechanism was considered not applicable while damping generated from internal friction within the structure was assumed adequate to assess damping. These conclusions indicate that the hysteretic damping model is more representative of behavior of real structures.

5.4 EVALUATION OF DAMAGE INDICES

Three modal damage indices were previously selected to quantify degradation sustained by the specimens tested. Two of these indicators, ultimate stiffness degradation and maximum softening, required evaluation of natural frequency history. The third one, normalized damping ratio, required computation of damping for each ductility level. The previous sections detailed extraction procedures of these two dynamic properties. The present section describes evaluation of the modal damage indices. As dynamic properties evaluated correspond to the first longitudinal mode, damage indices will also refer to that direction of motion.

5.4.1 ULTIMATE STIFFNESS DEGRADATION

In section 2.2.1, the ultimate stiffness degradation was defined as:

$$D = \frac{T_i - T_0}{T_0} \dots\dots\dots [5.27]$$

where T_0 is the undamaged fundamental period of the structure and T_i represents the fundamental period at cycle i . As natural frequencies were identified instead of natural periods, it was convenient to transform this equation in terms of frequencies:

$$D = \frac{f_0 - f_i}{f_i} \dots\dots\dots [5.28]$$

where f_0 refers to the undamaged fundamental frequency and f_i represents the fundamental frequency at cycle i . For every specimen, f_0 corresponded to the natural longitudinal frequency obtained at ductility level $\mu=0$ while f_i referred to its fundamental longitudinal frequencies of subsequent ductility cycles. Based on values of f_0 and f_i , ultimate stiffness degradation was computed using Equation 5.28 for each damage level. This procedure was repeated for each specimen.

5.4.2 MAXIMUM SOFTENING

Maximum softening was introduced in section 2.2.1 as:

$$D_m = 1 - \frac{T_0}{T_m} \dots\dots\dots [5.29]$$

where T_0 and T_m respectively refer to the undamaged natural period and the maximum period value experienced by the structure during loading. These parameters were schematically defined in Figure 2.1. As for the ultimate stiffness degradation, it was useful to express this index in terms of frequencies. However, the maximum period will correspond in this case to the lowest frequency:

$$D_m = 1 - \frac{f_{min}}{f_0} \dots\dots\dots [5.30]$$

As for ultimate stiffness degradation, f_0 referred to the natural longitudinal frequency obtained at ductility level $\mu=0$. f_{min} had an initial value of f_0 . For each ductility level i , the fundamental longitudinal frequency, f_i , was compared to f_{min} , which was updated with this examined frequency f_i if necessary. Based on values of f_0 and f_{min} , maximum softening was computed using Equation 5.30 for each damage level. These calculations were repeated for all five specimens.

5.4.3 NORMALIZED DAMPING RATIO

From section 2.2.1, the normalized damping ratios are evaluated from damping histories. Two approaches were used to evaluate experimental damping, viscous and hysteretic damping. Comparison of resulting

damping histories showed that hysteretic damping was more representative of real structure behaviors. Hence, calculations of the normalized damping ratio indices were performed on hysteretic damping histories only. Equation 5.31 gives the formulation of this index.

$$D = \frac{\xi_i - \xi_0}{\xi_0} \dots\dots\dots [5.31]$$

where ξ_0 is the equivalent damping value of the undamaged structure and ξ_i represents the damping value evaluated at cycle i . Since no damping value was obtained for $\mu=0$, for which no hysteresis curve was measured, the undamaged damping ratio, ξ_0 , was then considered equivalent to the value obtained for the next ductility level, $\mu=0.75$, for which data was available. This assumption was considered adequate since at ductility 0.75 the specimen behavior was still within the linear range. The term ξ_i denotes the equivalent damping values of subsequent ductility cycles. Based on ξ_0 and ξ_i values, normalized damping ratio indices were computed with Equation 5.31. Each specimen indices were evaluated using the same procedure.

5.5 RESULTS AND COMPARISON OF DAMAGE INDICES

Ultimate stiffness degradation, maximum softening and normalized damping ratio were calculated for every ductility level sustained by each specimen. These indices provide useful information for comparison of specimen behaviors. This section presents a comparison of index histories for each of the specimens tested. The similarity between damage characterization provided by each index is also investigated.

5.5.1 COMPARISON OF SPECIMEN BEHAVIORS

Three modal damage indices were evaluated for each specimen tested in the laboratory. Specimen performances were compared by examining each index evaluated for the five experimental specimens. Figures 5.12a to 5.12c show these comparisons for ultimate stiffness degradation, maximum softening and

normalized damping ratio, respectively. Index histories are presented with increasing ductility levels. The displacement ductilities refer to real ductility values, evaluated from experimental hysteresis loops. As demonstrated in Chapter 4, these real displacement ductilities were more representative of the structure behavior than the nominal ductilities, derived during the testing procedure.

5.5.1.1 ULTIMATE STIFFNESS DEGRADATION

Figure 5.12a shows the variation of ultimate stiffness degradation with increasing ductility level. The index values range approximately from 0 to 0.8. Maximum damage indices reached 0.56 (OSB1), 0.73 (OSB2), 0.52 (OSB3), 0.43 (OSB4) and 0.16 (OSB5). They were obtained at failure for specimens OSB1, OSB3 and OSB4 while intermediate sequences provided maximum index values for OSB2 and OSB5. Figure 5.12a also shows negative index values for low ductility levels of specimen OSB5. Anomalies observed in OSB2 and OSB5 frequency histories (see Section 5.2.3), where some frequencies were increasing instead of decreasing, explain these disparities in the index history. Ultimate stiffness degradation obtained at failure of specimens OSB2 and OSB5 were 0.51 and 0.10.

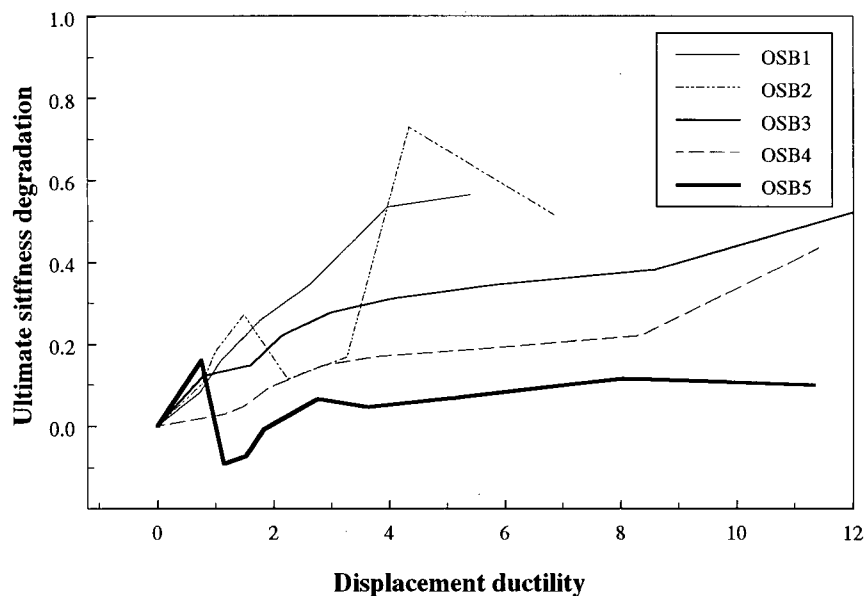


Figure 5.12a Comparison of specimen behaviors: ultimate stiffness degradation

Trends of index histories also provide information on the responses of the specimens. For all five specimens, the damage indices overall increase with increasing structural damage. Damage rates were calculated as the slopes of fitted curves, obtained from linear regressions on the index values. For specimens OSB1 and OSB2, damage rates were similar, 0.112 for OSB1 and 0.096 for OSB2. Similarly, the computed slopes of the fitted curves for OSB3, OSB4, and OSB5 were 0.051, 0.035 and 0.011, respectively. Table 5.7 summarizes index these characteristics, including maximum and final values as well as calculated slopes or damage rates.

Specimen	Peak Index Value	Final Index Value	Calculated Damage Rate
OSB1	0.56	0.56	0.112
OSB2	0.73	0.51	0.096
OSB3	0.52	0.52	0.051
OSB4	0.43	0.43	0.035
OSB5	0.16	0.10	0.011

Table 5.7 Ultimate stiffness degradation characteristics

High ultimate stiffness degradation values are associated with high structural damage. Looking at final indices, performance of specimens would then be ranked, starting with the poorest behavior, OSB1, OSB3, OSB2, OSB4 and OSB5. This classification is comparable with the one obtained from preliminary observations of specimen damage (see Section 3.5). However, from experimental observations, OSB2 indicated a poorer behavior than OSB3.

Comparison of damage rates can as well serve as performance indicator, where higher slopes would indicate significant degradation at low ductility level. According to this performance classification, the best specimen response would be OSB5 followed by OSB4, OSB3, OSB2 and finally the original design OSB1. This classification agrees with observations of damage during the test (see Chapter 3).

5.5.1.2 MAXIMUM SOFTENING

Histories of maximum softening index with respect to increasing degradation is shown in Figure 5.12b. Index values vary roughly from 0 to 0.5. Unlike ultimate stiffness degradation, each highest maximum softening index matches its corresponding final values for all five specimens. Since this index is partially derived from the maximum value of the natural period (Equation 5.29), it accounts for the maximum solicitation experienced by the structure up to the cycle under study. Consequently, final index values will always coincide with the maximum indices. Corresponding final maximum softening reached 0.36 (OSB1), 0.42 (OSB2), 0.34 (OSB3), 0.30 (OSB4) and 0.14 (OSB5).

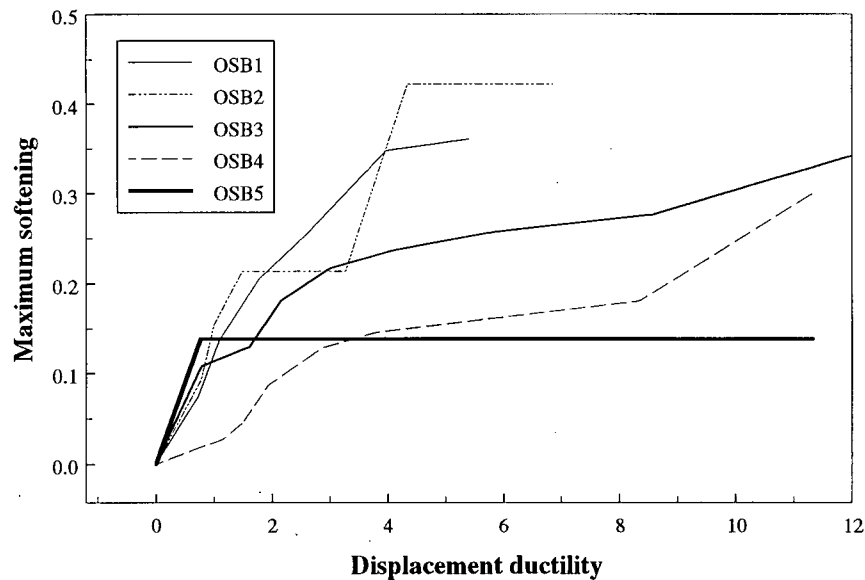


Figure 5.12b Comparison of specimen behaviors: maximum softening

Trends of index histories were also investigated to assess structural response. Figure 5.12b shows that damage of all five specimens indicates a steady increase of index values. For specimens OSB1 and OSB2, damage rates, associated to computed slopes of the fitted curves, are similar with 0.081 (OSB1) and 0.076 (OSB2). Damage rates of specimens OSB3, OSB4 and OSB5 are all comparable with values of 0.036, 0.027 and 0.021, respectively. Table 5.8 summarizes index characteristics described above, including final index values and calculated damage rates.

Specimen	Final Index Value	Calculated Damage Rate
OSB1	0.36	0.081
OSB2	0.42	0.076
OSB3	0.34	0.036
OSB4	0.30	0.027
OSB5	0.14	0.021

Table 5.8 Maximum softening characteristics

As for ultimate stiffness degradation, high maximum softening values correspond to high structural degradation. Looking at final index values, performance of specimens would then be ranked, starting with the poorest behavior, as follows: OSB2, OSB1, OSB3, OSB4 and OSB5. Since this performance classification shows that the original design OSB1 behaved in a superior way than retrofitted version OSB2, it was considered inadequate to assess damage.

If damage rate is the basis for damage comparison, the best specimen response would be OSB5 followed by OSB4, OSB3, OSB2 and OSB1. As for ultimate stiffness degradation, this classification agrees with preliminary observations of damage.

5.5.1.3 NORMALIZED DAMPING RATIO

Figure 5.12c shows normalized damping ratio histories compared to increasing degradation. Index values range between 0 and 10. As for maximum softening, final and highest indices of damping indices coincide for all five specimens. However, this index does not directly account for the maximum damping affecting the structure up to the cycle under study. The correspondence between final and maximum values originates from the constant increasing hysteretic damping trends obtained from experimental damping (refer to Figure 5.10). Figure 5.12c indicates that the maximum index values attained were 4.28 (OSB1),

5.84 (OSB2), 2.95 (OSB3), 9.10 (OSB4) and 9.17 (OSB5).

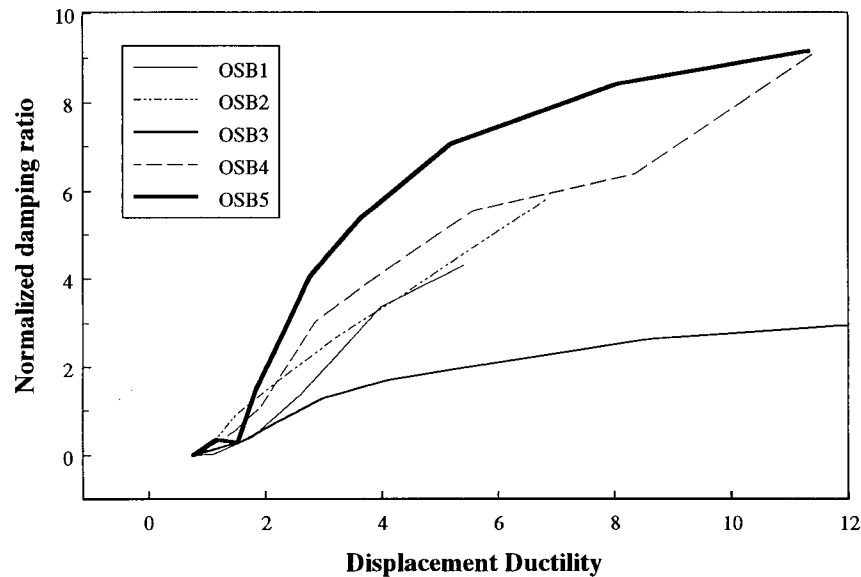


Figure 5.12c Comparison of specimen behaviors: normalized damping ratio

Based on these index variations, damage rates were investigated to assess structural response. Figure 5.12c indicates that damage of all five specimens increases constantly. Damage rate of specimens OSB1, OSB2, OSB4 and OSB5 correspond to 1.005, 0.963, 0.851 and 0.943, respectively. Specimen OSB3, however, shows a lower damage rate of 0.262. Table 5.9 gives a summary of characteristic values related to this index, including final index values as well as computed damage rates.

Specimen	Final Index Value	Calculated Damage Rate
OSB1	4.28	1.005
OSB2	5.84	0.963
OSB3	2.95	0.262
OSB4	9.10	0.851
OSB5	9.17	0.943

Table 5.9 Normalized damping ratio characteristics

As explained in Section 5.3.1.2, hysteretic damping forces are characterized by energy loss. As these energy losses increase with damage, experimental hysteretic damping increased with degradation. Based on these observations and on the equation of normalized damping ratio, high index values correspond to high damage. Looking at final index values, the performance of specimens would then be ordered, starting with the poorest behavior, as OSB5, OSB4, OSB2, OSB1 and OSB3. Comparing this sequence to the one obtained from preliminary observations, this classification approach was considered inadequate for damage assessment of these types of structures.

Taking damage rate as the basis for damage comparison, the specimen with the best response would be OSB3 followed by OSB4, OSB5, OSB2 and OSB1. Except for specimens OSB3 and OSB5, which were reversed in performance order, this classification agrees with observations of damage obtained during testing.

5.5.1.4 SUMMARY OF SPECIMEN CLASSIFICATION

For each damage index evaluated, Table 5.10 provides a summary of specimen ranking, starting with the poorest specimen behavior. Two classification approaches were used to assess performance of the specimens: the final index value and the degradation rate, referring to the fitted curve slope. Note that observations of damage and hysteresis loops suggested a ranking like OSB1, OSB2, OSB3, OSB4 and OSB5.

Damage Index	by Final Index Value	by Damage Rate
ultimate stiffness degradation	OSB1, OSB3, OSB2, OSB4, OSB5	OSB1, OSB2, OSB3, OSB4, OSB5
maximum softening	OSB2, OSB1, OSB3, OSB4, OSB5	OSB1, OSB2, OSB3, OSB4, OSB5
normalized damping ratio	OSB5, OSB4, OSB2, OSB1, OSB3	OSB1, OSB2, OSB5, OSB4, OSB3

Table 5.10 Ranking of specimen behaviors

5.5.2 DAMAGE INDICES CORRELATION

It is of interest to compare results obtained from the three damage indices computed and investigate how they represent damage. The three indices were normalized with respect to their peak value to allow a comparison of their relative ability to assess damage. Figures 5.13a to 5.13c show relationships obtained comparing ultimate stiffness degradation with maximum softening, ultimate stiffness degradation and normalized damping ratio as well as maximum softening compared with normalized damping ratio.

Correlation studies evaluated the similarity between the damage characterization provided by each index at different states of damage. As mentioned previously, damage characterization is understood here to be how physical elements, such as displacement, crack propagation, yielding, stiffness degradation, etc., are taken into account in the failure process defined in a particular damage index.

Results that fall on the line with a unit slope imply similar damage characterization of the two normalized indices. When a series of data points progresses close to this reference line, corresponding damage indices (ordinates and abscissas) are considered to be converging to failure at a comparable rate. On the other hand, curves above this unit line would suggest that the ordinate index converges more rapidly to failure than the abscissa index. Inversely, curves below the unit reference line would indicate that the abscissa index converges faster to failure than the ordinate index.

From Figures 5.13a, 5.13b and 5.13c, the best similarity of rate to failure was obtained from comparison of ultimate stiffness degradation and maximum softening, although curve of specimen OSB5 seems totally uncorrelated because of the anomalies present in its frequency history.

Figure 5.13a compares ultimate stiffness degradation and maximum softening. As mentioned above, this graph shows the least dispersion among the three comparisons. Specimens OSB1, OSB3 and OSB4 curves

all indicate that these two indices carry very similar damage information. However, specimens OSB2 and OSB5 show more scattered data points. Anomalies encountered in their frequency histories could explain these uncorrelated trends. From these observations, it was concluded that ultimate stiffness degradation and maximum softening converge to failure at very comparable rates, when frequency histories show a constant decrease.

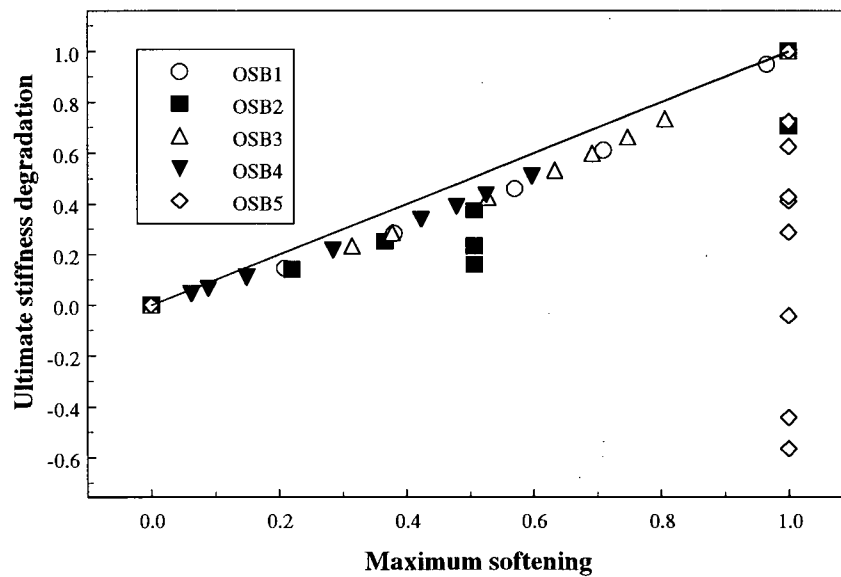


Figure 5.13a Index correlation: ultimate stiffness degradation vs maximum softening

Figure 5.13b compares ultimate stiffness degradation and normalized damping ratio. Data points of Specimens OSB1 to OSB4 progress close to the unit line. Specimen OSB5 shows data points further from the unit reference line. This was once more attributed to anomalies encountered in its frequency history. From these observations, it was concluded that ultimate stiffness degradation and normalized damping ratio transfer converge to failure at a comparable rate when frequency histories show constant decrease.

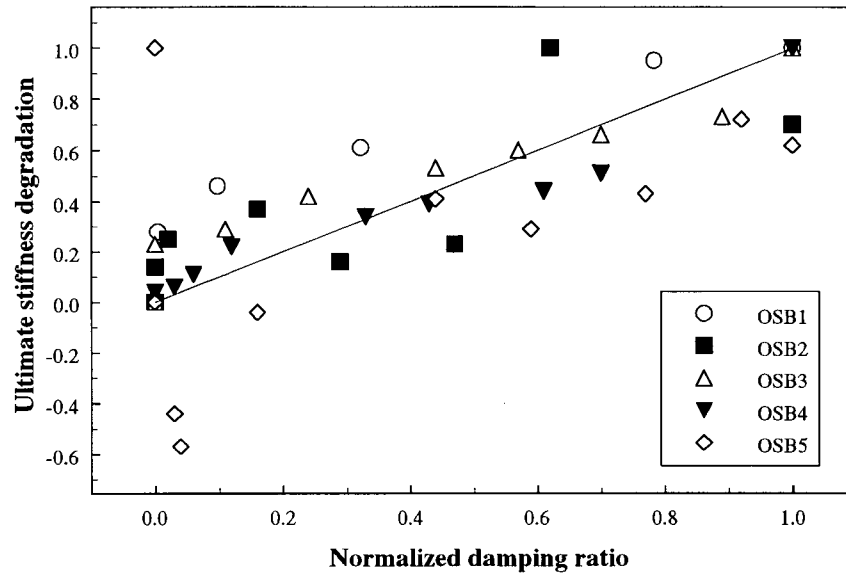
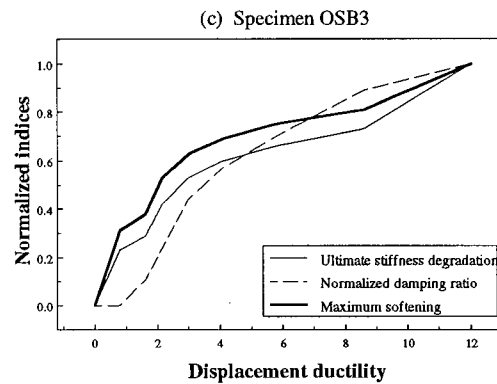
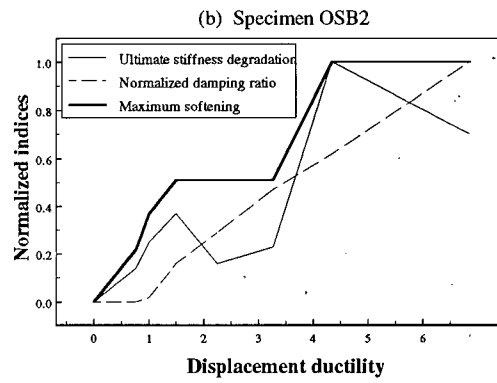
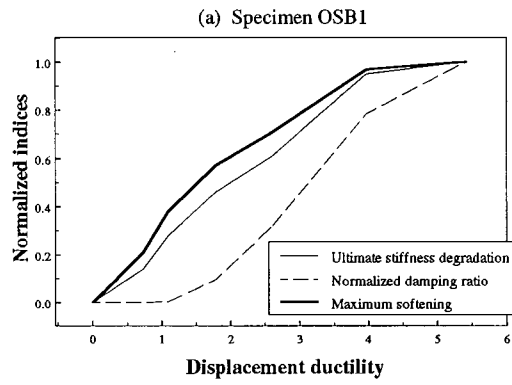


Figure 5.13b Index correlation: ultimate stiffness degradation vs normalized damping ratio

Figure 5.13c compares maximum softening and normalized damping ratio. Data points resulting from the comparison were quite scattered. This was observed for all five specimens. Looking at Figure 5.13c, it was concluded that maximum softening generally converges to failure more rapidly than normalized damping ratio.



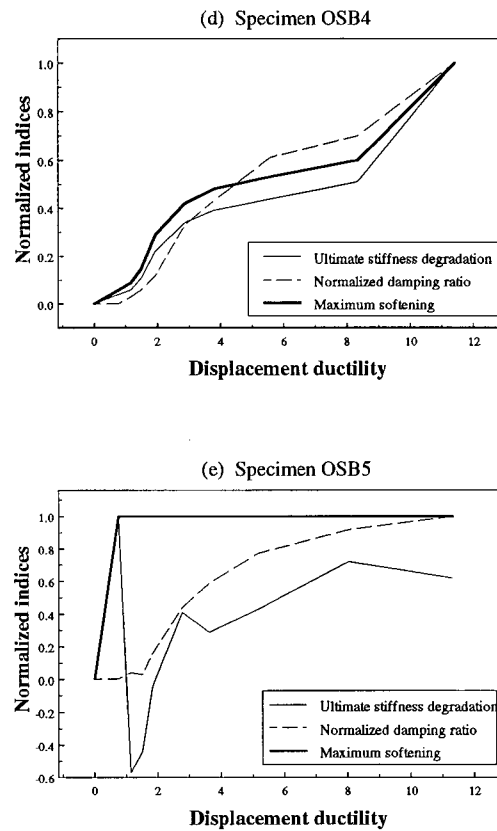


Figure 5.14 Comparison of normalized damage indices

5.6 CONCLUDING REMARKS

This chapter investigated damage assessment based on modal properties, such as natural frequencies and damping ratios. Impact testing, combined with calculations of frequency response functions, was found a useful mean for identification of these modal properties. For the five specimens tested in the laboratory, three indices were evaluated at each of their nominal ductilities.

Based on the index values, the specimen performance was compared and ranked according to different classification approaches. None of the modal indices investigated could provide indication on the failure mode experienced by the specimens. For the specimen behavior comparison, two approaches gave a

ranking similar to the one suggested by the observations of damage and the hysteresis loops: the **damage rate of the ultimate stiffness degradation** and the **damage rate of the maximum softening**.

In addition, index correlation was investigated to verify similarity between the damage characterization provided by each index at different states of damage. When normalized indices were compared, the most significant similarity was obtained from a comparison between the **ultimate stiffness degradation** and the **maximum softening** while ultimate stiffness degradation and normalized damping ratio only showed a trend of similarity. It was also shown that maximum softening converged to failure more rapidly than normalized damping ratio.

The following chapter presents a comparative analysis of the two damage assessment approaches explored in this study, structural damage indices and modal damage indices.

CHAPTER 6

COMPARATIVE ANALYSIS

In Chapters 4 and 5, two approaches were implemented to assess structural damage experienced by the five bent specimens tested in the laboratory. The first approach evaluated damage indices based on structural properties, such as displacement, stiffness and energy absorption. For the five specimens tested, three structural damage indices, namely displacement ductility, modified stiffness ratio and modified Park and Ang index, were evaluated at each of their ductility levels. The second approach investigated damage assessment based on modal properties like natural frequencies and damping ratios. Similarly, three modal damage indices, ultimate stiffness degradation, maximum softening and normalized damping ratio, were computed at each of the selected nominal ductility levels at which measurements were taken.

Although these two categories of indices are based on different parameters, they attempt to quantify the same phenomenon. Comparing how these two approaches differ in their damage evaluation is then of significant interest. This chapter first presents a correlation study to assess the similarity between the index values calculated from these two approaches. Thereafter, a comparison of both approaches is presented and advantages and limitations of both methods are discussed.

6.1 DAMAGE INDICES CORRELATION

The similarities between damage characterization provided by each index were determined from a correlative study. Damage indices were normalized with respect to their peak value in order to facilitate the comparison of their ability to assess damage. Figures 6.1 to 6.9 show nine relationships obtained from comparisons of the three modal damage indices with respect to the three structural damage indices. For reference, a line of unit slope is also included on these graphs. Results that fall on the line with a unit

slope imply similar damage characterization of the two normalized indices. When a series of data points progresses close to this reference line, corresponding damage indices (ordinates and abscissas) are considered to be converging to failure at a comparable rate.

6.1.1 ULTIMATE STIFFNESS DEGRADATION

Figure 6.1 to 6.3 show relationships between ultimate stiffness degradation and the three structural damage indices. The correlation between the ultimate stiffness degradation and the displacement ductility is shown in Figure 6.1.

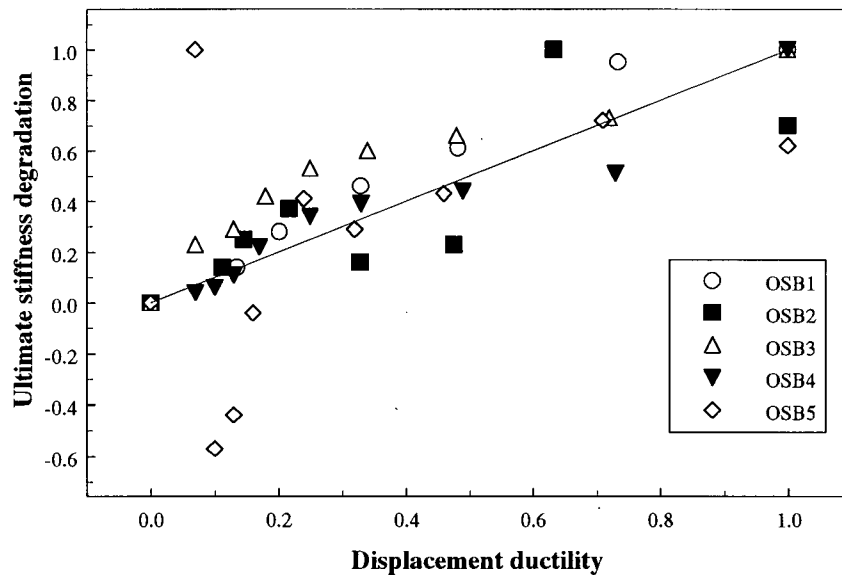


Figure 6.1 Correlation between ultimate stiffness degradation and displacement ductility

Data points lying close to the unit slope line suggest a very good correlation between these two damage indices. Note that specimen OSB5 indicate some uncorrelated data points in the low ductility levels, where some ultimate stiffness degradation indices are negative. Anomalies in the frequency history of specimen OSB5 could explain this low correlation of OSB5 data points. These observations suggest that ultimate stiffness degradation and displacement ductility converge to failure at comparable rate and, hence, there is no significant difference in their damage characterization.

Figure 6.2 shows the correlation between the ultimate stiffness degradation and the modified stiffness ratio.

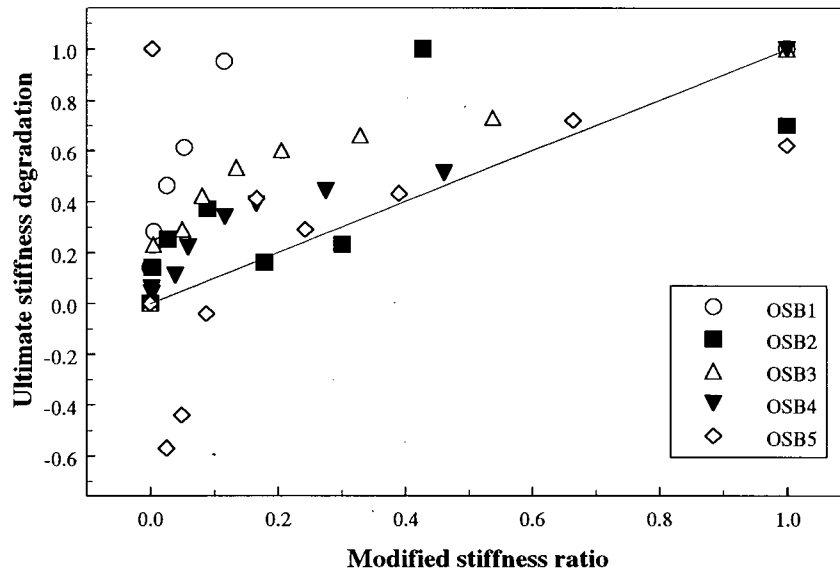


Figure 6.2 Correlation between ultimate stiffness degradation and modified stiffness ratio

Data points are not as close to the unit slope line as in the case for Figure 6.1. In this case, specimens OSB5 as well as specimens OSB1 and OSB2 show some data points distant from the perfect correlation. Again, anomalies in the frequency history of specimens OSB5 could explain these negative values in the low damage levels. For specimen OSB1 and OSB2, the uncorrelated data points could be related to the failure mode experienced by these two specimens, shear failure in the cap beam (OSB1) and shear failure in the columns (OSB2). Overall, these observations suggest that the ultimate stiffness degradation index converges slightly more rapidly to failure than the modified stiffness ratio index.

Figure 6.3 shows the correlation between the ultimate stiffness degradation and the modified Park and Ang index.

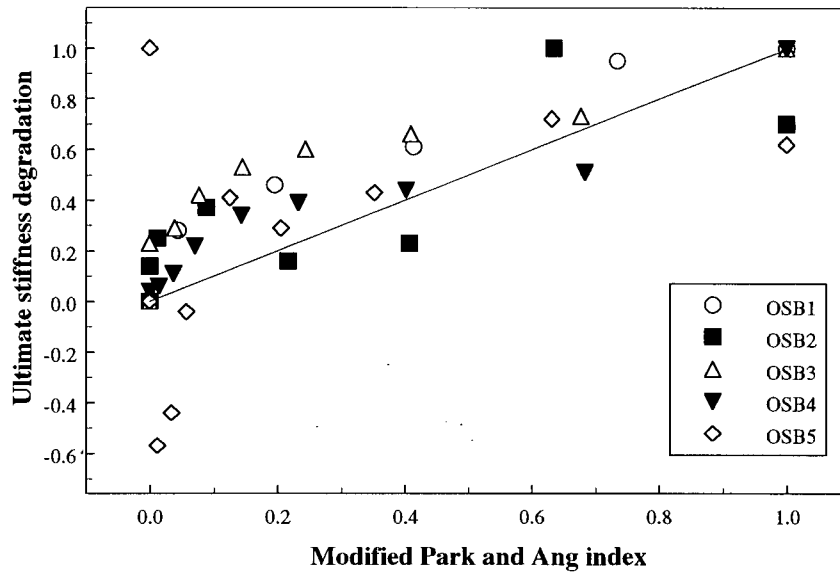


Figure 6.3 Correlation between ultimate stiffness degradation and modified Park and Ang index

This comparison is similar to the one obtained in Figure 6.1, where a good correlation is observed, except for specimen OSB5. Ultimate stiffness degradation and modified Park and Ang index were considered to converge to failure with similar damage rate.

6.1.2 MAXIMUM SOFTENING

Figure 6.4 to 6.6 show relationships obtained comparing maximum softening with the three structural damage indices investigated. Correlation between the maximum softening and the displacement ductility is shown in Figure 6.4.

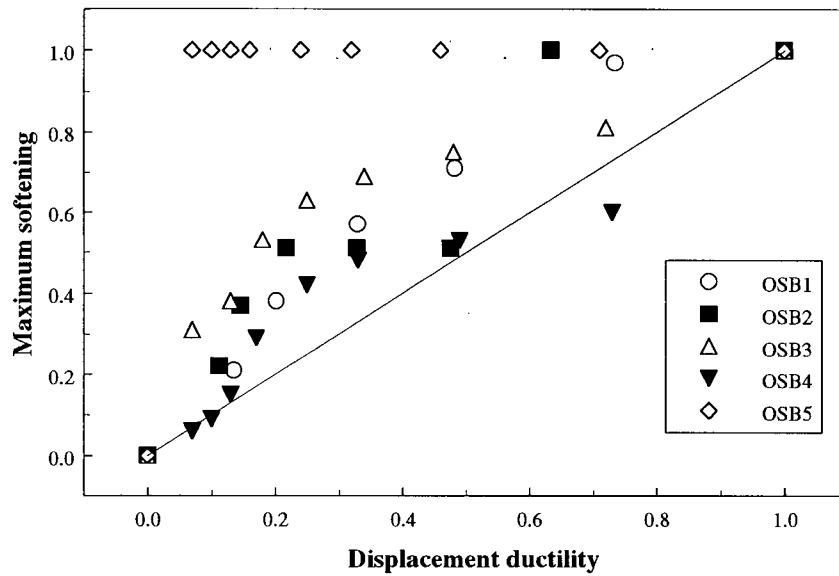


Figure 6.4 Correlation between maximum softening and displacement ductility

It can be seen, in this figure, that data points are, in general, located above the unit slope line. For specimen OSB5, data points of high value could be once more related to anomalies of its frequency history. From these observations, it was concluded that the maximum softening index indicates a higher rate of approach to failure than displacement ductility.

Figure 6.5 shows the correlation between the maximum softening and the modified stiffness ratio.

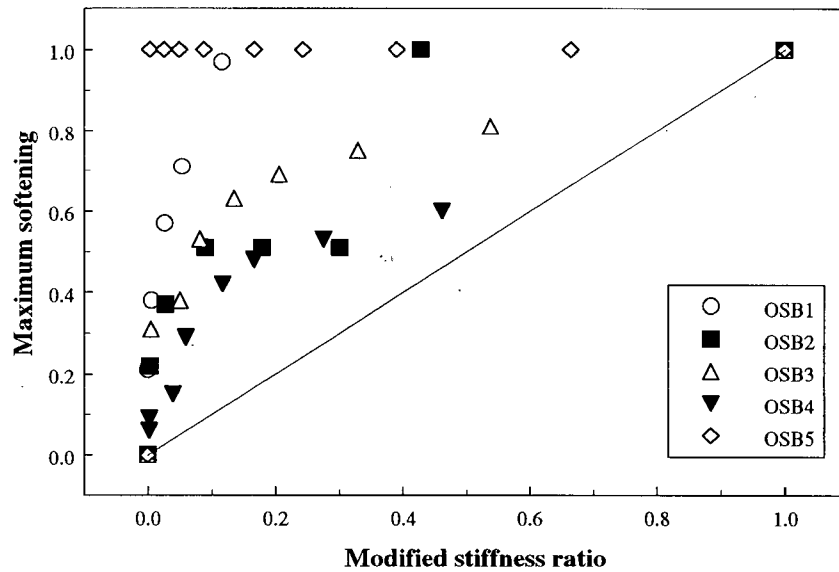


Figure 6.5 Correlation between maximum softening and modified stiffness ratio

This figure reveals that, with no exceptions, all data points are located above the unit slope line, indicating that the maximum softening index converges more rapidly to failure than the modified stiffness ratio index. It should be noted that results for specimen OSB5 still shows high values for the maximum softening index.

Figure 6.6 shows the correlation between the maximum softening and the modified Park and Ang index.

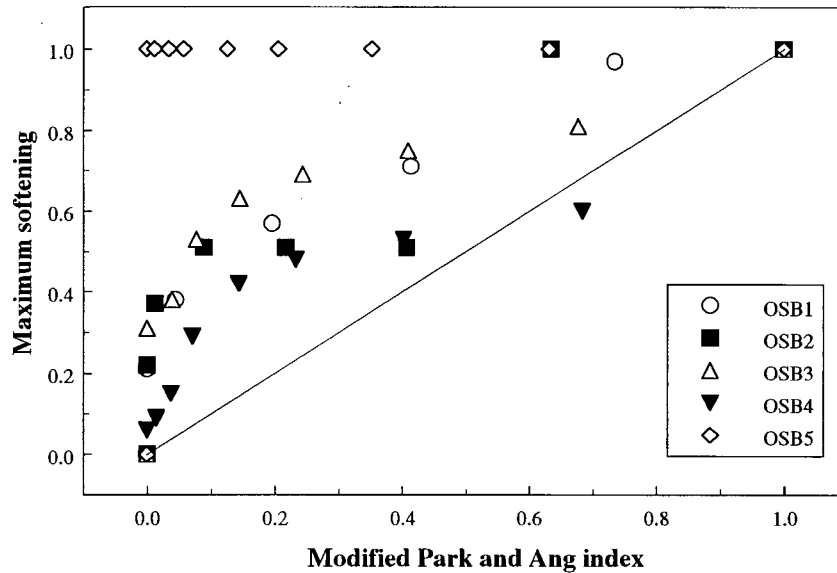


Figure 6.6 Correlation between maximum softening and modified Park and Ang index

This comparison graph indicates that the location of data points is mostly above the unit slope line. Specimen OSB5 indicated once again high value data points. The maximum softening index was then considered to show a higher rate of approach to failure than the modified Park and Ang index.

6.1.3 NORMALIZED DAMPING RATIO

Figure 6.7 to 6.9 show comparisons of normalized damping ratios with respect to each of the three structural damage indices investigated. The correlation between the normalized damping ratio and the displacement ductility is shown in Figure 6.7.

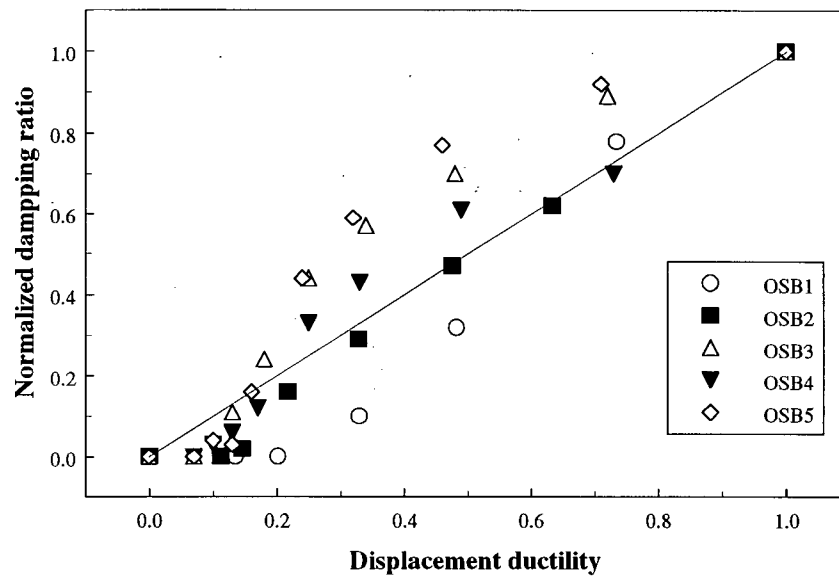


Figure 6.7 Correlation between normalized damping ratio and displacement ductility

In this figure, it can be seen that the data points are located close to the unit slope line. Since the frequency history results are not used in the evaluation of the normalized damping ratio index, specimen OSB5 data points do not indicate a particular behavior. These observations suggest that the normalized damping ratio index and the displacement ductility converge to failure at a comparable rate.

Figure 6.8 shows the correlation between the normalized damping ratio and the modified stiffness ratio.

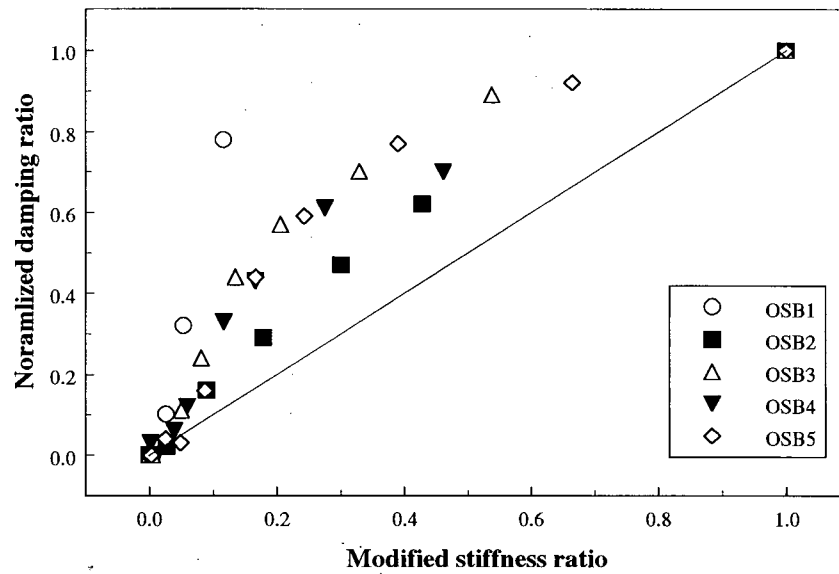


Figure 6.8 Correlation between normalized damping ratio and modified stiffness ratio

The comparison graph shows that, with no exception, all data points are located above the unit slope line. This observation suggests that the normalized damping ratio progresses to failure at a higher rate than the modified stiffness ratio index.

Finally, Figure 6.9 shows the correlation between the normalized damping ratio and the modified Park and Ang index.

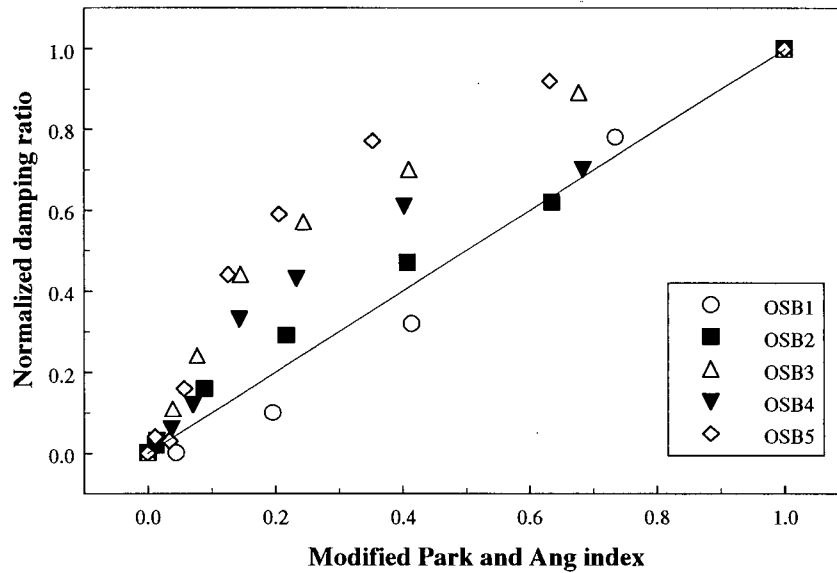


Figure 6.9 Correlation between normalized damping ratio and modified Park and Ang index

Although evaluation of these two damage indices use energy concepts, Figure 6.9 does not indicate a perfect correlation, since most of the data points are lying above the unit slope line. Instead, it is suggested that the normalized damping ratio index converges to failure at a higher rate than the modified Park and Ang index.

6.1.4 SUMMARY OF INDICES CORRELATION

Figures 6.1 to 6.9 showed the relationships obtained from comparison of the three modal damage indices with respect to the three structural damage indices. Table 6.1 summarizes the similarity between the index values calculated from these two approaches.

Damage Index	Displacement Ductility [μ]	Modified Stiffness Ratio [MSR]	Modified Park & Ang Index [P&A]
Ultimate Stiffness Degradation [USD]	USD $\sim \mu$	USD > MSR	USD \sim P&A
Maximum Softening [Ms]	MS > μ	MS > MSR	MS > P&A
Normalized Damping Ratio [NDR]	NDR $\sim \mu$	NDR > MSR	NDR > P&A

Table 6.1 Summary of index correlation

In Table 6.1, the symbol “>” refers to “converges to failure at a higher rate” and the character “ \sim ” means “converges to failure at comparable rate”. The comparison summary shows that damage indices based on modal properties converge to failure at comparable or higher rate than structural damage indices.

6.2 GENERAL COMPARISON OF DAMAGE ASSESSMENT APPROACHES

The two approaches investigated in this study provided efficient tools to quantify structural damage sustained by the specimens tested in the laboratory. Advantages of each approach are outlined in this section as well as limitations that could restrain their use.

Evaluation of structural damage indices usually requires that the hysteresis loops for the structure under study are available. However some indices, like displacement ductility, are exclusively based on displacement history. If required, hysteresis curves can be analytically predicted or experimentally measured. Modelling of hysteretic behavior can represent a complex assignment while measuring

experimental hysteresis responses imply complex instrumentation of the structure, in order to record the force applied and the corresponding displacements. Modal damage indices are based on dynamic properties of the structure studied. These modal properties can also be obtained analytically or measured experimentally. As for the hysteresis loops, modelling of a real structure dynamic behavior does not represent a straightforward process. However, unlike experimental hysteresis curves, vibration measurements can be recorded with a rather simple testing system, according more flexibility to this approach.

Considering the type of instrumentation involved, the approach based on structural damage indices is not applicable to all situations of damage assessment. For example, post-earthquake damage assessment can not be performed with this approach, unless the structure is fully instrumented prior to the seismic event. Hysteresis curves are usually predicted from non-linear models in this case. However, vibration tests can be easily performed on site after the structure has sustained damage. Assuming that dynamic parameters were measured prior to a seismic event, modal damage assessment can be used in post-earthquake damage assessment.

Although hysteresis curves necessitate either modelling effort or complex instrumentation, evaluation of structural damage indices use *directly* force and displacement measurements obtained from these procedures. Inversely, evaluation of modal damage indices are not based on direct measurements recorded during vibration testing. They rather require *extraction* of dynamic properties from these vibration measurements, implying additional analysis before computation of the damage indices. Moreover, the modal properties used in the modal damage assessment are not always obtained from vibration measurements. For example, hysteretic damping values are calculated from the load-displacement hysteresis curves.

If data are obtained experimentally, the information needed to evaluate the damage indices involve different types of tests. Development of hysteresis curves generally imply partial or total destruction of the structure. On the other hand, vibration tests represent a non-destructive assessment technique that do not involve damaging the structure during the testing procedure, although other types of vibration test may involve structural damage (for example, shake table tests).

However, once these hysteresis loops are available, structural damage indices serve as reliable indicators of structural damage. Likely, damage assessment based on modal properties quantify adequately structural degradation. Testing and modelling objectives will then guide the choice of damage assessment to be performed.

6.3 CONCLUDING REMARKS

This chapter compared the two approaches investigated in this study, damage assessment based on structural properties and damage assessment based on modal properties. First a correlation study assessing the similarity between the index values calculated from these two approaches was presented. It was shown that modal damage indices generally converge to failure at a higher rate than the structural damage indices. Thereafter, a general comparison of both approaches was presented, including advantages and limitations of both methods.

The following chapter will present conclusions of this study, including details on further research topics relevant to the investigation performed here.

CHAPTER 7

CONCLUSIONS AND FURTHER STUDIES

In order to investigate different damage assessment approaches and different damage indicators within a particular approach, this study developed and implemented a combined experimental and analytical program on damage assessment. As part of this study, structural and dynamic properties of five bent specimens tested in the laboratory were determined. From these measurements, damage indices based on structural properties and damage indices based on modal properties were evaluated for each specimen. Finally, comparative analyses of damage indices were performed to assess the specimens performance and to investigate damage characterization provided by the damage indicators.

Damage assessment based on structural properties was investigated evaluating three indices, displacement ductility, modified stiffness ratio and modified Park and Ang index. Results from this investigation showed that:

- the modified stiffness ratio and modified Park and Ang index could provide good indication on the failure mode sustained by the specimens (shear/flexural);
- the highest value of displacement ductility and the damage rate gradient of the modified stiffness ratio gave a ranking similar to that from the experimental observations;
- the modified Park and Ang index and the displacement ductility converged to failure at a similar rate while modified stiffness ratio seemed to progress to failure at a lower rate than other two indices.

Damage assessment based on modal properties was investigated by reference to three indices, ultimate stiffness degradation, maximum softening and normalized damping ratio. Index comparisons indicated that:

- none of the modal indices investigated could provide indication on the failure mode experienced by the specimens;
- the damage rate of the ultimate stiffness degradation and the damage rate of the maximum softening gave a specimen ranking similar to that from the experimental observations;
- the ultimate stiffness degradation and the maximum softening showed similar convergence rate to failure while ultimate stiffness degradation and normalized damping ratio only showed a trend of similarity in their rate of approach to failure;
- maximum softening yielded to a higher rate to failure than normalized damping ratio.

Although none of the modal indices investigated could provide indication on the failure mode experienced by the specimens, comparison of the two approaches, including six damage indices, showed that modal damage indices generally converge to failure at a higher rate than the structural damage indices.

Considering the extensive and complete database obtained experimentally, several research topics could be investigated in the future.

- More complex damage indices, based on both structural and dynamic properties, could be evaluated and subsequently investigated in comparative analyses;
- a detailed exploration of the neural network approach could be performed. This method could be compared with the two approaches already investigated;
- modal damage assessment could be completed using dynamic properties in the two other principal directions;
- finite element models of the specimens could be developed and used to experiment some updating techniques for different damage states of the specimens;
- other damping approaches (half-power method, for example) could be investigated;
- comparative analyses of mode shapes describing the undamaged structure and the structure at failure state could be performed in the three principal directions of motion;
- uses of ambient vibration data could be investigated to assess damage;
- considering damage indices on a time scale, a model to characterize their growth rate could be investigated. This model could be dependent on several parameters such as the types of loading involved, the stress range sustained by the structure under a specific loading pattern and the previous damage level of the structure.

REFERENCES

- Allemang R. J., Brown D. L. (1982) A correlation coefficient for modal vector analysis, *Proc. 1st Int. Modal Analysis Conf., Soc. for Experimental Mech., Conn.*, 110-116.
- Anderson D.L., Sexsmith R.G., English D., Kennedy D.W., Jennings D.B., (1995) *Oak Street And Queensborough Bridges: Two Column Bent Tests*, Earthquake Engineering Research Facility, Technical Report 95-02, University of British Columbia and Klohn-Crippen Consultants.
- Ang A. H.-S. (1987) Basis for earthquake-resistant design with tolerable structural damage, *Proc. 5th Int Conf. on Applications of Statistics and Probability in Soil and Structural Engineering (ICASP5)*, Vancouver BC, Canada, Vol. 1, 407-416.
- Banon H., Biggs J.M., Irvine H.M. (1981) Seismic damage in reinforced concrete frames, *Journal of Structural Engineering, ASCE*, Vol. 107, No. 9, 1713-1729.
- Barenberg M.E., Foutch D.A. (1988) Evaluation of seismic design procedures for highway bridges, *Journal of Structural Engineering, ASCE*, Vol. 114, No. 7, 1588-1605.
- Bendat J. S., Piersol A. G. (1993) *Engineering Applications Of Correlation And Spectral Analysis*, 2nd Edition, John Wiley and Sons, New York.
- Bernasconi O., Ewins D. J. (1989), Application of strain modal testing to real structures, *Proc. 7th Int. Modal Analysis Conf., Las Vegas Nevada*, Vol. II, 1453-1464.
- Bracci J.M., Reinhorn A.M., Mander J.B., Kunnath S.K. (1989) Deterministic model for seismic damage evaluation of RC structures, *Technical Report NCEER-89-0033*, National Center for Earthquake Engineering Research, State University of New-York, Buffalo NY.
- Carydis P., Mouzakis H.P. (1986) Small amplitude vibration measurement of buildings undamaged, damaged, and repaired after earthquakes, *Earthquake Spectra*, Vol. 3, No.2.
- Caudill M., & Butler C. (1992) *Understanding Neural Networks: Computer Explorations*, Volumes 1&2, MIT Press, Cambridge Massachusetts.

-
- Casas J. R., Aparicio A. C. (1994) Structural damage identification from dynamic-test data, *Journal of Structural Engineering, ASCE*, Vol. 120, No. 8, 2437-2450.
- Cawley P., Adams R. D. (1979) The location of defects in structures from measurements of natural frequencies, *Journal of Strain Analysis*, Vol. 14, No. 2, 49-57.
- Chen S., Shah K. (1992) Neural networks in dynamic analysis of bridges, *Proc. 8th Annual Conf. of Computing in Civil Eng., ASCE*, 1058-1065.
- Chen Y., Swamidass A.S.J. (1993) Change of modal parameters due to crack growth in a tripod tower platform, *Canadian Journal of Civil Engineering*, Vol. 20, 801-813.
- Cherng A.-P., Abdelhamid M. K. (1994) A validation of the signal subspace correlation (SSC) methodology for detection of structural changes, *Proc. 12th Int. Modal Analysis Conf., Honolulu Hawaii*, Vol. I, 133-136.
- Chung Y.S., Meyer C., Shinozuka M. (1990) Automatic seismic design of reinforced concrete building frames, *Structural Journal, American Concrete Institute*, Vol. 87, No. 3, 326-340.
- Ciampoli M., Giannini R., Nuti C., Pinto P.E. (1989) Seismic reliability of non-linear structures with stochastic parameters by directional simulation, *Proc. 5th Int. Conf. on Structural Safety and Reliability (ICOSSAIR 89)*, San Francisco CA, Vol. II, 1121-1128.
- Clough R. W., & Penzien J. (1993) *Dynamics of Structures*, 2nd Edition, McGraw Hill, New York.
- DiPasquale E., Cakmak A. S. (1987) Detection and assessment of seismic structural damage, *Technical Report NCEER-87-0015*, National Center for Earthquake Engineering Research, State University of New-York, Buffalo NY.
- DiPasquale E., Cakmak A. S. (1988) Identification of the serviceability limit state and detection of seismic structural damage, *Technical Report NCEER-88-0022*, National Center for Earthquake Engineering Research, State University of New-York, Buffalo NY.
- DiPasquale E., Cakmak A. S. (1989) On the relation between local and global damage indices, *Technical Report NCEER-89-0034*, National Center for Earthquake Engineering Research, State University of New-York, Buffalo NY.
- DiPasquale E., Ju J.-W., Cakmak A. S. (1990) Relation between global damage indices and local stiffness degradation, *Journal of Structural Engineering, ASCE*, Vol. 116, No.5, 1440-1456.

-
- Dowell E.H., (1979) On some general properties of combined dynamical systems, *Journal of Applied Mechanics, ASME*, Vol. 46, 206-209.
- Elkordy M. F., Chang K. C., Lee G. C. (1992) Neural networks based classifiers in vibrational signature analysis, *Proc. 8th Annual Conf. of Computing in Civil Eng., ASCE*, 1066-1073.
- Elkordy M. F., Chang K. C., Lee G. C. (1993) Neural networks trained by analytically simulated damage states, *Journal of Computing in Civil Engineering, ASCE*, Vol. 7, No. 2, 130-145.
- Ewins D. J. (1984) *Modal Testing: Theory and Practice*, John Wiley and Sons, New York.
- Felber A. J. (1993) *Development of A Hybrid Bridge Evaluation System*, Doctoral Dissertation, University of British Columbia, Canada.
- Garrett J. H. (1992) Neural networks and their applicability within civil engineering, *Proc. 8th Annual Conf. of Computing in Civil Eng., ASCE*, 1155-1162.
- Haroun M. A., Mourad S. A., Flynn N. H. (1993) Modal characteristics of RC pier walls before and after cyclic testing, *Proc. 11th Int. Modal Analysis Conf.*, Kissimmee Florida, Vol. II, 1299-1302.
- Hearn G., Testa R. B. (1991) Modal analysis for damage detection in structures, *Journal of Structural Engineering, ASCE*, Vol. 117, No. 10, 3042-3063.
- Hemez F. M., Farhat C. (1992) A finite element model updating methodology and its applications to structural damage detection, *2nd ESA Workshop on Modal Representation of Flexible Structures by Continuum Methods*.
- Horyna T. (1995) Master Dissertation, to be published, University of British Columbia, Canada.
- Humar J. L. (1990) *Dynamics of Structures*, Prentice Hall, New Jersey.
- Jeong G.D., Iwan W.D. (1988) Effect of earthquake duration on the damage of structures, *Earthquake Engineering and Structural Dynamics*, Vol. 16, No. 8, 1201-1211.

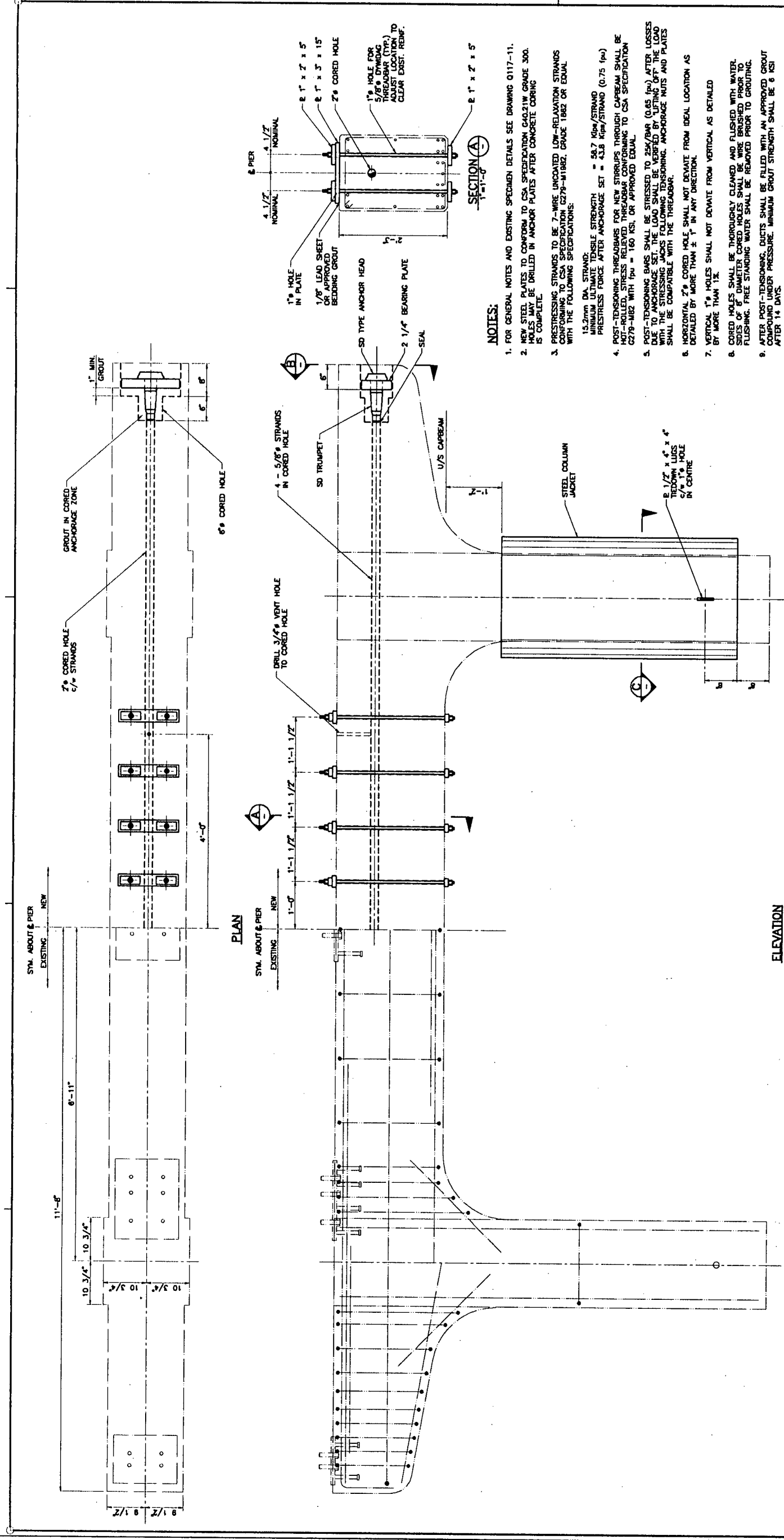
- Kaouk M., Zimmerman D. C. (1993) Evaluation of the minimum rank update in damage detection: an experimental study, *Proc. 11th Int. Modal Analysis Conf.*, Kissimmee Florida, Vol. II, 1061-1068.
- Kratzig W.B., Meyer I.F., Meskouris K. (1989) Damage evolution in reinforced concrete members under cyclic loading, *Proc. 5th Int. Conf. on Structural Safety and Reliability (ICOSSAIR 89)* San Francisco CA, Vol. II, 795-802.
- Kunnath S.K., Reinhorn A.M., Lobo R.F. (1992) IDARC version 3.0: A program for the inelastic damage analysis of RC structures, *Technical Report NCEER-92-0022*, National Center for Earthquake Engineering Research, State University of New-York, Buffalo NY.
- Lammens S., Heylen W., Sas P. (1994) The selection of updating frequencies and the choice of a damping approach for model updating procedures using experimental frequency response functions, *Proc. 12th Int. Modal Analysis Conf.*, Honolulu Hawaii, Vol. II, 1383-1389.
- Li D., Zhuge H., Wang B. (1989) The principle and techniques of experimental strain modal analysis, *Proc. 7th Int. Modal Analysis Conf.*, Las Vegas Nevada, Vol. II, 1285-1289.
- Lieven N. A., Ewins D. J. (1988) Spatial correlation of mode shapes, the coordinate modal assurance criterion (COMAC), *Proc. 6th Int. Modal Analysis Conf., Soc. for Experimental Mech.*, Kissimmee Florida, 690-695.
- Meyer C., Roufaiel M.S.L. (1984) Reliability of damaged concrete frames, *Proc. 8th World Conf. on Earthquake Engineering*, San Francisco CA, Vol.4, 535-543.
- Mihai C. Manolovici M., Carian St., Marinescu St. (1980) Static and seismic model behavior of a new type of mixed structure for RC industrial buildings, *Proc. 7th World Conf. on Earthquake Engineering*, Istanbul, Turkey, Vol. 7, 107-110.
- Newmark N.M., Rosenblueth E., *Fundamentals of Earthquake Engineering*, Prentice Hall, 1974.
- Ogawa J., Abe Y. (1980) Structural damage and stiffness degradation of buildings caused by severe earthquakes, *Proc. 7th World Conf. on Earthquake Engineering*, Istanbul, Turkey, Vol. 7, 527-534.
- Ojalvo I. U., Pilon D. (1988) Diagnostics for geometrically locating structural math model errors from modal test data, *Proc. 29th AIAA Structures, Structural Dynamics and Materials Conf.*, Williamsburg VA, 1174-1186.

-
- Park Y.J., Ang A.H.-S. (1985) Mechanistic seismic damage model for reinforced concrete, *Journal of Structural Engineering, ASCE*, Vol. 111, No. ST4, 722-739.
- Park Y. J., Ang A.H.-S., Wen Y.K. (1987) Damage-limiting aseismic design of buildings, *Earthquake Spectra*, Vol. 3, No. 1, 1-26.
- Penny J.E.T., Wilson D.A.L., Friswell M.I. (1993) Damage location in structures using vibration data, *Proc. 11th Int. Modal Analysis*, Kissimmee Florida, Vol. II, 861-867.
- Raghavendrachar M., Aktan A. E. (1992) Flexibility by multireference impact testing for bridge diagnostics, *Journal of Structural Engineering, ASCE*, Vol. 118, No. 8, 2186-2203.
- Richardson M. H., Mannan M. A. (1993) Correlating minute structural faults with changes in modal parameters, *Proc. 11th Int. Modal Analysis Conf.*, Kissimmee Florida, Vol. II, 893-898.
- Roufaiel M.S.L., Meyer C. (1987a) Analytical modelling of hysteretic behavior of RC frames, *Journal of Structural Engineering, ASCE*, Vol. 113, No. 3, 429-444.
- Roufaiel M.S.L., Meyer C. (1987b) Reliability of RC frames damaged by earthquakes, *Journal of Structural Engineering, ASCE*, Vol. 113, No. 3, 445-457.
- Salawu O.S., Williams C. (1994) Damage location using vibration mode shapes, *Proc. 12th Int. Modal Analysis Conf.*, Honolulu Hawaii, Vol. I, 933-939.
- Salawu O.S., Williams C. (1995) Bridge assessment using forced-vibration testing, *Journal of Structural Engineering, ASCE*, Vol. 121, No. 2, 161-173.
- Samman M. M., Biswas M. (1994a) Vibration testing for nondestructive evaluation of bridges I: Theory, *Journal of Structural Engineering, ASCE*, Vol. 120, No. 1, 269-289.
- Samman M. M., Biswas M. (1994b) Vibration testing for nondestructive evaluation of bridges II: Results, *Journal of Structural Engineering, ASCE*, Vol. 120, No. 1, 290-309.
- Schuster N. D. (1994) *Dynamic Characteristics of A 30 Storey Building During Construction Detected From Ambient Vibration Measurements*, Master Dissertation, University of British Columbia, Canada.

-
- Seidel M.J., Reinhorn A.M., Park Y.J. (1989) Seismic damageability assessment of RC buildings in eastern U.S., *Journal of Structural Engineering, ASCE*, Vol. 115, No. 9, 2184-2260.
- Slanstan J., Pietrzko S. (1993) Changes of RC-beam modal parameters due to cracks, *Proc. 11th Int. Modal Analysis Conf.*, Kissimmee Florida, Vol. I, 70-76.
- Sordo E., Teran A., Guerrero J.J., Juarez H., Iglesias J. (1989) Ductility and resistance requirements imposed on a concrete building, *Earthquake Spectra*, Vol. 5, No. 1, 41-50.
- Stephens J.E., Yao J.T.P. (1987) Damage assessment using response measurement, *Journal of Structural Engineering, ASCE*, Vol. 113, No. 4, 787-801.
- Stone W. C., Taylor A. W. (1991) System identification of spirally reinforced circular bridge columns subjected to cyclic lateral loading, *Wind and Seismic Effects: Proc. 23rd Joint Meeting UJNR, NIST SP 820*, National Institute of Standards and Technology.
- Szewczyk P., Hajela P. (1994) Damage detection in structures based on feature-sensitive neural networks, *Journal of Computing in Civil Engineering, ASCE*, Vol. 8, No. 2, 163-178.
- Tsang W. F. (1990) Use of dynamic strain measurements for modelling of structures, *Proc. 8th Int. Modal Analysis Conf.*, Kissimmee Florida, Vol. II, 1246-1251.
- Wang M.L., Shah S.P. (1987) Reinforced concrete hysteresis model based in the damage concept, *Earthquake Engineering and Structural Dynamics*, Vol. 15, No. 8, 993-1003.
- Williams M. S., Sexsmith R. G. (1995) Seismic Damage Indices for Concrete Structures: A-State-of-the-Art Review, *Earthquake Spectra*, accepted for publication.
- Williams M. S., Villemure I., Sexsmith R. G. (1995) *Evaluation Of Seismic Damage Indices For Concrete Elements Loaded In Combined Shear And Flexure*, to be published, University of British Columbia.
- Wolff T., Richardson M. (1989) Fault detection in structures from changes in their modal parameters, *Proc. 7th Int. Modal Analysis Conf., Soc. for Experimental Mech.*, Las Vegas Nevada 87-94.
- Wu X., Ghaboussi J., Garrett J. H. (1992) Use of neural networks in detection of structural damage *Comput. and Struct.*, Vol. 42, No. 4, 649-659.

APPENDIX A

The first part of Appendix A contains a drawing of the original design of bent S28 as well as drawings of the five specimens tested in the laboratory. These drawings were provided by Crippen International Ltd (except for Figure Q-1). The second part of this appendix includes pictures of the experimental vibration procedure and pictures of the damaged specimens.



- NOTES:**
- FOR GENERAL NOTES AND EXISTING SPECIMEN DETAILS SEE DRAWING 0117-11.
 - NEW STEEL PLATES TO CONFORM TO CSA SPECIFICATION G40.21W GRADE 300. ALL PLATES TO BE DRILLED IN ANCHOR PLATES AFTER CONCRETE CURING IS COMPLETE.
 - PRESTRESSING STRANDS TO BE 7-WIRE UNCOATED LOW-RELAXATION STRANDS CONFORMING TO CSA SPECIFICATION G279-M1982, GRADE 1982 OR EQUAL WITH THE FOLLOWING SPECIFICATIONS:
 15.2mm DIA. STRAND;
 MINIMUM ULTIMATE TENSILE STRENGTH = 58.7 Kip/STRAND
 PRESTRESS FORCE AFTER ANCHORAGE SET = 43.8 Kip/STRAND (0.75 fu)
 4. POST-TENSIONING TUBES FOR NEW STRANDS THROUGH CAPBEAM SHALL BE NOT-ROLLED, STRESS RELIEVED THREADBAR CONFORMING TO CSA SPECIFICATION G279-M82 WITH fu = 160 KSI, OR APPROVED EQUAL.
 - POST-TENSIONING BARS SHALL BE STRESSED TO 25K/5M (0.65 fu) AFTER LOSSES DUE TO ANCHORAGE SET. THE LOAD SHALL BE VERIFIED BY LIFTING OFF THE LOAD AND RE-ANCHORING THE STRANDS. ANCHORAGE NUTS AND PLATES SHALL BE COMPATIBLE WITH THE THREADBAR.
 - HORIZONTAL 2" CORED HOLES SHALL NOT DEVIATE FROM IDEAL LOCATION AS DETAILED BY MORE THAN ± 1" IN ANY DIRECTION.
 - VERTICAL 1" CORED HOLES SHALL NOT DEVIATE FROM VERTICAL AS DETAILED BY MORE THAN 1/8".
 - CORED HOLES SHALL BE THOROUGHLY CLEANED AND FLUSHED WITH WATER. SIDES OF 6" DIAMETER CORED HOLES SHALL BE WIRE BRUSHED PRIOR TO FLUSHING. FREE STANDING WATER SHALL BE REMOVED PRIOR TO GROUTING.
 - AFTER POST-TENSIONING, DUCTS SHALL BE FILLED WITH AN APPROVED GROUT COMPOUND UNDER PRESSURE. MINIMUM GROUT STRENGTH SHALL BE 6 KSI AFTER 14 DAYS.
 - GROUT VENT TUBES SHALL BE PROVIDED AT EACH END OF THE TENDON AND AT THE TOP OF EACH THREADBAR. GROUTING SHALL BE INJECTED FROM THE LOW END OF EACH HOLE.
 - ANCHORAGE DETAILS SHOWN CONFORM TO A MODIFIED DS D TYPE SYSTEM. EQUIVALENT ALTERNATIVE SYSTEMS MUST BE APPROVED.
 - GROUT IN CORED ANCHORAGE ZONE SHALL BE A NON-METALLIC NON-SHRINK GROUT WITH A MINIMUM COMPRESSIVE STRENGTH OF 5 KSI AFTER 7 DAYS.
 - CONCRETE FOR RETILING COLUMN JACKETS SHALL HAVE A MINIMUM COMPRESSIVE STRENGTH OF 5 KSI AT 14 DAYS, AND SHALL HAVE A MAXIMUM W/C RATIO OF 0.40.
 - COLUMN JACKET STEEL SHALL CONFORM TO CSA SPECIFICATION G40.21 GRADE 300.

CRIPPEN INTERNATIONAL LTD.
 100 - 40 WEST GERRARD STREET / WILLOWDALE, ONT. / CANADA M2B 3K1
 TEL: (416) 491-3333 / FAX: (416) 491-3334

SCALE: 1" = 1'-0" U/N

DESIGNED BY	DATE	DES. NO.
CHECKED BY	DATE	CHECK NO.
DRAWN BY	DATE	DRAWING NO.

REVISIONS

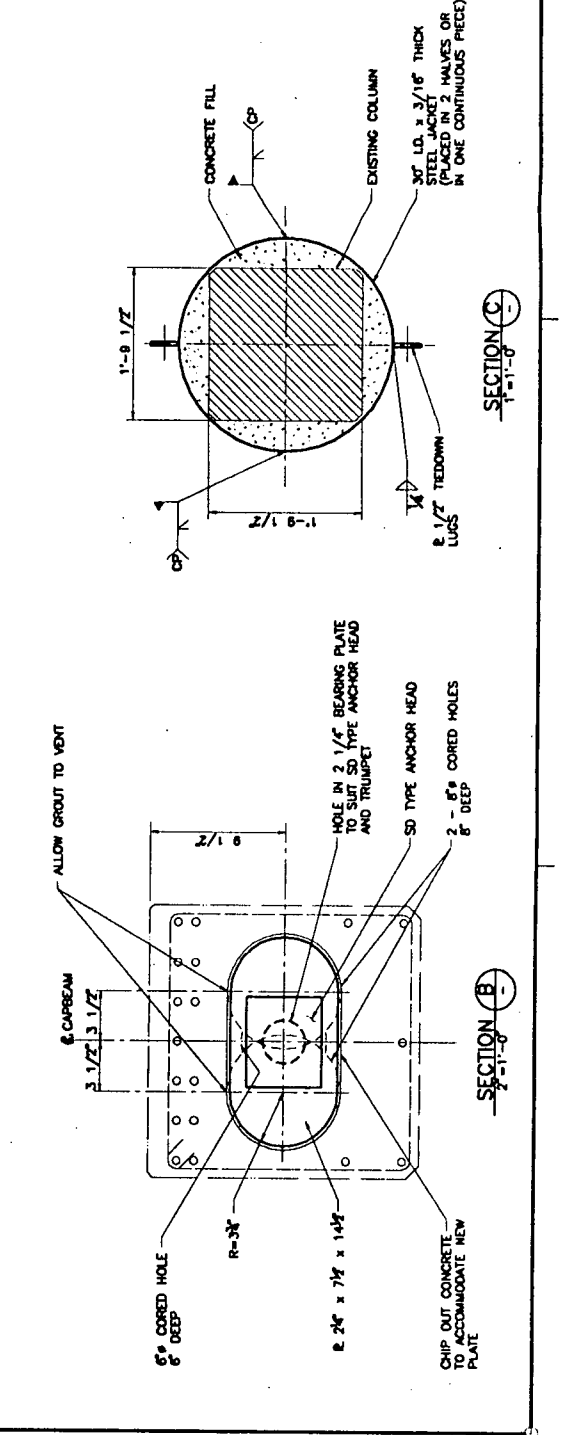
No.	Date	Description

Province of British Columbia
 MINISTRY OF TRANSPORTATION AND HIGHWAYS
 BRIDGE ENGINEERING BRANCH

SEISMIC RETROFIT
 CONCRETE PIER PROOF TESTS
 OAK STREET BRIDGE - PIER S28 MODEL
 CAPBEAM RETROFIT SCHEME 3

PREPARED UNDER THE DIRECTION OF: [Name]
 RECOMMENDED: [Name]
 CHECKED BY: [Name]
 DATE: [Date]

FILE NO. [Number] DRAWING NO. 0117-14
 CANCEL PRINTS BEARING PREVIOUS LETTER



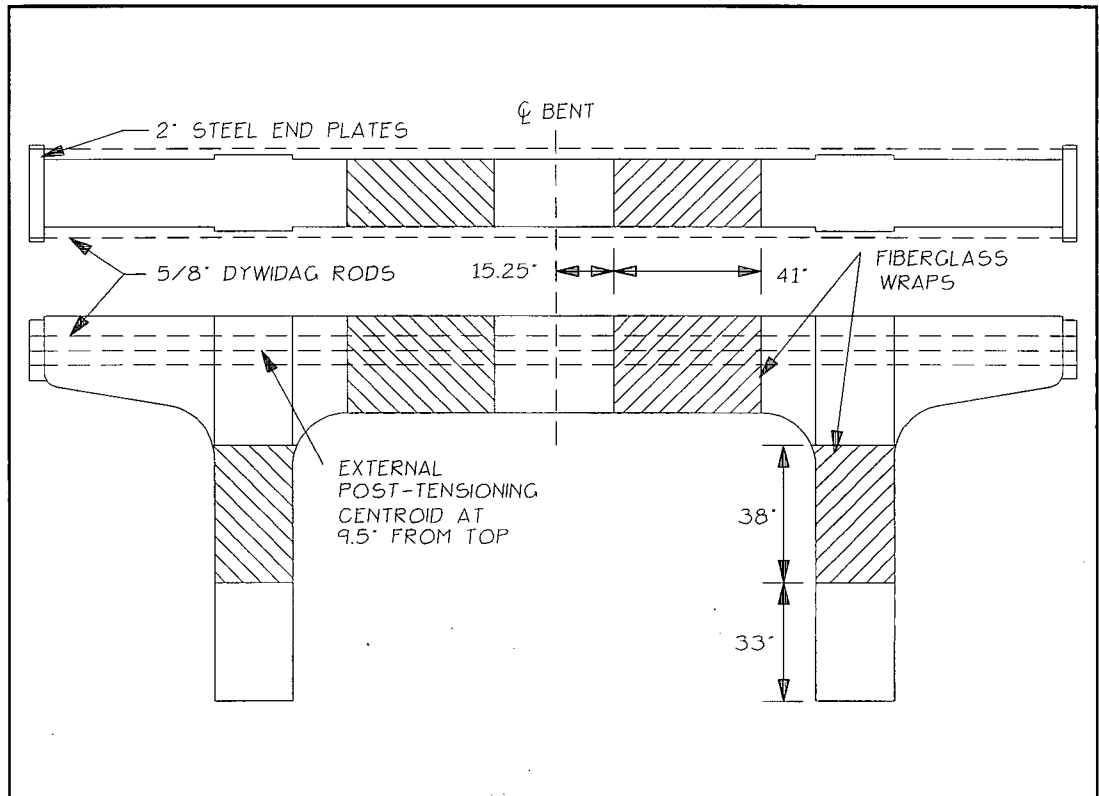


Figure Q-1 Elevation view of specimen OSB5

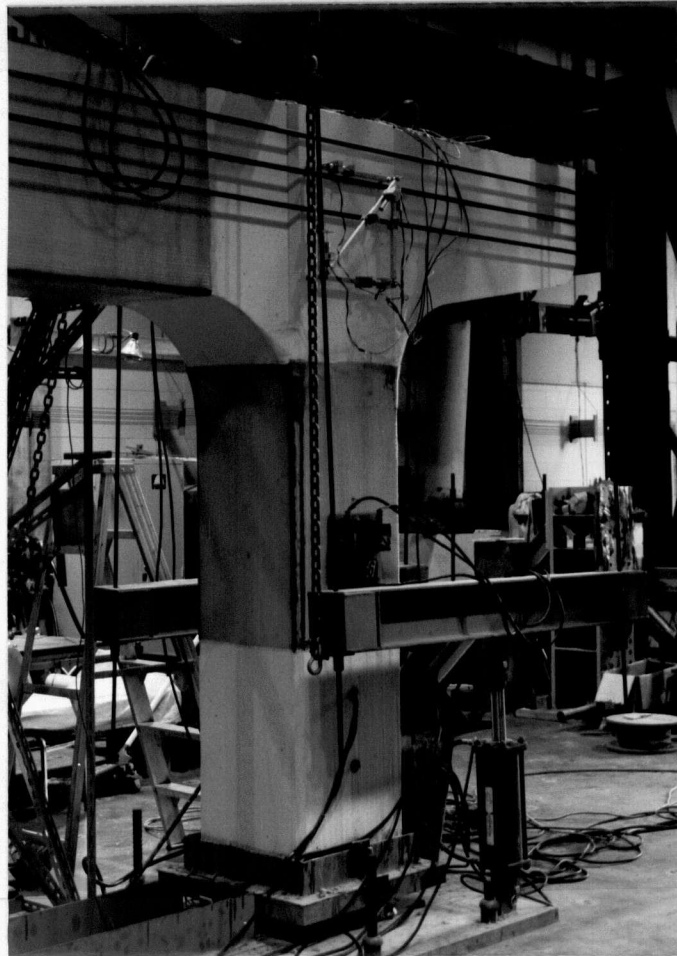


Figure A.1 Typical accelerometer setup on a column

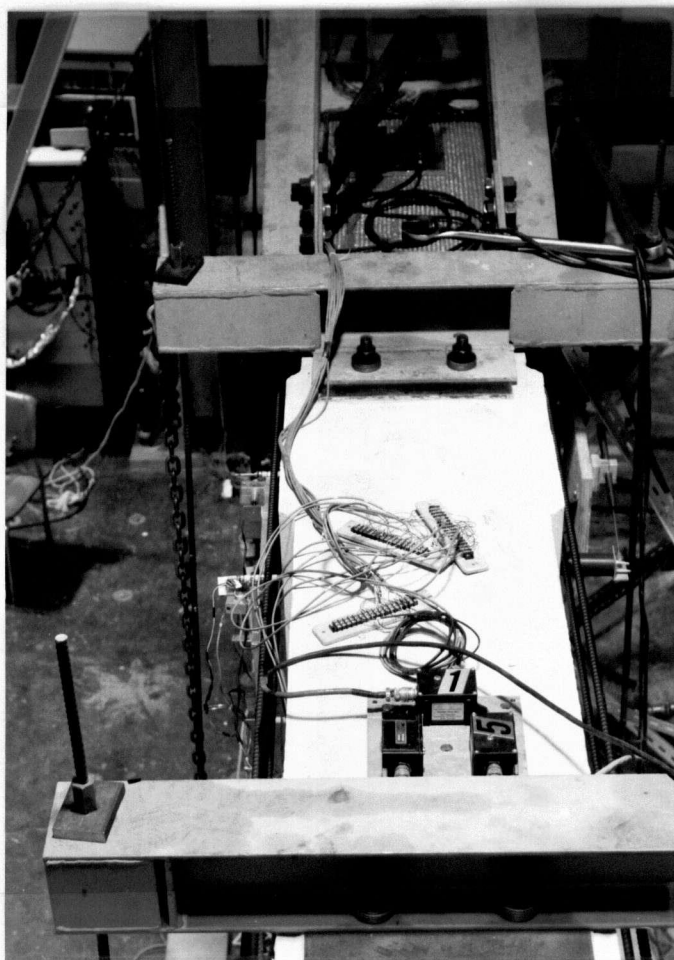


Figure A.2 Typical accelerometer setup on the cap beam



Figure A.3 Instrumented hammer



Figure A.4 Transverse impact applied with the instrumented hammer



Figure A.5 Vertical impact applied with the instrumented hammer



Figure A.6 Data acquisition system

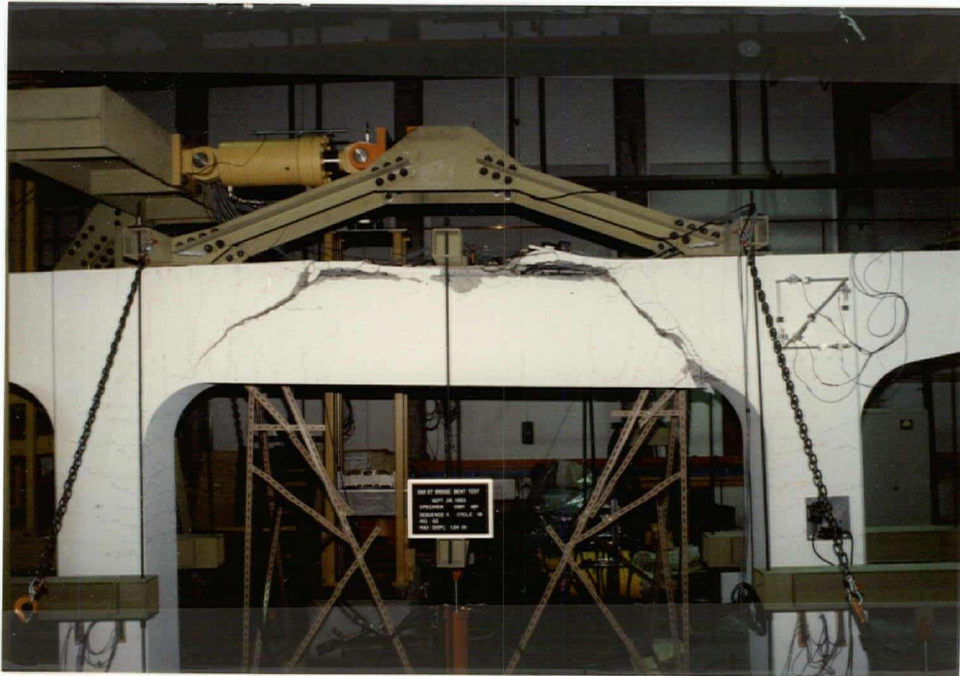
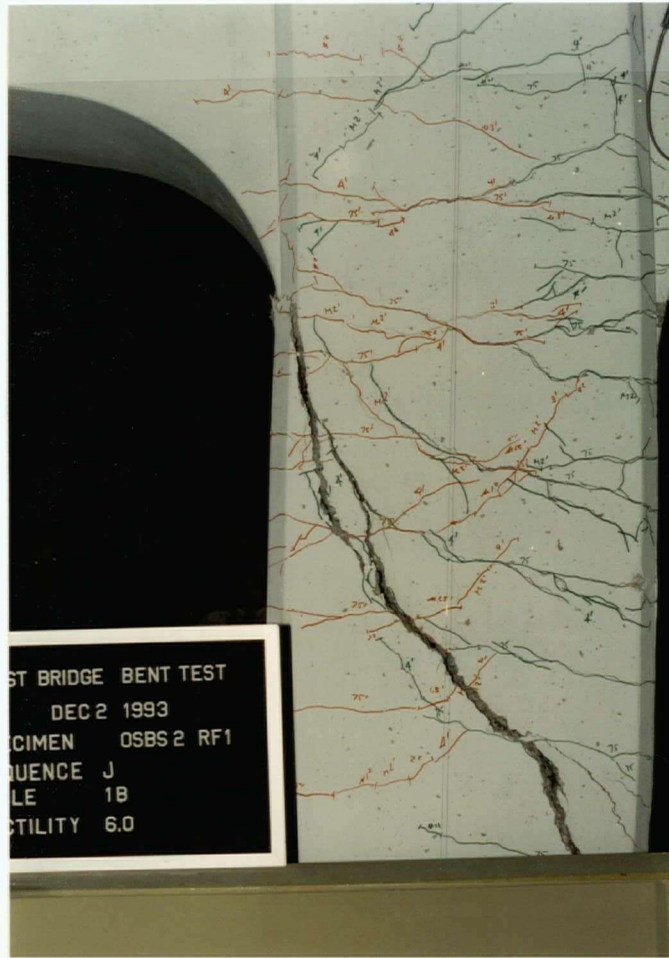


Figure A.7 Overall view of specimen OSB1 at failure



Figure A.8 View of specimen OSB2 at failure (north column, east side)



ST BRIDGE BENT TEST
DEC 2 1993
CIMEN OSBS 2 RF1
SEQUENCE J
LE 1B
CTILITY 6.0

Figure A.9 View of specimen OSB2 at failure (north column, west side)



UBC OSB 3
SEQ P CYCLE 6
APR 8 1994
U 9,0

Figure A.10 Overall view of specimen OSB3 at failure

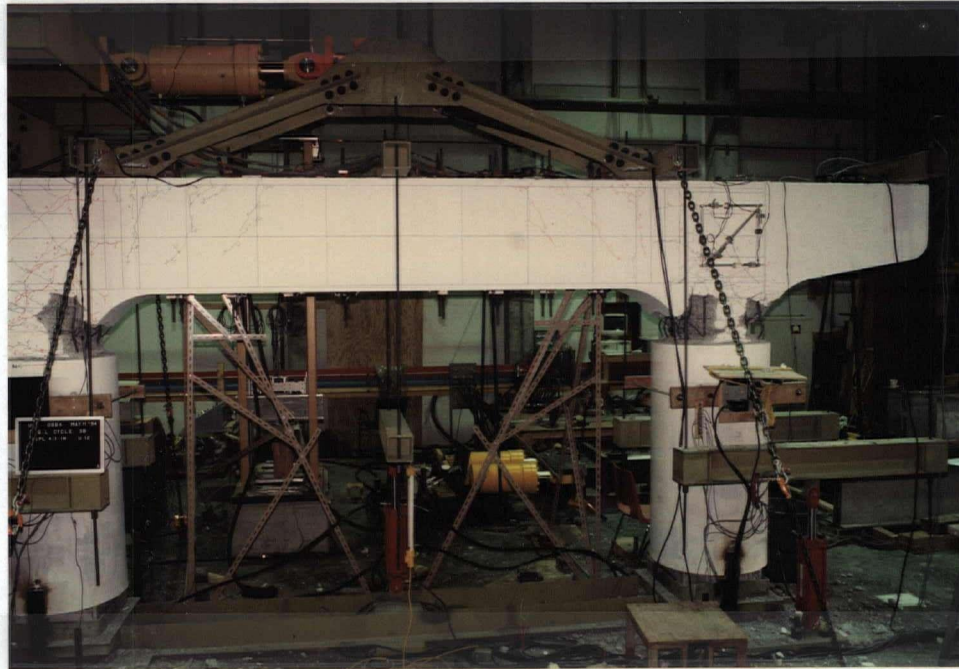


Figure A.11 Overall view of specimen OSB4 at failure



Figure A.12 View of specimen OSB5 at failure (north half)



Figure A.13 View of specimen OSB5 at failure (south half)

APPENDIX B

Appendix B presents the typical testing procedure. Detailed testing characteristics of the five specimens follow in section B.2. Section B.3 presents sensor locations for each specimen tested and, finally, details on processing of the longitudinal frequencies are included in section B.4.

B.1 TYPICAL TESTING PROCEDURE

Using the instrumented hammer, a typical testing procedure is as follow:

1. Verify connections between the A/D converter (Keithley), the conditioner and the computer;
2. Connect the instrumented hammer to the A/D converter and to its power box;
3. Turn power switches to ON for all these equipment components;
4. Balance the sensors;
5. Install the sensors at selected locations;
6. Connect cables between sensors and signal conditioner;
7. Set the signal conditioner to TEST;
8. Run "h AVDA" (usually from the KEITHLEY directory) and verify the input parameters (for details on the input parameters, see Schuster, 1994);
9. If calibration is desired:
 - (a) set the attenuation to 66dB and filters to OUT for all channels;
 - (b) press any key to begin sampling;
 - (c) after the beep, the signal conditioner key should be turned from TEST to CALIBRATE;
 - (d) after approximately one second, the key should be turned from CALIBRATE to NATURAL FREQUENCY and should remain in this position until calibration is completed;
 - (e) while data is acquiring, inspect the individual calibration records to ensure that sensors are working correctly;
 - (f) turn the key back to TEST position;
 - (g) after display of all calibration records, calibration can be repeated or one can proceed with data acquisition. If any of the sensors are not functioning, they can be verified before proceeding;
10. Set attenuation (usually 54dB) and filters for recording;
11. Proceed with data acquisition;
12. If calibration is desired after the data acquisition, repeat the procedure described in step no.9;
13. For quality control, inspect time histories using THV program;
14. If needed, relocate sensors;
15. Repeat steps no.4 to no.14 until the test is completed.

For details about balancing of sensors, see the operating instructions (Kinematics FBA-11).

B.2 DETAILED TESTING CHARACTERISTICS

Setup no.: refer to Figure 3.7

Dead load: on=vertical loading system activated / off=vertical loading system not applied

Actuator: in=lateral actuator installed / out=lateral actuator not installed

Test type: ambient=ambient vibrations / I/long, vert, trans=impact testing in the longitudinal, vertical or transverse direction

B.2.1 SPECIMEN OSB1

Test date: 09/16/1993 to 09/29/1993

SEQUENCE	SETUP NO.	DEAD LOAD	ACTUATOR	GAIN [dB]	TEST TYPE	DISK NO.	FILENAME
PRELIMINARY	1	on	in	6	ambient	1	O11D1A
		on	in	54	I/long	2	O11D1L
		on	in	54	I/vert	2	O11D1V
		on	in	54	I/trans	2	O11D1T
	2	on	in	6	ambient	3	O11D2A
		on	in	54	I/long	4	O11D2L
		on	in	54	I/vert	4	O11D2V
		on	in	54	I/trans	4	O11D2T
PRELIMINARY	2	off	in	12	ambient	5	O10D1A*
		off	in	54	I/long	6	O10D1L*
		off	in	54	I/vert	6	O10D1V*
		off	in	54	I/trans	6	O10D1T**
	1	off	in	12	ambient	7	O10D2A**
		off	in	54	I/long	8	O10D2L**
		off	in	54	I/vert	8	O10D2V**
		off	in	54	I/trans	8	O10D2T**
E	1	on	in	12	ambient	9	O1011A
$\mu = 0.50$		on	in	54	I/long	10	O1011L
		on	in	54	I/vert	10	O1011V
		on	in	54	I/trans	10	O1011T
	2	on	in	18	ambient	11	O1012A
		on	in	54	I/long	12	O1012L
		on	in	54	I/vert	12	O1012V
		on	in	54	I/trans	12	O1012T
F	2	on	in	54	I/long	54	O1022L
$\mu = 0.75$		on	in	54	T/vert	54	O1022V
		on	in	54	I/trans	54	O1022T
	1	on	in	54	I/long	54	O1021L
		on	in	54	I/vert	54	O1021V
		on	in	54	I/trans	54	O1021T
G	1	on	in	18	ambient	15	O1031A
$\mu = 1.0$		on	in	54	I/long	16	O1031L
		on	in	54	I/vert	16	O1031V
		on	in	54	I/trans	16	O1031T
	2	on	in	18	ambient	17	O1032A
		on	in	54	I/long	18	O1032L
		on	in	54	I/vert	18	O1032V
		on	in	54	I/trans	18	O1032T
H	2	on	in	54	I/long	19	O1042L
$\mu = 1.5$		on	in	54	I/vert	19	O1042V

SEQUENCE	SETUP NO.	DEAD LOAD	ACTUATOR	GAIN (aB)	TEST TYPE	DISK NO.	FILENAME
		on	in	54	I/trans	19	LOST
	1	on	in	54	I/long	20	O1041L
		on	in	54	I/vert	20	O1041V
		on	in	54	I/trans	20	O1041T
I	1	on	in	18	ambient	21	O1051A
$\mu = 2$		on	in	54	I/long	22	O1051L
		on	in	54	I/vert	22	O1051V
		on	in	54	I/trans	22	O1051T
	2	on	in	18	ambient	23	O1052A
		on	in	54	I/long	24	O1052L
		on	in	54	I/vert	24	O1052V
		on	in	54	I/trans	24	O1052T
J	2	on	in	54	I/long	25	O1062L
$\mu = 3$		on	in	54	I/vert	25	O1062V
		on	in	54	I/trans	25	O1062T
	1	on	in	54	I/long	26	O1061L
		on	in	54	I/vert	26	O1061V
		on	in	54	I/trans	26	O1061T
FINAL	1	off	in	24	ambient	27	O1171A
$\mu = 4$		off	in	54	I/long	28	O1171L
		off	in	54	I/vert	28	O1171V
		off	in	54	I/trans	28	O1171T
	2	off	in	24	ambient	29	O1172A
		off	in	54	I/long	30	O1172L
		off	in	54	I/vert	30	O1172V
		off	in	54	I/trans	30	O1172T
FINAL	2	on	in	24	ambient	31	O1071A*
		on	in	54	I/long	32	O1072L
		on	in	54	I/vert	32	O1072V
		on	in	54	I/trans	32	O1072T
	1	on	in	24	ambient	33	O1072A**
		on	in	54	I/long	34	O1071L
		on	in	54	I/vert	34	O1071V
		on	in	54	I/trans	34	O1071T
FINAL	2	off	out	18	ambient	35	O1182A
		off	out	54	I/long	36	O1182L
		off	out	54	I/vert	36	O1182V
		off	out	54	I/trans	36	O1182T
FINAL	2	on	out	18	ambient	37	O1082A
		on	out	54	I/long	38	O1082L
		on	out	54	I/vert	38	O1082V
		on	out	54	I/trans	38	O1082T

* These files correspond to setup no.2

** These files correspond to setup no.1

B.2.2 SPECIMEN OSB2

Test date: 11/30/1993 to 12/03/1993

SEQUENCE	SETUP NO.	DEAD LOAD	ACTUATOR	GAIN (dB)	TEST TYPE	DISK NO.	FILENAME
PRELIMINARY	2	off	in	12	ambient	1	O2PR2A
		off	in	54	I/trans,vert,long,long	1	O2PR2H
PRELIMINARY	2	on	in	12	ambient	2	O2PD2A
		on	in	54	I/trans,vert,long,long	2	O2PD2H
PRELIMINARY	1	on	in	18	ambient	3	O2PD1A
		on	in	54	I/trans,vert,long,long	3	O2PD1H
PRELIMINARY	1	off	in	12/6 ⁽¹⁾	ambient	4	O2PR1A
		off	in	54	I/trans,vert,long,long	4	O2PR1H
C	1	on	in	12	ambient	5	O2OC1A
$\mu = 0.50$		on	in	54	I/trans,vert,long,long	5	O2OC1H
D	1	on	in	6	ambient	6	O2OD1A
$\mu = 0.75$		on	in	54	I/trans,vert,long,long	6	O2OD1H
E	1	on	in	12	ambient	7	O2OE1A
$\mu = 1$		on	in	54	I/trans,vert,long,long	7	O2OE1H
F	1	on	in	12	ambient	8	O2OF1A
$\mu = 1.5$		on	in	54	I/trans,vert,long,long	8	O2OF1H
G	1	on	in	6,12 ⁽²⁾	ambient	9	O2OG1A
$\mu = 2$		on	in	54	I/trans,vert,long,long	9	O2OG1H
H	1	on	in	12	ambient	10	O2OH1A
$\mu = 3$		on	in	54	I/trans,vert,long,long	10	O2OH1H
I	1	on	in	6	ambient	11	O2OI1A
$\mu = 4$		on	in	54	I/trans,vert,long,long	11	O2OI1H
FINAL	1	off	in	6	ambient	12	O2A01A
$\mu = 6$		off	in	54	I/trans,vert,long,long	12	O2A01H
FINAL	1	on	in	12	ambient	13	O2OJ1A
		on	in	54	I/trans,vert,long,long	13	O2OJ1H
FINAL	2	on	in	18	ambient	14	O2OJ2A
		on	in	54	I/trans,vert,long,long	14	O2OJ2H
FINAL	2	off	in	6,24 ⁽³⁾	ambient	15	O2A02A
		off	in	54	I/trans,vert,long,long	15	O2A02H

I/trans,vert,long,long=one file with:

- segment 1 = impact in the transverse direction
- segment 2 = impact in the vertical direction
- segment 3 = impact in the longitudinal direction
- segment 4 = impact in the longitudinal direction

(1): segment 1 = 6 dB / segment 2 = 12dB

(2): segments 1,2,3 = 6 dB / segment 4 = 12 dB

(3): segment 1 =6 dB / segments 2,3,4 = 12 dB

B.2.3 SPECIMEN OSB3

Test date: 03/23/1994 to 03/31/1994

SEQUENCE	SETUP NO.	DEAD LOAD	ACTUATOR	GAIN (Hz)	TEST TYPE	DISK NO.	FILENAME
PRELIMINARY	1	off	out	12	ambient	1	O3P11A
		off	out	54	I/long	2,3	O3P11L (and G)*
		off	out	54	I/vert	2,3	O3P11V
		off	out	54	I/trans	2,3	O3P11T
PRELIMINARY	1	on	out	54	I/long	4,5	O3P21L (and G)
		on	out	54	I/vert	4,5	O3P21V
		on	out	54	I/trans	4,5	O3P21T
PRELIMINARY	2	on	out	54	I/long	6,7	O3P32L (and G)
		on	out	54	I/vert	6,7	O3P32V
		on	out	54	I/trans	6,7	O3P32T
PRELIMINARY	2	off	out	54	I/long	8,9	O3P42L (and G)
		off	out	54	I/vert	8,9	O3P42V
		off	out	54	I/trans	8,9	O3P42T
PRELIMINARY	2	off	in	18	ambient	10	O3P52A
		off	in	54	I/long	11,12	O3P52L (and G)
		off	in	54	I/vert	11,12	O3P52V
		off	in	54	I/trans	11,12	O3P52T
PRELIMINARY	2	on	in	24	ambient	13	O3P62A
		on	in	54	I/long	14,15	O3P62L (and G)
		on	in	54	I/vert	14,15	O3P62V
		on	in	54	I/trans	14,15	O3P62T
PRELIMINARY	1	on	in	18	ambient	16	O3P71A
		on	in	54	I/long	17,18	O3P71L (and G)
		on	in	54	T/vert	17,18	O3P71V
		on	in	54	I/trans	17,18	O3P71T
PRELIMINARY	1	off	in	12	ambient	19	O3P81A
		on	in	54	I/long	20,21	O3P81L (and G)
		off	in	54	I/vert	20,21	O3P81V
		off	in	54	I/trans	20,21	O3P81T
G	1	on	in	18	ambient	22	O30G1A
$\mu = 0.75$		on	in	54	I/long	23,24	O30G1L (and G)
		on	in	54	I/vert	23,24	O30G1V
		on	in	54	I/trans	23,24	O30G1T
I	1	on	in	12	ambient	25	O30I1A
$\mu = 1.5$		on	in	54	I/long	26,27	O30I1L (and G)
		on	in	54	I/vert	26,27	O30I1V
		on	in	54	I/trans	26,27	O30I1T
J	1	on	in	12	ambient	28	O30J1A
$\mu = 2$		on	in	54	I/long	29,30	O30J1L (and G)
		on	in	54	I/vert	29,30	O30J1V
		on	in	54	I/trans	29,30	O30J1T
K	1	on	in	6	ambient	31	O30K1A
$\mu = 3$		on	in	54	I/long	32,33	O30K1L (and G)
		on	in	54	I/vert	32,33	O30K1V
		on	in	54	I/trans	32,33	O30K1T
L	1	on	in	6	ambient	34	O30L1A
$\mu = 4$		on	in	54	I/long	35,36	O30L1L (and G)
		on	in	54	I/vert	35,36	O30L1V
		on	in	54	I/trans	35,36	O30L1T

SEQUENCE	SETUP NO.	DEAD LOAD	ACTUATOR	GAIN [dB]	TEST TYPE	DISK NO.	FILENAME
M	1	on	in	12	ambient	37	O30M1A
$\mu = 6$		on	in	54	I/long	38,39	O30M1L (and G)
		on	in	54	I/vert	38,39	O30M1V
		on	in	54	I/trans	38,39	O30M1T
N	1	on	in	54	I/long	40,41	O30N1L (and G)
$\mu = 9$		on	in	54	I/vert	40,41	O30N1V
		on	in	54	I/trans	40,41	O30N1T
FINAL	1	off	in	18	ambient	42	O3F81A
$\mu = 12$		off	in	54	I/long	43,44	O3F81L (and G)
		off	in	54	I/vert	43,44	O3F81V
		off	in	54	I/trans	43,44	O3F81T
FINAL	1	on	in	18	ambient	45	O3F71A
		on	in	54	I/long	46,47	O3F71L (and G)
		on	in	54	I/vert	46,47	O3F71V
		on	in	54	I/trans	46,47	O3F71T
FINAL	2	on	in	24	ambient	48	O3F62A
		on	in	54	I/long	49,50	O3F62L (and G)
		on	in	54	I/vert	49,50	O3F62V
		on	in	54	I/trans	49,50	O3F62T
FINAL	2	off	in	24	ambient	51	O3F52A
		off	in	54	I/long	52,53	O3F52L (and G)
		off	in	54	I/vert	52,53	O3F52V
		off	in	54	I/trans	52,53	O3F52T
FINAL	2	off	out	30	ambient	54	O3F42A
		off	out	54	I/long	55,56	O3F42L (and G)
		off	out	54	I/vert	55,56	O3F42V
		off	out	54	I/trans	55,56	O3F42T
FINAL	2	on	out	24	ambient	57	O3F32A
		on	out	54	I/long	58,59	O3F32L (and G)
		on	out	54	I/vert	58,59	O30I1V
		on	out	54	I/trans	58,59	O3F32T
FINAL	1**	on	out	54	I/long	61,62	O3F31L (and G)
		on	out	54	I/vert	61,62	O3F31V
		on	out	54	I/trans	61,62	O3F31T
FINAL	1**	off	out	54	I/long	63,64	O3F11L (and G)
		off	out	54	I/vert	63,64	O3F11V
		off	out	54	I/trans	63,64	O3F11T

* Two different filenames, O3P11L and O3P11G, for two longitudinal impact sets

** Sensors 2,3,6 correspond to the nodes and directions of setup no.2

B.2.4 SPECIMEN OSB4

Test date: 05/09/1994 to 05/12/1994

SEQUENCE	SETUP NO.	DEAD LOAD	ACTUATOR	GAIN (dB)	TEST TYPE	DISK NO.	FILENAME
PRELIMINARY	1	off	out	12	ambient	1	O4P11A
		off	out	54	I/long	1,2	O4P11L (and G)
		off	out	54	I/vert	1,2	O4P11V
		off	out	54	I/trans	1,2	O4P11T
PRELIMINARY	1	on	out	12	ambient	3	O4P21A
		on	out	54	I/long	3,4	O4P21L (and G)
		on	out	54	I/vert	3,4	O4P21V
		on	out	54	I/trans	3,4	O4P21T
PRELIMINARY	2	on	out	12	ambient	5	O4P32A
		on	out	54	I/long	5,6	O4P32L (and G)
		on	out	54	I/vert	5,6	O4P32V
		on	out	54	I/trans	5,6	O4P32T
PRELIMINARY	2	off	out	24	ambient	7	O4P42A
		off	out	54	I/long	7,8	O4P42L (and G)
		off	out	54	I/vert	7,8	O4P42V
		off	out	54	I/trans	7,8	O4P42T
PRELIMINARY	2	off	in	18	ambient	9	O4P52A
		off	in	54	I/long	9,10	O4P52L (and G)
		off	in	54	I/vert	9,10	O4P52V
		off	in	54	I/trans	9,10	O4P52T
PRELIMINARY	2	on	in	18	ambient	11	O4P62A
		on	in	54	I/long	11,12	O4P62L (and G)
		on	in	54	I/vert	11,12	O4P62V
		on	in	54	I/trans	11,12	O4P62T
PRELIMINARY	1	on	in	18	ambient	13	O4P71A
		on	in	54	I/long	13,14	O4P71L (and G)
		on	in	54	I/vert	13,14	O4P71V
		on	in	54	I/trans	13,14	O4P71T
PRELIMINARY	1	off	in	18	ambient	15	O4P81A
		off	in	54	I/long	15,16	O4P81L (and G)
		off	in	54	I/vert	15,16	O4P81V
		off	in	54	I/trans	15,16	O4P81T
D	1	on	in	18	ambient	17	O40D1A
$\mu = 0.75$		on	in	54	I/long	17,18	O40D1L (and G)
		on	in	54	I/vert	17,18	O40D1V
		on	in	54	I/trans	17,18	O40D1T
E	1	on	in	18	ambient	19	O40E1A
$\mu = 1$		on	in	54	I/long	19,20	O40E1L (and G)
		on	in	54	I/vert	19,20	O40E1V
		on	in	54	I/trans	19,20	O40E1T
F	1	on	in	18	ambient	21	O40F1A
$\mu = 1.5$		on	in	54	I/long	21,22	O40F1L (and G)
		on	in	54	I/vert	21,22	O40F1V
		on	in	54	I/trans	21,22	O40F1T
G	1	on	in	18	ambient	23	O40G1A
$\mu = 2$		on	in	54	I/long	23,24	O40G1L (and G)
		on	in	54	I/vert	23,24	O40G1V
		on	in	54	I/trans	23,24	O40G1T
H	1	on	in	18	ambient	25	O40H1A

SEQUENCE	SETUP NO.	DEAD LOAD	ACTUATOR	GAIN (aB)	TEST TYPE	DISK NO.	FILENAME
$\mu = 3$		on	in	54	I/long	25,26	O40H1L (and G)
		on	in	54	I/vert	25,26	O40H1V
		on	in	54	I/trans	25,26	O40H1T
I	1	on	in	18	ambient	27	O40I1A
$\mu = 4$		on	in	54	I/long	27,28	O40I1L (and G)
		on	in	54	I/vert	27,28	O40I1V
		on	in	54	I/trans	27,28	O40I1T
J	1	on	in	18	ambient	29	O40J1A
$\mu = 6$		on	in	54	I/long	29,30	O40J1L (and G)
		on	in	54	I/vert	29,30	O40J1V
		on	in	54	I/trans	29,30	O40J1T
K	1	on	in	18	ambient	31	O40K1A
$\mu = 9$		on	in	54	I/long	31,32	O40K1L (and G)
		on	in	54	I/vert	31,32	O40K1V
		on	in	54	I/trans	31,32	O40K1T
FINAL	1	off	in	18	ambient	33	O40L1A
$\mu = 12$		off	in	54	I/long	33,34	O40L1L (and G)
		off	in	54	I/vert	33,34	O40L1V
		off	in	54	I/trans	33,34	O40L1T
FINAL	1	on	in	18	ambient	35	O4F71A
		on	in	54	I/long	35,36	O4F71L (and G)
		on	in	54	I/vert	35,36	O4F71V
		on	in	54	I/trans	35,36	O4F71T
FINAL	2	on	in	30	ambient	37	O4F62A
		on	in	54	I/long	37,38	O4F62L (and G)
		on	in	54	I/vert	37,38	O4F62V
		on	in	54	I/trans	37,38	O4F62T
FINAL	2	off	in	30	ambient	39	O4F52A
		off	in	54	I/long	39,40	O4F52L (and G)
		off	in	54	I/vert	39,40	O4F52V
		off	in	54	I/trans	39,40	O4F52T
FINAL	2	off	out	24	ambient	41	O4F42A
		off	out	54	I/long	41,42	O4F42L (and G)
		off	out	54	I/vert	41,42	O4F42V
		off	out	54	I/trans	41,42	O4F42T
FINAL	2	on	out	18	ambient	43	O4F32A
		on	out	54	I/long	43,44	O4F32L (and G)
		on	out	54	I/vert	43,44	O40I1V
		on	out	54	I/trans	43,44	O4F32T
FINAL	1	on	out	18	ambient	45	O4F21A
		on	out	54	I/long	45,46	O4F21L (and G)
		on	out	54	I/vert	45,46	O4F21V
		on	out	54	I/trans	45,46	O4F21T
FINAL	1	off	out	24	ambient	47	O4F11A
		off	out	54	I/long	47,48	O4F11L (and G)
		off	out	54	I/vert	47,48	O4F11V
		off	out	54	I/trans	47,48	O4F11T

B.2.5 SPECIMEN OSB5

Test date: 09/02/1994 to 09/09/1994

SEQUENCE	SETUP NO.	DEAD LOAD	ACTUATOR	GAIN (lb)	TEST TYPE	DISK NO.	FILENAME
PRELIMINARY	1	off	out	12	ambient	1	O5P11A
		off	out	54	I/long	1,2	O5P11L (and G)
		off	out	54	I/vert	1,2	O5P11V
		off	out	54	I/trans	1,2	O5P11T
PRELIMINARY	1	on	out	12	ambient	3	O5P21A
		on	out	54	I/long	3,4	O5P21L (and G)
		on	out	54	I/vert	3,4	O5P21V
		on	out	54	I/trans	3,4	O5P21T
PRELIMINARY	2	on	out	12	ambient	5	O5P32A
		on	out	54	I/long	5,6	O5P32L (and G)
		on	out	54	I/vert	5,6	O5P32V
		on	out	54	I/trans	5,6	O5P32T
PRELIMINARY	2	off	out	12	ambient	7	O5P42A
		off	out	54	I/long	7,8	O5P42L (and G)
		off	out	54	I/vert	7,8	O5P42V
		off	out	54	I/trans	7,8	O5P42T
PRELIMINARY	2	off	in	12	ambient	9	O5P52A
		off	in	54	I/long	9,10	O5P52L (and G)
		off	in	54	I/vert	9,10	O5P52V
		off	in	54	I/trans	9,10	O5P52T
PRELIMINARY	2	on	in	12	ambient	11	O5P62A
		on	in	54	I/long	11,12	O5P62L (and G)
		on	in	54	I/vert	11,12	O5P62V
		on	in	54	I/trans	11,12	O5P62T
PRELIMINARY	1	on	in	12	ambient	13	O5P71A
		on	in	54	I/long	13,14	O5P71L (and G)
		on	in	54	T/vert	13,14	O5P71V
		on	in	54	I/trans	13,14	O5P71T
PRELIMINARY	1	off	in	18	ambient	15	O5P81A
		off	in	54	I/long	15,16	O5P81L (and G)
		off	in	54	I/vert	15,16	O5P81V
		off	in	54	I/trans	15,16	O5P81T
D	1	on	in	12	ambient	17	O50D1A
$\mu = 0.75$		on	in	54	I/long	17,18	O50D1L (and G)
		on	in	54	I/vert	17,18	O50D1V
		on	in	54	I/trans	17,18	O50D1T
E	1	on	in	12	ambient	19	O50E1A
$\mu = 1$		on	in	54	I/long	19,20	O50E1L (and G)
		on	in	54	I/vert	19,20	O50E1V
		on	in	54	I/trans	19,20	O50E1T
F	1	on	in	12	ambient	21	O50F1A
$\mu = 1.5$		on	in	54	I/long	21,22	O50F1L (and G)
		on	in	54	I/vert	21,22	O50F1V
		on	in	54	I/trans	21,22	O50F1T
G	1	on	in	12	ambient	23	O50G1A
$\mu = 2$		on	in	54	I/long	23,24	O50G1L (and G)
		on	in	54	I/vert	23,24	O50G1V
		on	in	54	I/trans	23,24	O50G1T
H	1	on	in	12	ambient	25	O50H1A

SEQUENCE	SETUP NO.	DEAD LOAD	ACTUATOR	GAIN [dB]	TEST TYPE	DISK NO.	FILENAME
$\mu = 3$		on	in	54	I/long	25,26	O50H1L (and G)
		on	in	54	I/vert	25,26	O50H1V
		on	in	54	I/trans	25,26	O50H1T
I	1	on	in	12	ambient	27	O50I1A
$\mu = 4$		on	in	54	I/long	27,28	O50I1L (and G)
		on	in	54	I/vert	27,28	O50I1V
		on	in	54	I/trans	27,28	O50I1T
J	1	on	in	12	ambient	29	O50J1A
$\mu = 6$		on	in	54	I/long	29,30	O50J1L (and G)
		on	in	54	I/vert	29,30	O50J1V
		on	in	54	I/trans	29,30	O50J1T
K	1	on	in	12	ambient	31	O50K1A
$\mu = 9$		on	in	54	I/long	31,32	O50K1L (and G)
		on	in	54	I/vert	31,32	O50K1V
		on	in	54	I/trans	31,32	O50K1T
FINAL	1	off	in	12	ambient	33	O5F81A
$\mu = 12$		off	in	54	I/long	33,34	O5F81L (and G)
		off	in	54	I/vert	33,34	O5F81V
		off	in	54	I/trans	33,34	O5F81T
FINAL	1	on	in	18	ambient	35	O50L1A
		on	in	54	I/long	35,36	O50L1L (and G)
		on	in	54	I/vert	35,36	O50L1V
		on	in	54	I/trans	35,36	O50L1T
FINAL	2	on	in	12	ambient	39	O5F62A
		on	in	54	I/long	39,40	O5F62L (and G)
		on	in	54	I/vert	39,40	O5F62V
		on	in	54	I/trans	39,40	O5F62T
FINAL	2	off	in	12	ambient	37	O5F52A
		off	in	54	I/long	37,38	O5F52L (and G)
		off	in	54	I/vert	37,38	O5F52V
		off	in	54	I/trans	37,38	O5F52T
FINAL	2	off	out	18	ambient	41	O5F42A
		off	out	54	I/long	41,42	O5F42L (and G)
		off	out	54	I/vert	41,42	O5F42V
		off	out	54	I/trans	41,42	O5F42T
FINAL	2	on	out	18	ambient	43	O5F32A
		on	out	54	I/long	43,44	O5F32L (and G)
		on	out	54	I/vert	43,44	O5F32V
		on	out	54	I/trans	43,44	O5F32T
FINAL	1	on	out	18	ambient	45	O5F21A
		on	out	54	I/long	45,46	O5F21L (and G)
		on	out	54	I/vert	45,46	O5F21V
		on	out	54	I/trans	45,46	O5F21T
FINAL	1	off	out	18	ambient	47	O5F11A
		off	out	54	I/long	47,48	O5F11L (and G)
		off	out	54	I/vert	47,48	O5F11V
		off	out	54	I/trans	47,48	O5F11T

B.3 DETAILED SENSOR LOCATION

AV = ambient vibration testing

IMP = impact testing with the instrumented hammer

ham = instrumented hammer

channel identification: example 5L = node 5 in the longitudinal direction (refer to Figure 3.7 and to section 5.2.2.2)

setup	channel	OSB1 AV	OSB1 IMP	OSB2 AV	OSB2 IMP	OSB3 AV	OSB3 IMP	OSB4 AV	OSB4 IMP	OSB5 AV	OSB5 IMP
1	1	1L	ham	5L	5L	5L	5L	5L	5L	5L	5L
1	2	6L	6L	-6L	-6L	6L	6L	6L	6L	-6L	-6L
1	3	5L	5L	6T	6T	6T	6T	6T	6T	6T	6T
1	4	6T	6T	4T	4T	4T	4T	4T	4T	4T	4T
1	5	4T	4T	5T	5T	5T	5T	5T	5T	5T	5T
1	6	5T	5T	6V	6V	6V	6V	6V	6V	6V	6V
1	7	4V	4V								
1	8	5V	5V								
1	9	n/a	n/a	n/a	n/a	n/a	ham	n/a	ham	n/a	ham
1	A	n/a	n/a	n/a	ham	n/a	n/a	n/a	n/a	n/a	n/a
2	1	2L	ham	2L	2L	2L	2L	2L	2L	2L	2L
2	2	1L	1L	-1L	-1L	1L	1L	1L	1L	-1L	-1L
2	3	5L	5L	1T	1T	1T	1T	1T	1T	1T	1T
2	4	1T	1T	3T	3T	3T	3T	-3T	-3T	3T	3T
2	5	3T	3T	2T	2T	2T	2T	2T	2T	2T	2T
2	6	2T	2T	1V	1V	1V	1V	1V	1V	1V	1V
2	7	3V	3V								
2	8	2V	2V								
2	9	n/a	n/a	n/a	n/a	n/a	ham	n/a	ham	n/a	ham
2	A	n/a	n/a	n/a	ham	n/a	n/a	n/a	n/a	n/a	n/a

B.4 HAMMER AND SENSOR SPECIFICATIONS

B.4.1 HAMMER SPECIFICATIONS

Model : DYTRAN / model 5803A 12 pound impulse hammer
Range : 5000 lbs (nominal range for +5 volts out)
Sensitivity : 1.0 mv/lb
Maximum input : 10000 lbs
Stiffness sensor : 110 lb/ μ in
Resonant frequency : 75 kHz (sensor with no impact cap);

B.4.2 SENSOR SPECIFICATIONS:

Model: : Kinematics FBA-11
Full scale range: : ± 0.5 g
Output range : ± 2.5 volts
Dynamic range : 130 dB from 0 to 50 Hz
: 140 dB from 0 to 10 Hz
Natural frequency: : 50 Hz (damping: 70% critical)

B.5 DETAILS ON PROCESSING OF LONGITUDINAL FREQUENCY

Ductility Level	Impact Set	Channel	OSB1 ham.	OSB2 ham.	OSB2 ambient	OSB3 ham.	OSB4 ham.	OSB5 ham.	OSB5 ambient
0	1	5L	20.28	20.09	19.63	22.31	21.00	18.92	19.35
	1	6L	20.28	20.09		22.31	21.00	18.92	
	2	5L	n/a	n/a		22.21	21.00	18.92	
	2	6L	n/a	n/a		22.21	21.00	18.92	
0.75	1	5L	18.75	18.22	19.63	19.93	20.60	16.30	17.77
	1	6L	18.75	18.22		19.93	20.60	16.30	
	2	5L	n/a	n/a		19.78	20.63	16.30	
	2	6L	n/a	n/a		19.78	20.63	16.20	
1.0	1	5L	17.5	17.11	18.16	*	20.43	20.80	20.78
	1	6L	17.5	17.11		*	20.43	20.80	
	2	5L	n/a	n/a		*	20.43	**	
	2	6L	n/a	n/a		*	20.43	**	
1.5	1	5L	16.11	15.86	16.5	19.35	20.02	20.51	19.22
	1	6L	16.11	15.86		19.35	20.08	20.51	
	2	5L	n/a	n/a		19.41	20.02	20.23	
	2	6L	n/a	n/a		19.41	20.08	20.23	
2.0	1	5L	15.09	18.01	18.16	18.31	19.17	19.07	19.32
	1	6L	15.09	18.01		18.31	19.20	19.07	
	2	5L	n/a	n/a		18.16	19.17	19.04	
	2	6L	n/a	n/a		18.16	19.20	19.04	
3.0	1	5L	13.22	17.18	17.38	17.43	18.34	17.79	18.13
	1	6L	13.22	17.18		17.43	18.25	17.79	
	2	5L	n/a	n/a		17.43	18.34	17.70	
	2	6L	n/a	n/a		17.43	18.25	17.70	
4.0	1	5L	12.97	11.54	12.5	16.97	17.95	18.01	18.09
	1	6L	12.97	11.54		16.99	17.95	18.01	
	2	5L	n/a	n/a		16.97	17.95	18.16	
	2	6L	n/a	n/a		16.99	17.95	18.16	
6.0	1	5L	n/a	13.28	14.5	16.54	17.64	17.67	17.7
	1	6L	n/a	13.28		16.57	17.64	17.67	
	2	5L	n/a	n/a		16.54	17.67	17.73	
	2	6L	n/a	n/a		16.57	17.67	17.73	
9.0	1	5L	n/a	n/a		16.08	17.21	16.91	16.95
	1	6L	n/a	n/a		16.08	17.21	16.91	
	2	5L	n/a	n/a		16.14	17.18	16.99	
	2	6L	n/a	n/a		16.18	17.18	16.99	
12.0	1	5L	n/a	n/a		14.68	14.62	17.18	17.2
	1	6L	n/a	n/a		14.68	14.62	17.18	
	2	5L	n/a	n/a		14.59	14.65	17.21	
	2	6L	n/a	n/a		14.59	14.65	17.21	

* Vibrations not measured

** Signals corrupted

APPENDIX C

Appendix C includes typical spreadsheets for the three structural damage indices evaluated in this study: displacement ductility, modified stiffness ratio and the modified Ppark and Ang index.

C.1 . TYPICAL SPREADSHEET FOR DISPLACEMENT DUCTILITY - SPECIMEN OSB1

$$\delta_y = 0.247 \text{ in}$$

sequence	displacement [in]	ductility	absolute ductility	maximum ductility
f1	0.206	0.836	0.836	0.836
	-0.183	-0.741	0.741	
f2	0.174	0.704	0.704	0.710
	-0.175	-0.710	0.710	
f3	0.175	0.711	0.711	0.729
	-0.180	-0.729	0.729	
g1	0.253	1.026	1.026	1.029
	-0.254	-1.029	1.029	
g2	0.258	1.047	1.047	1.047
	-0.217	-0.879	0.879	
g3	0.269	1.090	1.090	1.090
	-0.248	-1.003	1.003	
h1	0.452	1.832	1.832	1.872
	-0.462	-1.872	1.872	
h2	0.427	1.732	1.732	1.784
	-0.440	-1.784	1.784	
h3	0.430	1.740	1.740	1.785
	-0.441	-1.785	1.785	
i1	0.602	2.439	2.439	2.639
	-0.651	-2.639	2.639	
i2	0.626	2.536	2.536	2.622
	-0.647	-2.622	2.622	
i3	0.637	2.580	2.580	2.606
	-0.643	-2.606	2.606	
j1	0.829	3.359	3.359	3.976
	-0.981	-3.976	3.976	
j2	0.875	3.547	3.547	3.968
	-0.979	-3.968	3.968	
j3	0.879	3.561	3.561	3.966
	-0.979	-3.966	3.966	
k1	1.174	4.756	4.756	5.414
	-1.336	-5.414	5.414	

C.2 . TYPICAL SPREADSHEET FOR MODIFIED STIFFNESS RATIO - SPECIMEN OSB1

$$\delta_y = 0.247 \text{ in}$$

$$\delta_f = 1.174 \text{ in}$$

$$F_y = 55.848 \text{ kips}$$

$$F_f = 6.23 \text{ kips}$$

sequence	displacement [in]	load [kips]	km+ and km- [kips/in] load/displacement	D+ and D-	Dmax
f1	0.206	43.186	209.336	0.002	0.002
	-0.183	-42.813	234.079	-0.001	
f2	0.174	41.679	239.950	-0.001	-0.001
	-0.175	-42.293	241.258	-0.001	
f3	0.175	40.792	232.567	-0.001	0.000
	-0.180	-40.367	224.258	0.000	
g1	0.253	48.200	190.365	0.005	0.005
	-0.254	-48.562	191.187	0.004	
g2	0.258	50.981	197.293	0.004	0.004
	-0.217	-42.631	196.454	0.004	
g3	0.269	49.168	182.847	0.006	0.006
	-0.248	-45.850	185.179	0.005	
h1	0.452	60.399	133.568	0.017	0.024
	-0.462	-51.837	112.178	0.024	
h2	0.427	58.437	136.727	0.016	0.023
	-0.440	-50.661	115.034	0.023	
h3	0.430	57.673	134.280	0.016	0.026
	-0.441	-47.571	107.993	0.026	
i1	0.602	55.066	91.486	0.035	0.047
	-0.651	-50.182	77.038	0.047	
i2	0.626	46.886	74.898	0.049	0.056
	-0.647	-43.672	67.478	0.056	
i3	0.637	44.480	69.849	0.054	0.054
	-0.643	-48.640	75.623	0.048	
j1	0.829	43.127	52.029	0.080	0.092
	-0.981	-46.080	46.963	0.092	
j2	0.875	36.068	41.207	0.108	0.108
	-0.979	-42.738	43.637	0.100	
j3	0.879	34.106	38.805	0.116	0.116
	-0.979	-40.095	40.959	0.109	
k1	1.174	6.226	5.304	1.000	1.000
	-1.336	-31.913	23.884	0.203	

C.3 . TYPICAL SPREADSHEET FOR MODIFIED PARK AND ANG INDEX - SPECIMEN OSB1

$\delta_y = 0.247 \text{ in}$

$F_y = 55.848 \text{ kips}$

$\delta_r = 1.174 \text{ in}$

sequence	energy at each 1/4 cycle [kips*in]	cumulative energy [kips]	energy term	δ_m [in]	deformation term	total D	total D+
f1	2.579	2.579	0.004			0.004	0.004
	0.184	2.763	0.004			0.004	0.004
	3.427	6.189	0.009			0.009	0.009
f2	0.166	6.356	0.010	0.206	-0.044	-0.034	0.000
	2.343	8.698	0.013			0.013	0.013
	0.051	8.750	0.013			0.013	0.013
	2.183	10.933	0.017			0.017	0.017
f3	0.117	11.049	0.017	0.175	-0.077	-0.060	0.000
	2.195	13.245	0.020			0.020	0.020
	0.000	13.245	0.020			0.020	0.020
g1	1.928	15.173	0.023			0.023	0.023
	0.000	15.173	0.023	0.180	-0.072	-0.049	0.000
	2.898	18.071	0.028			0.028	0.028
	0.280	18.350	0.028			0.028	0.028
g2	5.138	23.488	0.036			0.036	0.036
	0.288	23.777	0.036	0.254	0.008	0.044	0.044
	4.151	27.928	0.043			0.043	0.043
	0.104	28.032	0.043			0.043	0.043
g3	2.914	30.947	0.047			0.047	0.047
	0.194	31.141	0.048	0.258	0.013	0.060	0.060
	3.937	35.078	0.054			0.054	0.054
	0.178	35.256	0.054			0.054	0.054
h1	3.719	38.975	0.059			0.059	0.059
	0.177	39.152	0.060	0.269	0.024	0.084	0.084
	10.485	49.637	0.076			0.076	0.076
	1.440	51.077	0.078			0.078	0.078
h2	15.431	66.508	0.101			0.101	0.101
	1.054	67.561	0.103	0.462	0.232	0.335	0.335
	9.574	77.135	0.118			0.118	0.118
	0.380	77.515	0.118			0.118	0.118
h3	8.380	85.895	0.131			0.131	0.131
	0.753	86.648	0.132	0.440	0.209	0.341	0.341
	8.430	95.079	0.145			0.145	0.145
	0.332	95.411	0.146			0.146	0.146
i1	7.983	103.394	0.158			0.158	0.158
	0.637	104.031	0.159	0.441	0.209	0.368	0.368
	16.856	120.887	0.184			0.184	0.184

	2.114	123.001	0.188			0.188	0.188
	21.912	144.913	0.221			0.221	0.221
	3.077	147.990	0.226	0.651	0.436	0.662	0.662
i2	20.284	168.273	0.257			0.257	0.257
	1.797	170.071	0.259			0.259	0.259
	17.263	187.334	0.286			0.286	0.286
	2.346	189.679	0.289	0.647	0.432	0.721	0.721
i3	17.327	207.006	0.316			0.316	0.316
	2.054	209.061	0.319			0.319	0.319
	16.730	225.791	0.344			0.344	0.344
	2.172	227.962	0.348	0.643	0.428	0.775	0.775
j1	23.806	251.768	0.384			0.384	0.384
	4.792	256.560	0.391			0.391	0.391
	28.706	285.266	0.435			0.435	0.435
	5.756	291.023	0.444	0.981	0.792	1.236	1.236
j2	20.503	311.526	0.475			0.475	0.475
	3.622	315.147	0.481			0.481	0.481
	19.981	335.128	0.511			0.511	0.511
	4.486	339.614	0.518	0.979	0.790	1.308	1.308
j3	17.677	357.291	0.545			0.545	0.545
	4.033	361.324	0.551			0.551	0.551
	19.779	381.103	0.581			0.581	0.581
	3.925	385.028	0.587	0.979	0.790	1.377	1.377
k1	17.890	402.918	0.615			0.615	0.615
	13.728	416.647	0.636			0.636	0.636
	36.301	452.948	0.691			0.691	0.691
	5.438	458.387	0.699	1.336	1.175	1.874	1.874

APPENDIX D

Appendix D presents the calculation sheet used for evaluation of the improved frequency response function, H_s . The method presented here uses a non-recursive approach based on the coherence function and is discussed in Park (1993).

IMPROVED FREQUENCY RESPONSE FUNCTION

$W_i = f(\text{COHERENCE FUNCTION})$

(from Mathcad ver. 5.0 - calculation sheet)

Inputs is vector X and Output is vector Y

Define array sizes and read X and Y vectors:

$$N := 16384 \quad dt := 0.001 \quad T := dt \cdot (N - 1) \quad M := 0.5 \cdot N \quad i := 0..N - 1 \quad j := 0..M \quad r := 1..M - 1 \quad df := \frac{1}{T}$$

Read Input and Output Signals

$$Y_i := \text{READ}(\text{out}) \quad X_i := \text{READ}(\text{inp})$$

Calculate Auto Spectra Spectra for X and Y :

$$\text{FTY} := \text{cfft}(Y) \quad \text{FTX} := \text{cfft}(X)$$

SMOOTHED DATA

Smooth the spectral estimates using "n" adjacent estimates:

$$n := 3 \quad m := -n..n \quad \Delta f := \frac{1}{T}$$

$$\text{SPEC}_j := \overline{\text{FTX}_j} \cdot \text{FTX}_j$$

$$\text{TEMP}_j := \frac{1}{2 \cdot n + 1} \sum_m \text{if}[(j + m) < 0 + ((j + m) > M), 0, \text{SPEC}_{j+m}]$$

$$\text{ASxx}_j := \text{TEMP}_j$$

(calculate only $N/2$ spectral values for each spectrum; the other half corresponds to the complex conjugates)

$$\text{SPEC}_j := \overline{\text{FTY}_j} \cdot \text{FTY}_j$$

$$\text{TEMP}_j := \frac{1}{2 \cdot n + 1} \sum_m \text{if}[(j + m) < 0 + ((j + m) > M), 0, \text{SPEC}_{j+m}]$$

$$\text{ASyy}_j := \text{TEMP}_j$$

$$\text{SPEC}_j := \overline{\text{FTX}_j} \cdot \text{FTY}_j$$

$$\text{TEMP}_j := \frac{1}{2 \cdot n + 1} \sum_m \text{if}[(j + m) < 0 + ((j + m) > M), 0, \text{SPEC}_{j+m}]$$

$$\text{CSxy}_j := \text{TEMP}_j$$

$$\text{SPEC}_j := \overline{\text{FTY}_j \cdot \text{FTX}_j}$$

$$\text{TEMP}_j := \frac{1}{2 \cdot n + 1} \sum_m \text{if} [((j + m) < 0) + ((j + m) > M), 0, \text{SPEC}_{j+m}]$$

$$\text{CSyx}_j := \text{TEMP}_j$$

Calculate Transfer Function and Coherence Between Y and X:

$$\text{TEMP}_j := \frac{\text{CSxy}_j}{\text{ASxx}_j} \quad \text{mHSxy} := \text{mag}(\text{TEMP})$$

$$\text{TEMP}_j := \frac{\text{ASyy}_j}{\text{CSyx}_j} \quad \text{mHSyx} := \text{mag}(\text{TEMP})$$

Coherence Function

$$\text{CHSxy}_j := \frac{\text{CSxy}_j \cdot \overline{\text{CSxy}_j}}{\text{ASxx}_j \cdot \text{ASyy}_j}$$

Case B: Wf is coherence dependant

$$\text{Wf}_j := \text{if} [(\text{Re}(\text{CHSxy}_j)) > 0.5, 1, 0]$$

Term Wx

$$\text{Wx}_j := \text{Wf}_j \cdot \text{CHSxy}_j$$

Term Wy

$$\text{Wy1}_j := 1$$

$$\text{Wy2}_j := \frac{\text{Wf}_j}{\text{mHSxy}_j \cdot \text{mHSyx}_j} \cdot (-1)$$

$$\text{Wy} := \text{stack}(\text{Wy1}^T, \text{Wy2}^T)$$

$$\text{F} := \text{Wy} \cdot \text{Wx}$$

$$\text{F} = \begin{pmatrix} 3.825 \cdot 10^3 \\ -1.043 \cdot 10^5 \end{pmatrix}$$

$$\text{aa} := \text{F}_0$$

$$\text{a} := \frac{1}{1 + \text{aa}}$$

$$\text{a} = 2.614 \cdot 10^{-4}$$

$$\text{bb} := \text{F}_1$$

$$\text{b} := \frac{\text{bb}}{(1 + \text{aa})^2}$$

$$\text{b} = -0.007$$

$$\text{mHtrue}_j := \sqrt{(1 + \text{a}) \cdot \text{mHSxy}_j \cdot \text{mHSyx}_j - \text{b}}$$